Supplementary information

Regio Isomers Containing Triarylboron-Based Motifs as Multi-Functional Photoluminescent Materials. From Dual-mode Delayed Emission to pH-Switchable Room-Temperature Phosphorescence

Ramar Arumugam†, [a] Akkarakkaran Thayyil Muhammed Munthasir†,[b] Ramkumar Kannan, [a] Dipanjan Banerjee,[c] Pagidi Sudhakar,[a] Venugopal Rao Soma,[c] Pakkirisamy Thilagar* [b] and Vadapalli Chandrasekhar* [a]

Table of contents

Supplementary information

1. General experimental procedures

1.1. Materials

All reactions were performed under an inert atmosphere of argon using standard Schlenk techniques.[1] Starting materials such as *n*-butyl lithium (2.5 M in hexane), dimethylamine (2M in THF), dimesitylboron fluoride, Lithium dimethylamide, 2,6-dibromo naphthalene, 1,4-dibromo naphthalene, paraffin, and ethylene glycol were obtained and used as received. Tetrahydrofuran, *n*-hexane, *n*-pentane, diethyl ether, DMSO, and DCM were dried and distilled by standard procedures.[2] Precursors such as 4-bromo-*N*, *N*-dimethylnaphthalen-1-amine (**P1**)[3] and 6-bromo-*N*, *N*-dimethylnaphthalen-2-amine (**P2**) [4] have been synthesized by following modified synthetic procedure as shown in Scheme S1.

1.2. Methods

Multi-nuclear NMR (^{1}H, ^{11}B, and ^{13}C) spectra were recorded in $CDCl_3$ at 25 °C on a Bruker Avance 400 MHz/300 MHz NMR spectrometer operating at a frequency of 300 MHz for ^{1}H, ^{11}B for 128 MHz, and ^{13}C for 75 MHz. ^{1}H NMR spectra were referenced to TMS (0.00 ppm) as an internal standard. Chemical shift multiplicities are reported as singlet (s), doublet (d), triplet (t), and multiplet (m). ^{13}C resonances were referenced to the $CDCl_3$ signal at ~77.67 ppm. ^{11}B NMR chemical shift values were referenced to the external standard boron signal of $BF_3{\cdot}Et_2O$. The ESI (HR-MS) mass spectra were recorded on a Bruker maXis mass spectrometer. Electronic absorption spectra, fluorescence emission spectra, and time-resolved fluorescence (TRF) decay measurements were recorded on a SHIMADAZU UV-2600 spectrophotometer and FLS-980 EDINBURGH spectrometer, respectively. Time-gated emission spectra were recorded using the same FLS 980 fluorimeter by excitation source of a pulsed microsecond flash lamp (μF1) with a pulse width of 1.1 μs. Temperature-dependent emission studies were also performed using the same instrument with the help of an OXFORD cryostat. Solutions of all the compounds for spectral measurements were prepared using anhydrous spectrophotometric grade solvents and standard volumetric glassware. Quartz cuvettes with sealing screw caps were used for the solution state spectral measurements. The intensity data of crystal **1** were collected on a Bruker D8 Quest diffractometer [λ(Mo Kα) = 0.71073 Å] and data reduction was performed using Apex3. The intensity data of crystal **2** were collected on an XtaLAB AFC12 (RINC) [λ(Mo Kα) = 0.71073 Å] (Rigaku Oxford Diffraction, 2017) diffractometer. The data were integrated using CrysAlisPro

1.171.39.29d software. [5a,c] The structures were solved by direct methods using SHELXS-97 and refined using the SHELXL-2018/3 program (within the WinGX program package) [5b] and non-H atoms were refined anisotropically. The CCDC numbers **1** and **2** are 2288523 and 2288524 respectively. Density functional theory (DFT) calculations were done using B3LYP functional with 6-31G(d) basis set as incorporated in the Gaussian 09 package for all the atoms. [6] The optimized structures and the frontier molecular orbitals (FMOs) were viewed using Gaussview 5.0. SOC calculations were done by ORCA 5.0 software, using B3LYP functional with a 6-31G (d, p) basis set.

2. Synthesis details

2.1 Synthesis of **P1** and **P2**

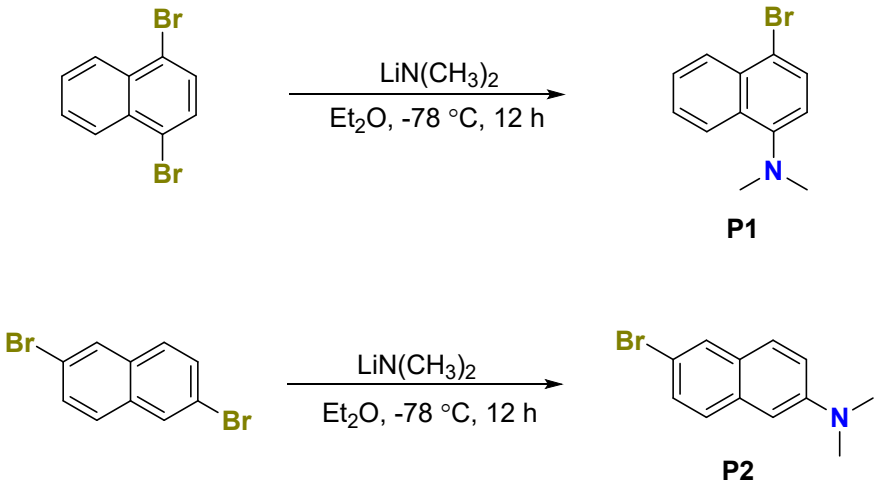

Scheme S1. Synthesis of precursor compounds **P1** and **P2**.

General procedure: To an oven-dried 100 mL Schlenk flask, 1,4-dibromo naphthalene / 2,6-dibromo naphthalene (1.00 g, 3.5 mmol) and dry Et_2O (30 mL) were added under argon atmosphere. Then lithium dimethylamide (304 mg, 3.5 mmol) in 5 mL Et_2O was added to the reaction flask at -78 °C. The reaction mixture was warmed to ambient temperature and stirred for 12 h. The volatiles were removed under vacuum, the compound extracted with dichloromethane, and dried over Na_2SO_4. The final product is purified by column chromatography on silica gel using petroleum ether, to give a white solid.

4-bromo-*N*, *N*-dimethylnaphthalen-1-amine (**P1**): White solid. Yield: 80%. ^{1}H NMR (300 MHz, $CDCl_3$): δ (ppm) 8.37 (s, 2H), 7.78-7.66 (m, 3H), 6.96 (d, *J* = 3.6 Hz, 1H), 2.94 (s, 6H).

6-bromo-*N*, *N*-dimethylnaphthalen-2-amine (**P2**): White solid. Yield: 65%. ^{1}H NMR (300 MHz, $CDCl_3$): δ (ppm) 7.83 (s, 1H), 7.61 (d, *J* = 9 Hz, 1H), 7.52 (d, *J* = 8.4 Hz, 1H), 7.42 (d, *J* = 8.4 Hz, 1H), 7.16 (d, *J* = 8.7 Hz, 1H), 6.87 (s, 1H), 3.05 (s, 6H).

2.2 Synthesis of **1** and **2**

General procedure: To an oven-dried 100 mL Schlenk flask*, n*-butyl lithium (2.5 M in hexane, 1.5 mmol) was added dropwise to a (15 mL) Et_2O of **P1**/**P2** (1.3 mmol) at -78 °C for 5 min. After 4 h, an (5 mL) Et_2O solution of dimesitylfluoroborane (1.3 mmol) was added, and the reaction mixture was warmed to ambient temperature and stirred for an additional 12 h. The resulting yellow color solution was extracted with a dichloromethane/water mixture (30 mL × 3). The crude products **1** /**2** were further purified by column chromatography on silica gel using petroleum ether and characterized by multinuclear NMR spectroscopy.

Synthesis of 4-(dimesitylboraneyl)-*N*, *N*-dimethylnaphthalen-1-amine (1)

Quantities used for the preparation of **1** as follows: **P1** (333 mg, 1.3 mmol), *n*-butyl lithium (2.5 M in *n*-hexane, 1.91 mL, 1.5 mmol), and dimesitylboron fluoride (357 mg, 1.3 mmol). Yield: 65 %. ^{1}H NMR (300 MHz, $CDCl_3$): δ (ppm) 8.17 (d, *J* = 8.4 Hz, 1H), 7.62 (d, *J* = 8.1 Hz, 1H), 7.44-7.36 (m, 2H), 7.23-7.16 (m, 1H), 6.89 (d, *J* = 7.5 Hz, 1H), 6.77 (s, 4H), 2.94 (s, 6H), 2.28 (s, 6H), 1.95 (s, 12H); ^{11}B NMR (128 MHz, $CDCl_3$): δ (ppm) 70.2; ^{13}C NMR (75 MHz, $CDCl_3$): δ (ppm) 154.58, 143.87, 141.81, 140.56, 138.45, 138.14, 136.18, 128.41, 128.27, 127.88, 125.90, 124.79, 124.66, 112.56, 44.83, 23.11, 21.29; ESI (HR-MS). Calcd for $C_{30}H_{35}BN$ $[M + H]^+$: *m*/*z* 420.2858. Found: *m*/*z* 420.2861.

Synthesis of 6-(dimesitylboraneyl)-*N*, *N*-dimethylnaphthalen-2-amine (2)

Quantities used for the preparation of **1** as follows: **P2** (333 mg, 1.3 mmol), *n*-butyl lithium (2.5 M in *n*-hexane 1.91 mL, 1.5 mmol), and dimesitylboron fluoride (357 mg, 1.3 mmol). Yield: 60%. ^{1}H NMR (300 MHz, $CDCl_3$): δ (ppm) 7.98 (s, 1H), 7.73 (d, *J* = 8.7 Hz, 1H), 7.62-7.54 (m, 2H), 7.14 (d, *J* = 8.9 Hz, 1H), 6.93 (s, 1H), 6.88 (s, 4H), 3.11 (s, 6H), 2.36 (s, 6H), 2.09 (s, 12H); ^{11}B NMR (128 MHz, $CDCl_3$): δ (ppm) 68.5; ^{13}C NMR (75 MHz, $CDCl_3$): δ (ppm) 149.98, 140.94, 139.07, 138.16, 137.48, 133.38, 130.97, 128.12, 126.19, 125.25, 115.57, 105.63, 40.64, 23.54, 21.28; ESI (HR-MS). Calcd for $C_{30}H_{35}BN$ $[M + H]^+$: *m*/*z* 420.2858. Found: *m*/*z* 420.2860.

3. Structural Characterization

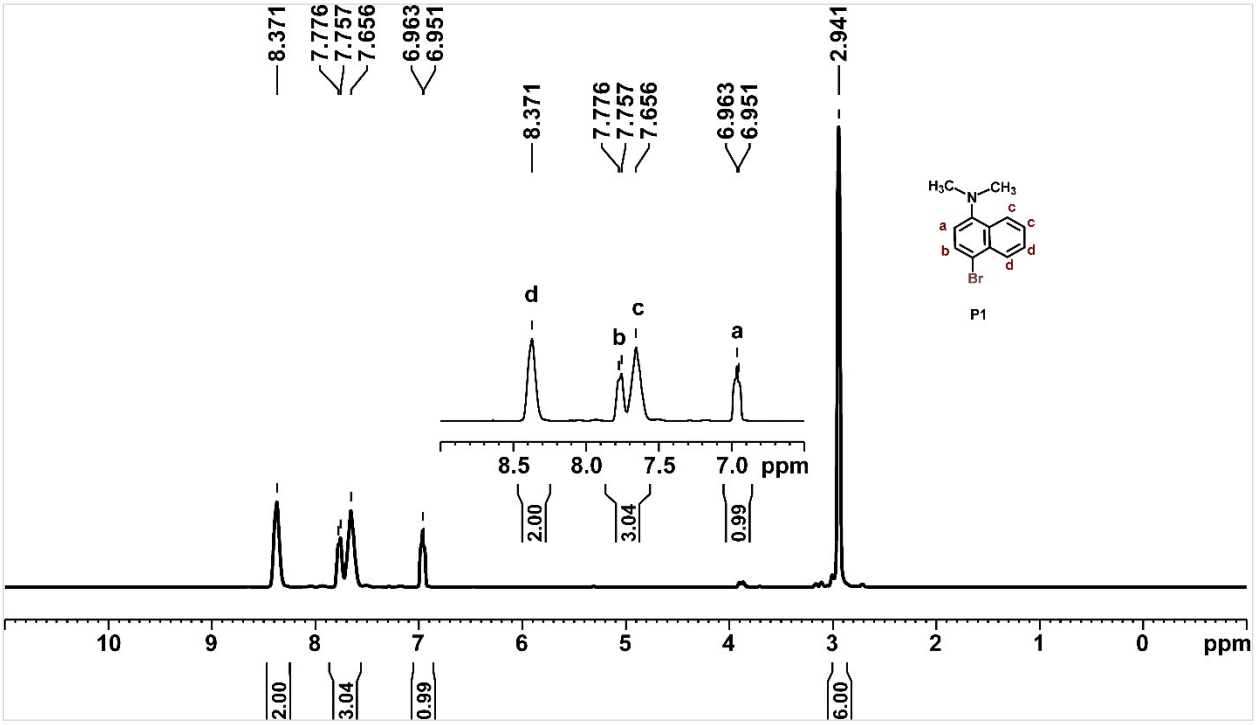

Figure S1. ^{1}H NMR spectrum of **P1** in $CDCl_3$.

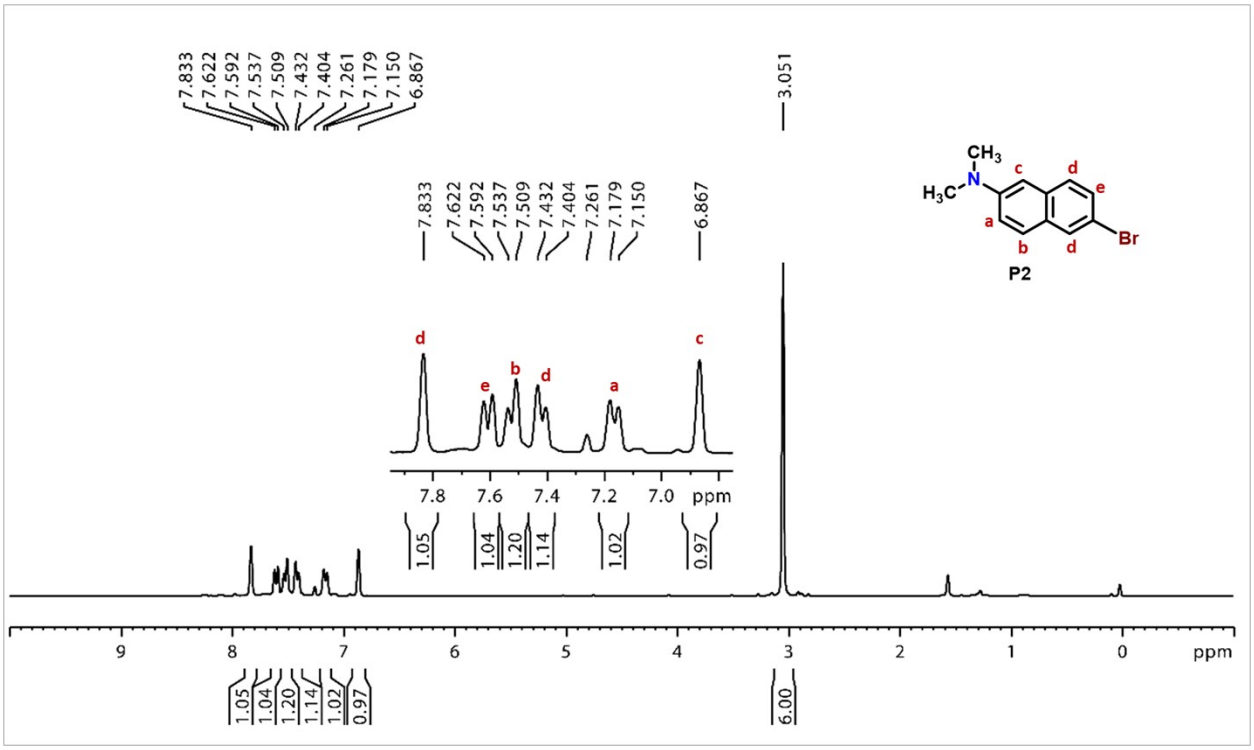

Figure S2. ^{1}H NMR spectrum of **P2** in $CDCl_3$.

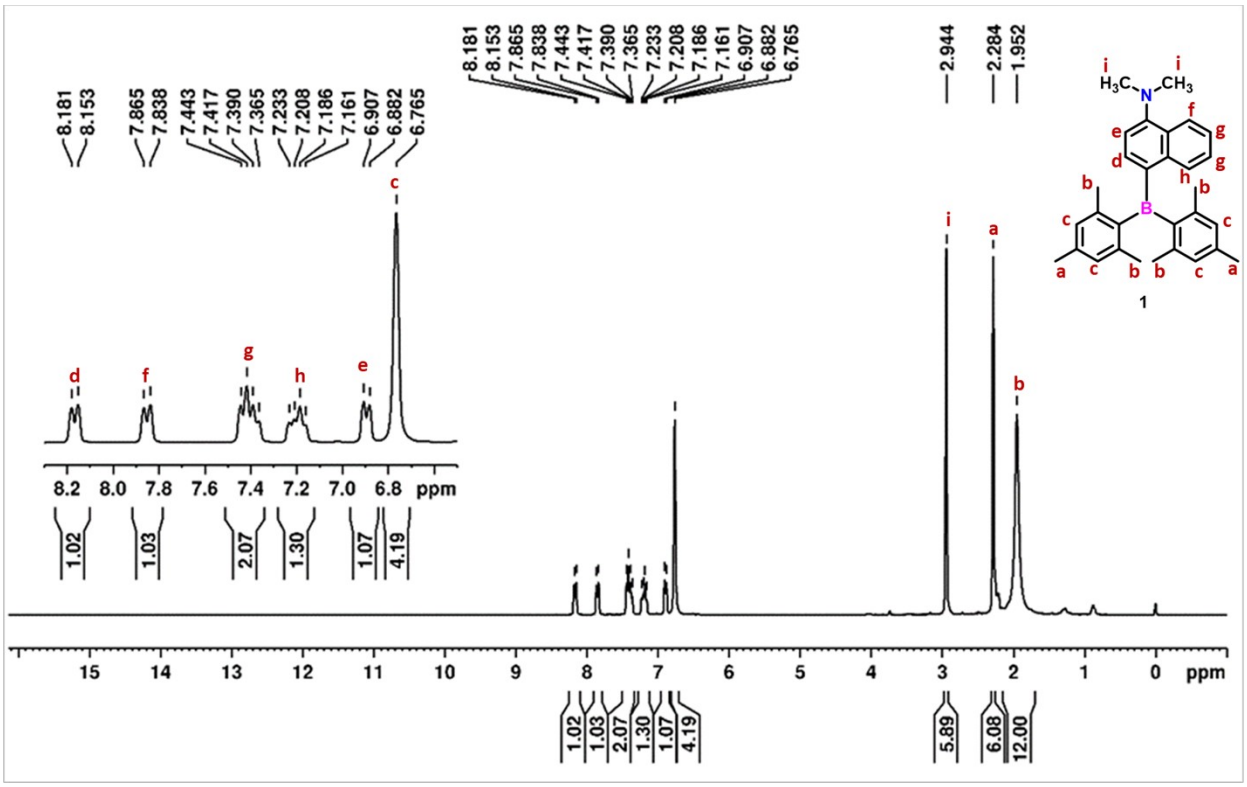

Figure S3. ^{1}H NMR spectrum of **1** in $CDCl_3$.

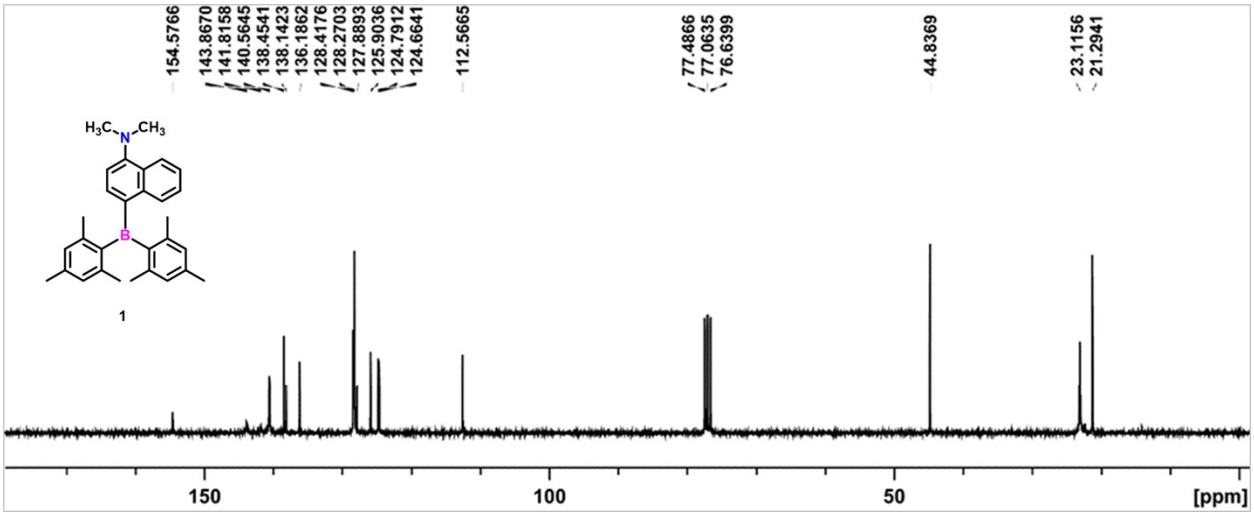

Figure S4. ^{13}C NMR spectrum of **1** in $CDCl_3$.

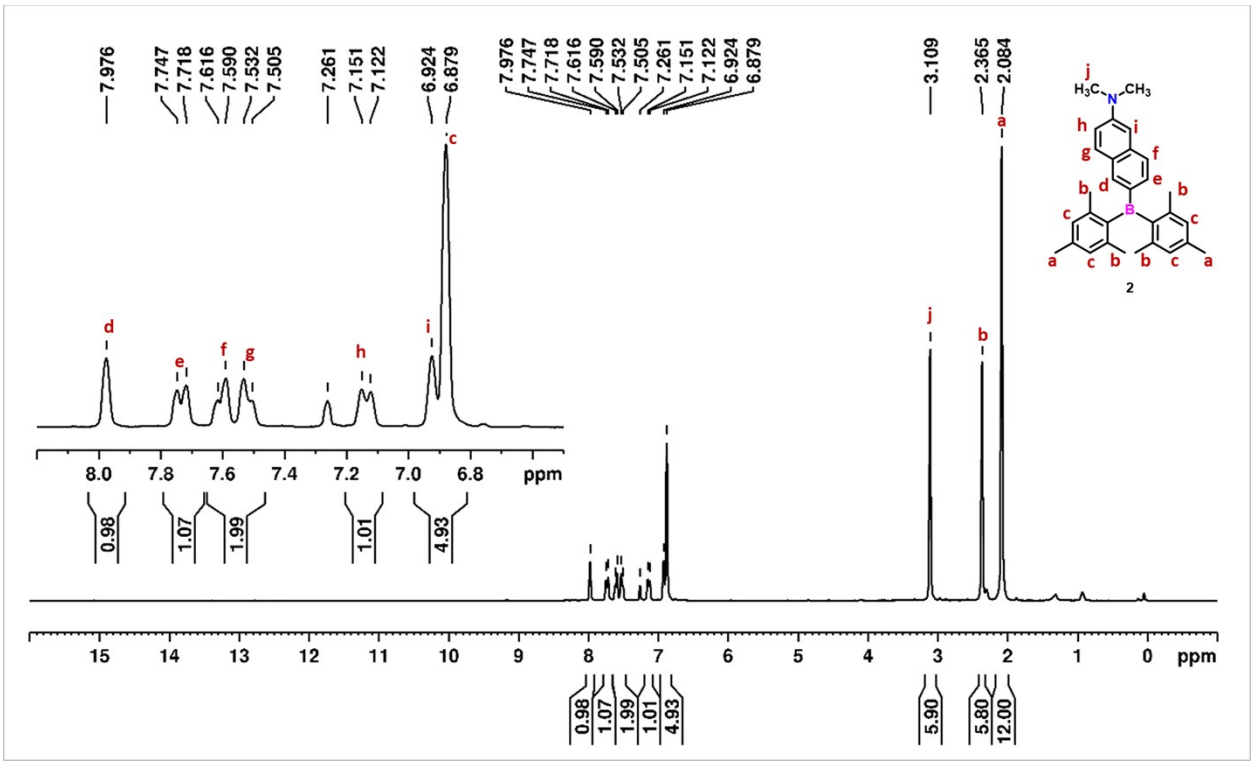

Figure S5. ^{1}H NMR spectrum of **2** in $CDCl_3$.

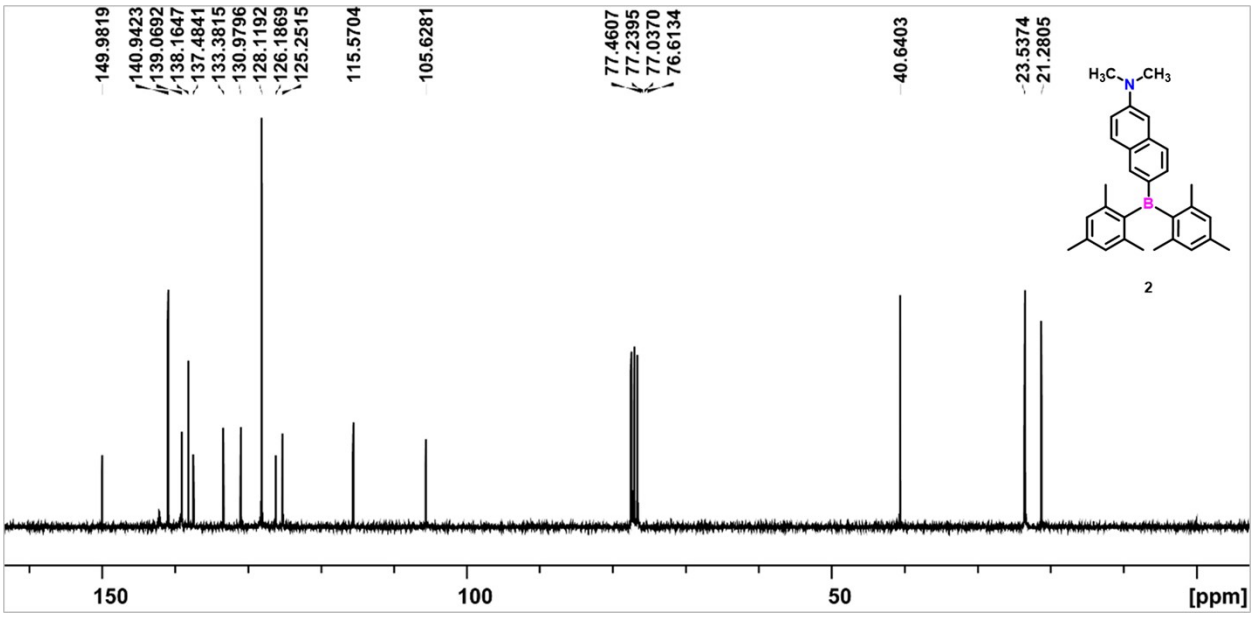

Figure S6. ^{13}C NMR spectrum of **2** in $CDCl_3$.

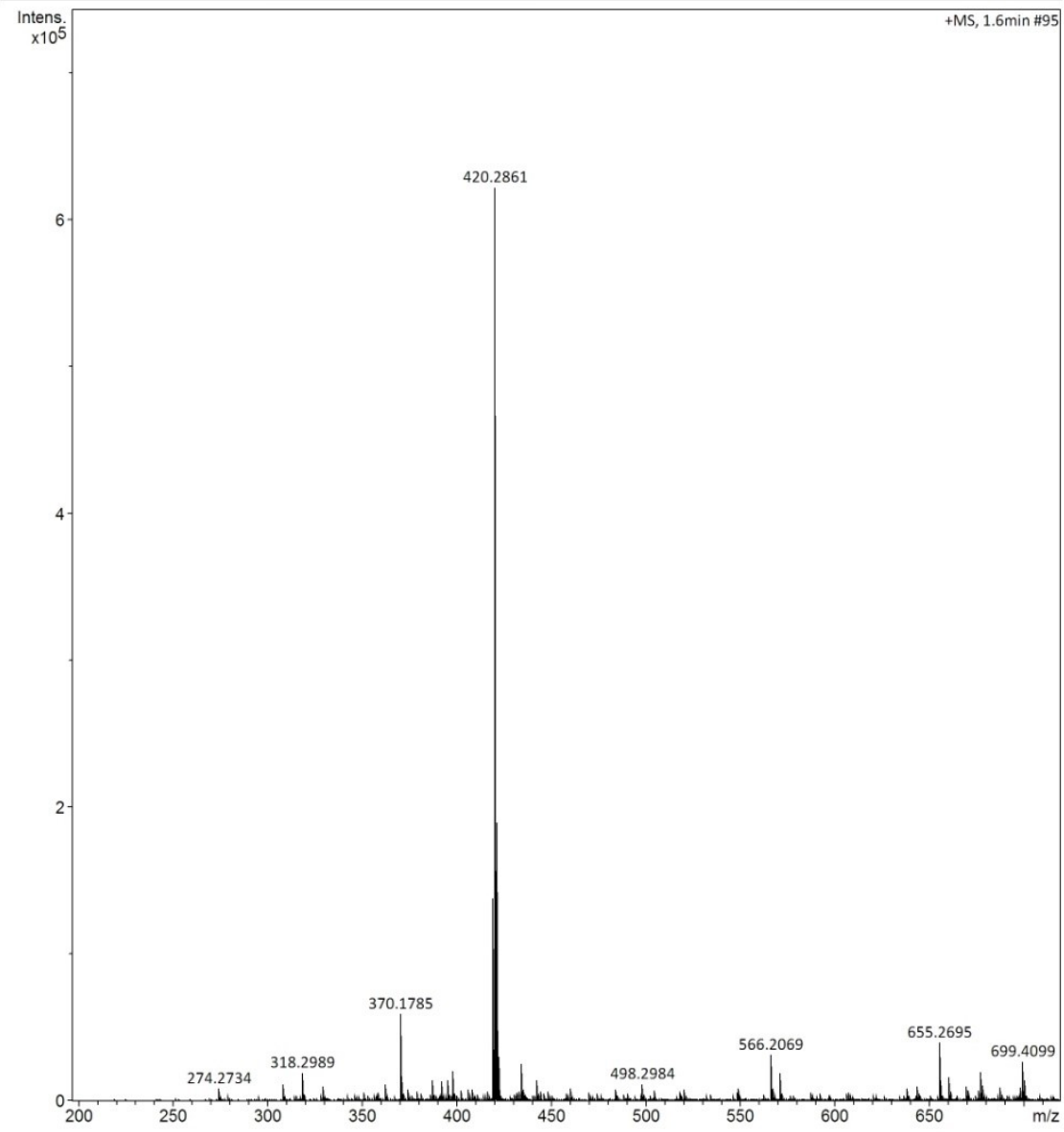

Figure S7. HRMS spectrum of **1**.

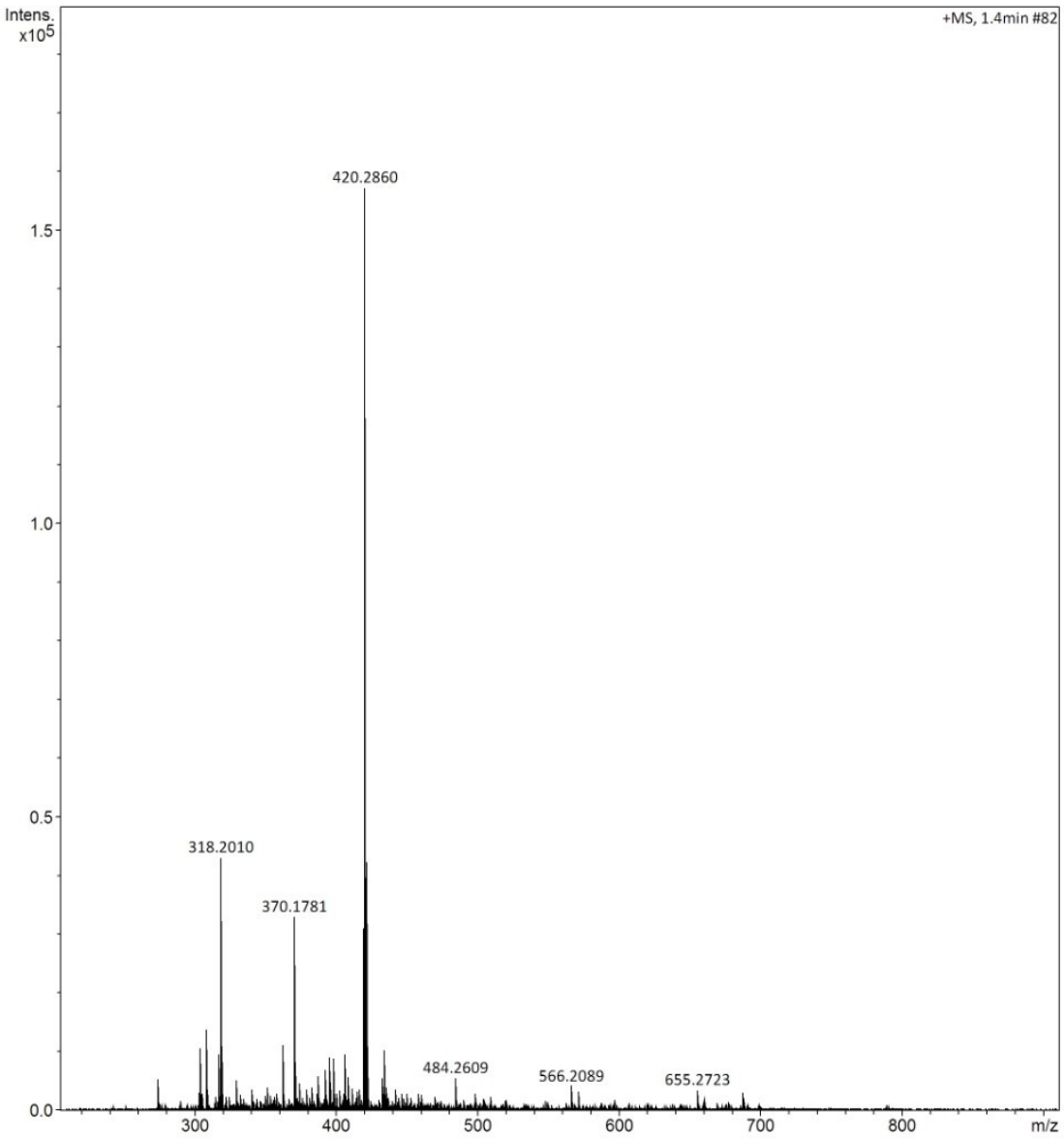

Figure S8. HRMS spectrum of **2**.

4. Single crystal X-ray diffraction Studies

	1	**2**
Empirical formula	$C_{30}H_{34}BN$	$C_{30}H_{34}BN$
FW	419.39	419.39
T (K)	296 K	298 K
Crystal system	orthorhombic	triclinic
Space group	*P 21 21 21*	*P -1*
a/Å	8.3637(3)	7.9503(4)
b/Å	14.3587(6)	8.3312(4)
c/Å	21.3790(8)	19.4228(9)
α/deg	90	78.527(4)
β/deg	90	89.087(4)
γ/deg	90	87.192(4)
V/Å^3	2567.44(17)	1259.24(11)
Z	4	2
ρ_{calcd} (gcm^{-3})	1.085	1.106
μ (Mo Kα) (mm^{-1})	0.061	0.062
λ/Å	0.71073	0.71073
F (000)	904.0	452.0
Collected reflections	5267	4372
Unique reflections	3071	3389
Goodness of Fit (GOF) [F2]	1.013	1.048
R1 [I>2σ(I)][a]	0.0584	0.0585
wR2 [I>2σ(I)][b]	0.1918	0.1787
CCDC Number	**2288523**	**2288524**

Table S1. Crystallographic data and refinement parameters for **1** and **2**

[a] $R1 = \Sigma||Fo| - |Fc||/\Sigma|Fo|$. [b] $wR2 = [\Sigma\{w(Fo^2 - Fc^2)^2\}/\Sigma\{w(Fo^2)$

Table S2. Comparison of selected bond lengths [Å] and angles [°] for Me_2N-C_6H_4–$B(Mes)_2$ (**R1**), [5] **1**, and **2**.

Compounds	Bond length (Å)			Bond angle (°)		Dihedral angle (°)		
	B-C(Mes)	B–C(Nap)	N–C(Nap)	C–B–C	C–N–C	θ_{B-N}	θ_{B-Nap}	θ_{N-Nap}
R1	1.586(2)	1.545(2)	1.368(1)	360	359.4	13.4	19.6	8.1
1	1.585(6) 1.571(6)	1.553(6)	1.409(5)	359.8	343.2	57.4	37	61.1
2	1.581(3) 1.578(3)	1.559(3)	1.371(2)	360	359.7	32.2	32.1	3.2

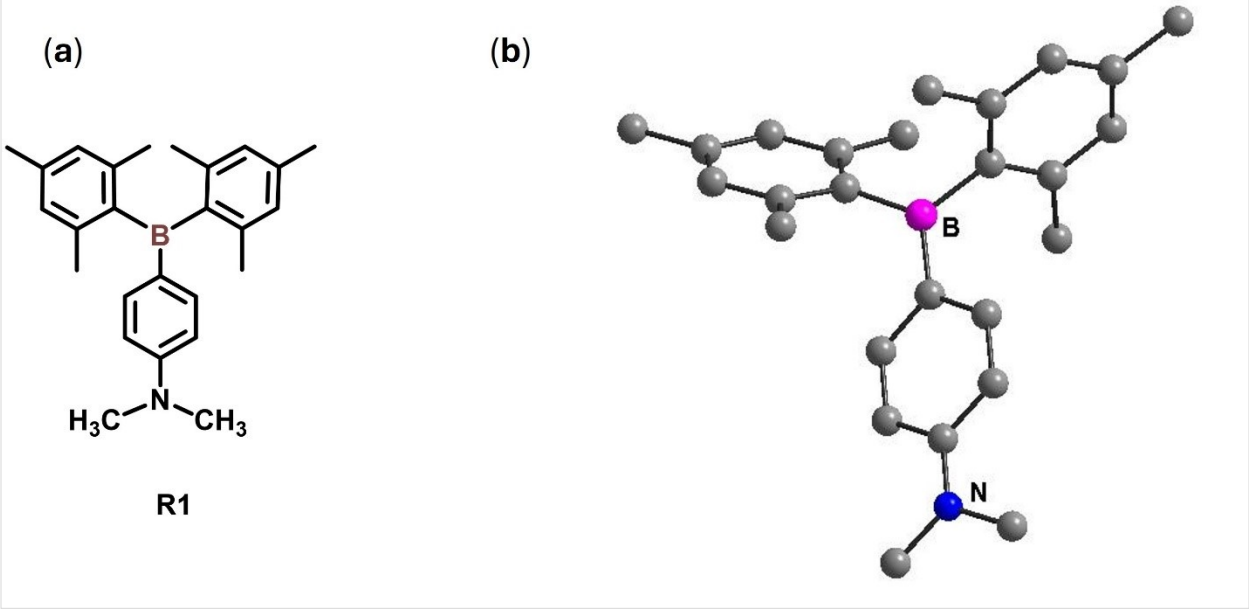

Figure S8a. a) Chemical structure b) molecular structure of **R1**[5] (All the hydrogen atoms are omitted for clarity).

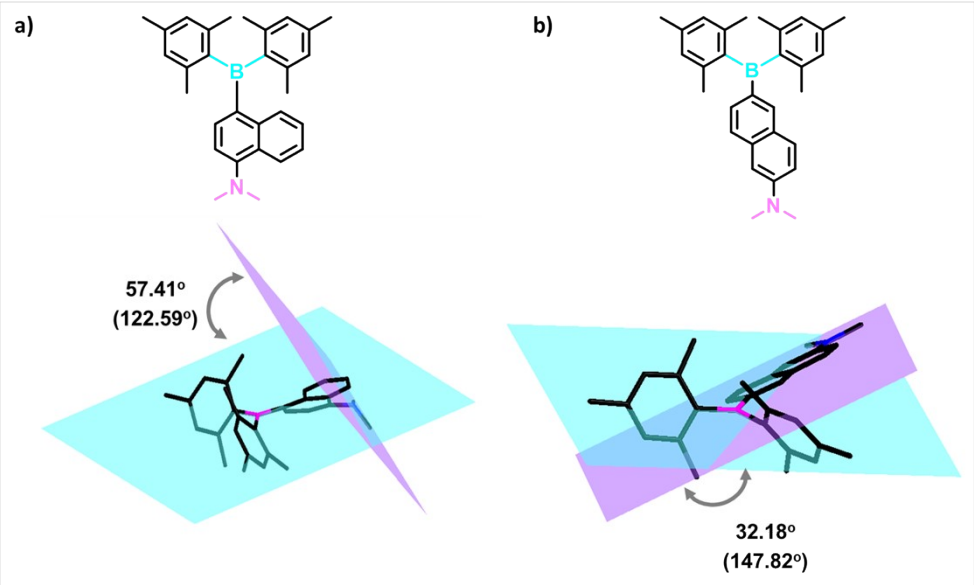

Figure S9. Dihedral angle (°) between the plane containing boron with carbons attached to B (cyan) and nitrogen with methyl carbon attached to N (magenta) [$\theta_{B\text{-}N}$] on (a) **1** and (b) **2**. [Carbon: black, nitrogen: blue, boron: magenta, and hydrogen are omitted for clarity]. The angles mentioned in parenthesis are obtained by subtracting the exact angle measured (from the crystal structure) from 180°.

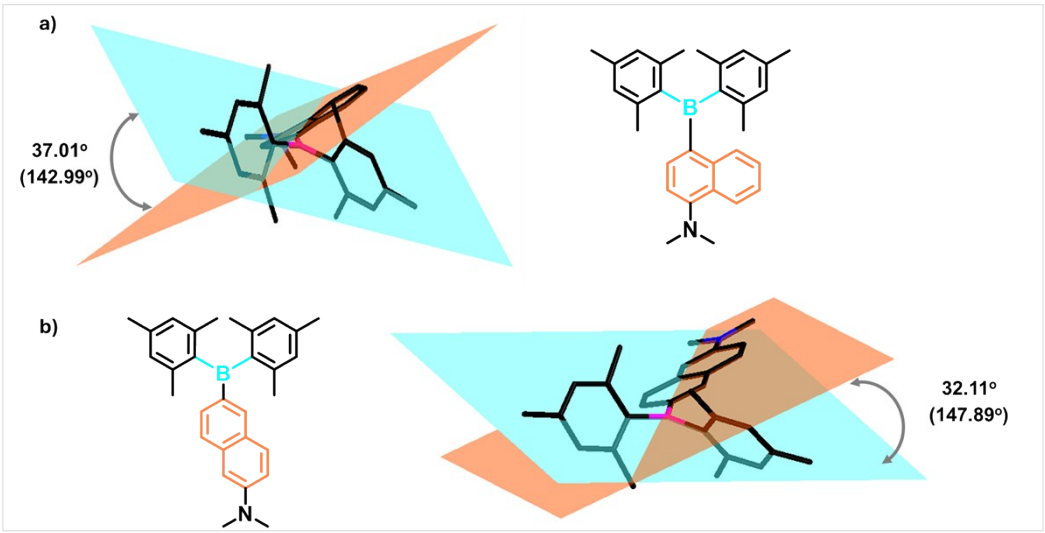

Figure S10. Dihedral angle (°) between the plane containing boron with carbons attached to B (cyan) and the mean plane containing all naphthalene carbon atoms (orange) [$\theta_{B\text{-}Nap}$] on (a) **1** and (b) **2**. [Carbon: black, nitrogen: blue, boron: magenta, and hydrogen are omitted for clarity]. The angles mentioned in parenthesis are obtained by subtracting the exact angle measured (from the crystal structure) from 180°.

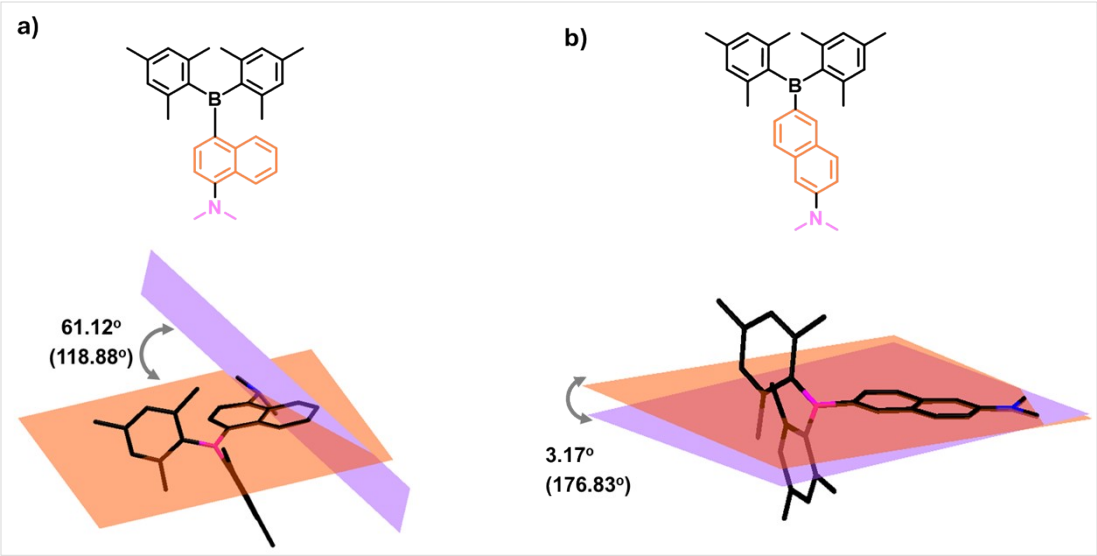

Figure S11. Dihedral angle (°) between the mean plane containing all naphthalene carbon atoms (orange) and nitrogen with methyl carbon attached to N (magenta) [$\theta_{N\text{-}Nap}$] on (a) **1** and (b) **2**. [Carbon: black, nitrogen: blue, boron: magenta, and hydrogen are omitted for clarity]. The angles mentioned in parenthesis are obtained by subtracting the exact angle measured (from the crystal structure) from 180°.

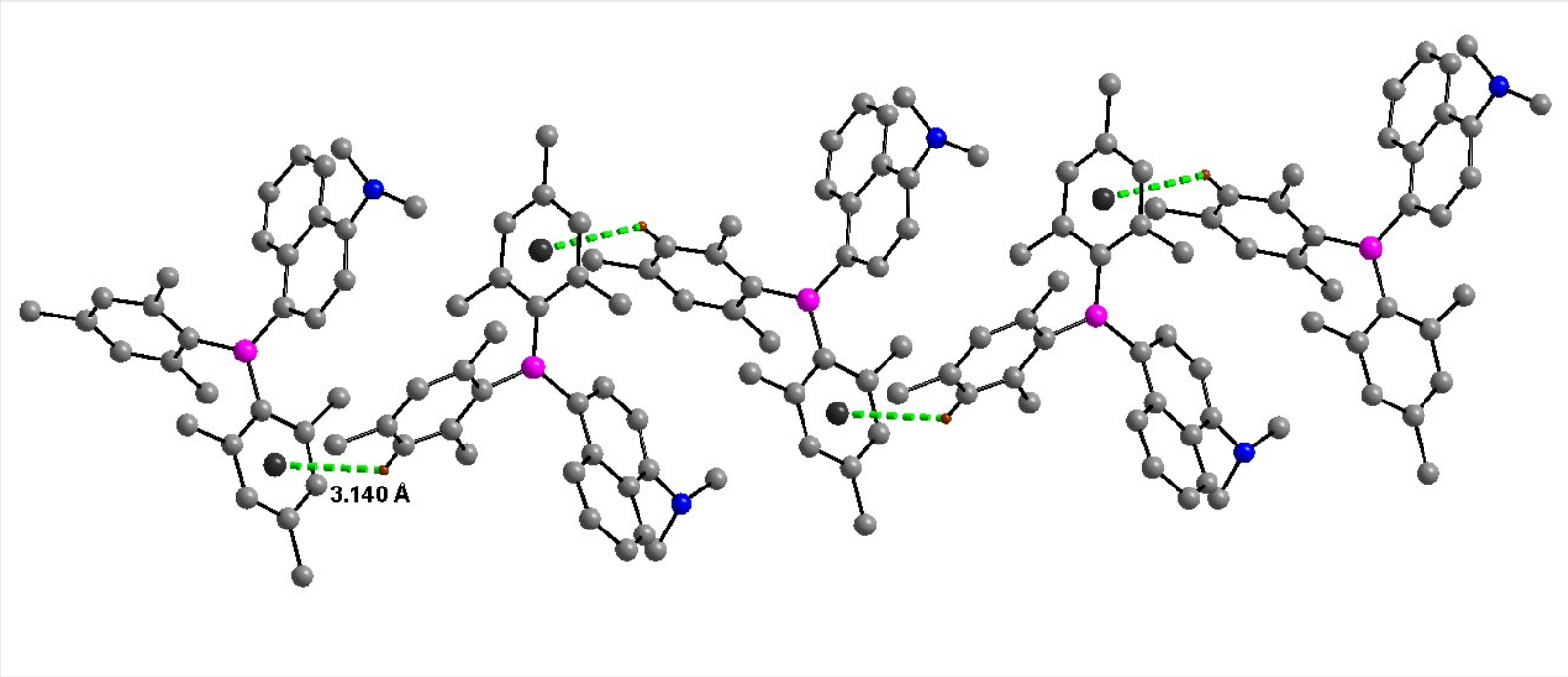

Figure S12. C-H···π (green line) intermolecular interactions in **1** which extended in one direction and formed a 1D chain. The twisted geometry of this system constrains these molecules from forming any further interaction leading to loose packing in the 3D lattice. Hydrogen atoms are omitted for clarity. Color code: carbon (gray 50), boron (magenta), and nitrogen (blue).

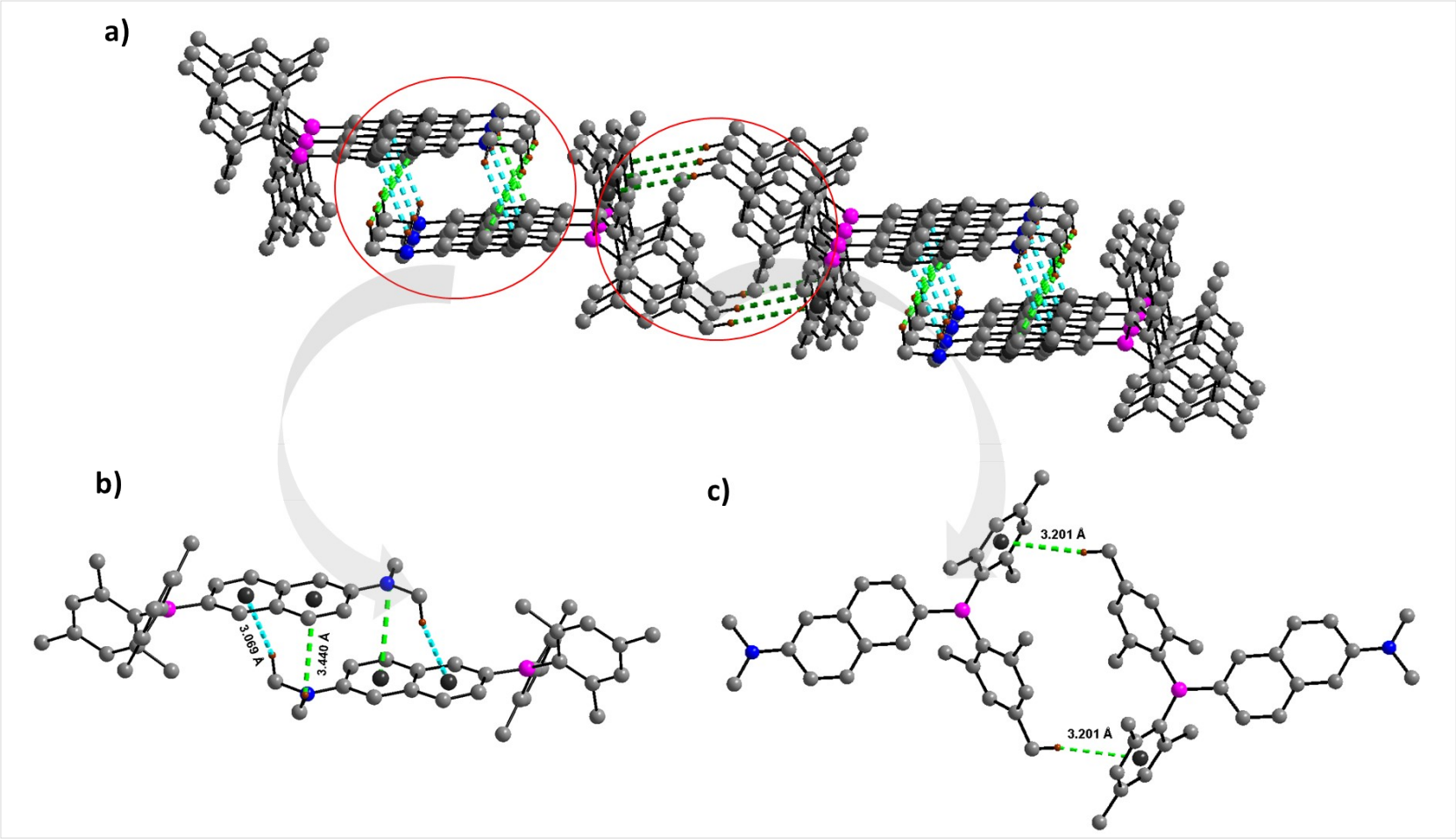

Figure S13. (a) Intermolecular interactions in **2** which hold the molecule to form the crystal lattice. (b) The intramolecular interaction that forms the 2D chain. [Intermolecular C-H---π_{Nap} interaction between the methyl hydrogen on N of one molecule with π cloud of naphthalene ring on the adjacent molecule (3.069 Å and 3.440 Å)]. (c) intermolecular interaction that connects the 2D chain to form the 3D structure. [Intermolecular C-H---π_{mes} interaction between the methyl hydrogen on the mesityl ring of one molecule with π cloud of mesityl ring on the adjacent molecule (3.201 Å)]. Hydrogen atoms are omitted for clarity. Color code: carbon (gray 50), boron (pink), and nitrogen (blue)

5. Photophysical and Theoretical Studies

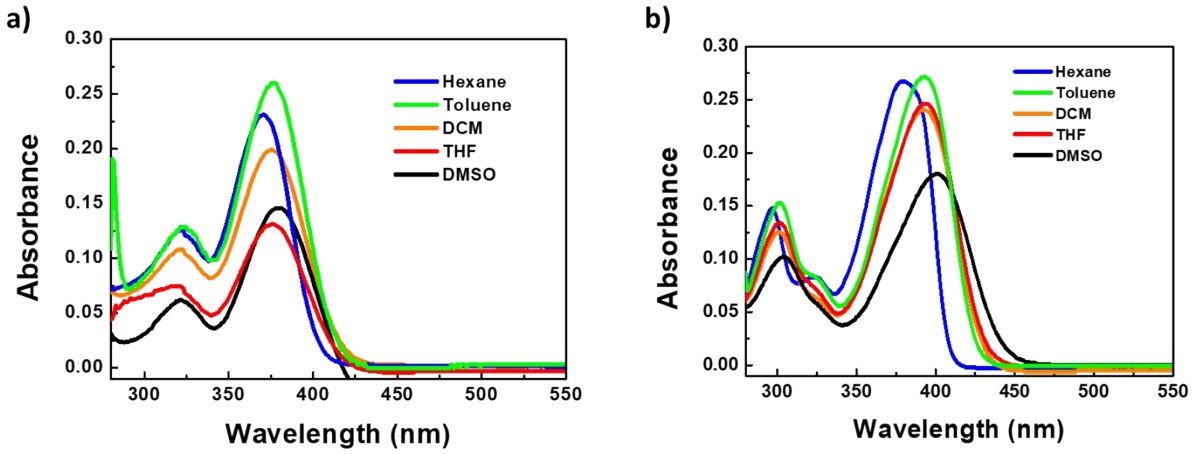

Figure S14. UV-visible absorption spectra of (a) **1** and (b) **2** in different solvents (conc. 10^{-5} M).

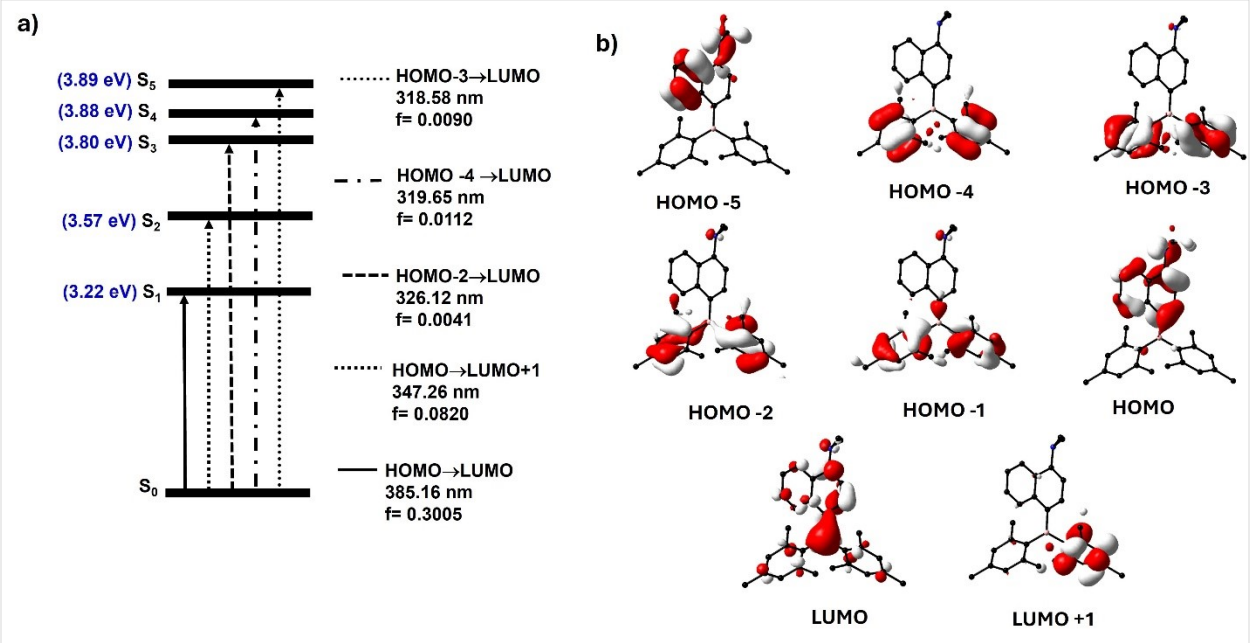

Figure S15. (a) Singlet energy level diagram, vertical transition involving first five singlet states, and (b) molecular orbitals involved in the transitions calculated through TD-DFT calculation using 6-31G (d, p)/B3LYP level of theory for **1**.

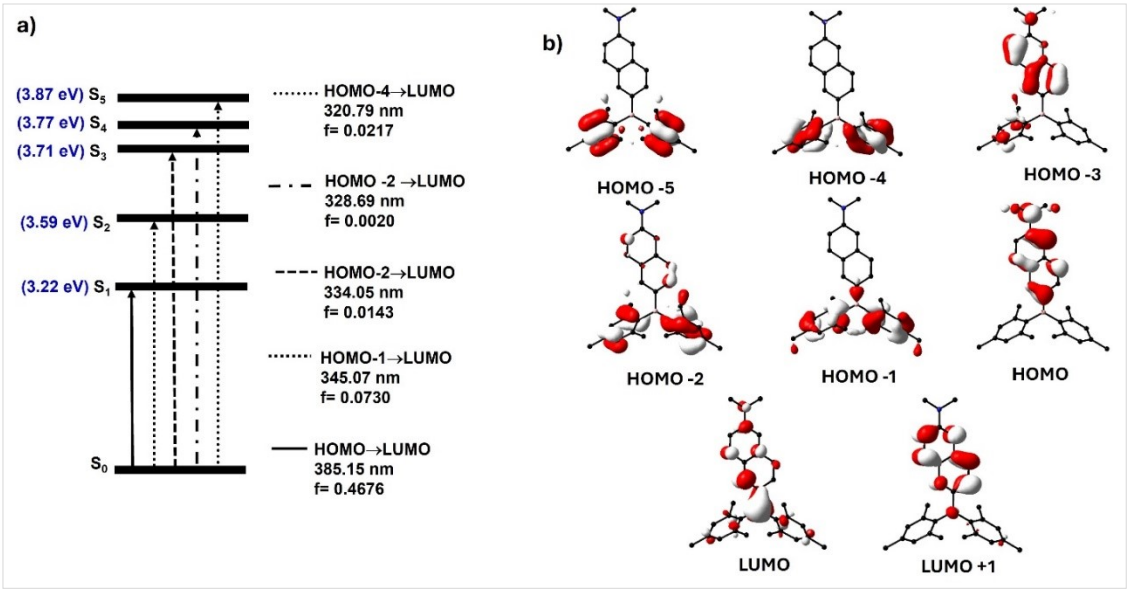

Figure S16. (a) Singlet energy level diagram, vertical transition involving first five singlet states, and (b) molecular orbitals involved in the transitions calculated through TD-DFT calculation using 6-31G (d,p)/B3LYP level of theory for **2**.

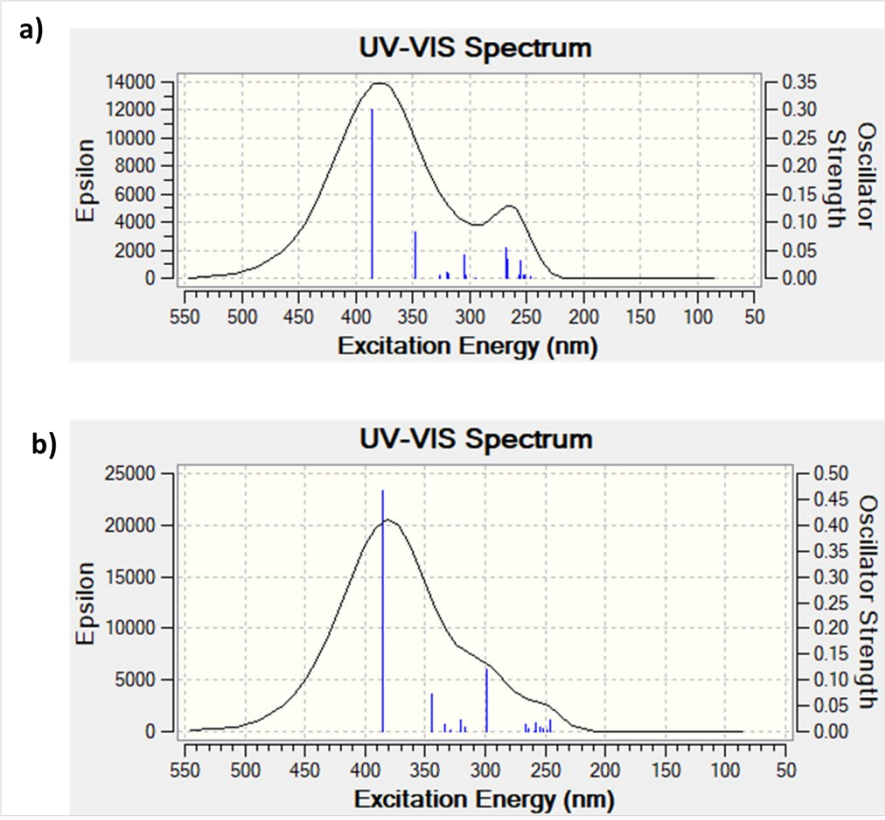

Figure S17. Theoretical UV-visible absorption spectra for (a) **1** and (b) **2** through TD-DFT calculation using 6-31G (d, p)/B3LYP level of theory.

Table S3: Comparison of different parameters for **1** and **2** obtained from crystal data and ground state optimized geometry through DFT calculation using 6-31G (d,p)/B3LYP level of theory.

Parameter	1			2		
	Ground state (S_0)	Excited state (S_1)	Crystal	Ground state (S_0)	Excited state (S_1)	Crystal
HOMO (eV)	-5.27	-	-	-5.04	-	-
LUMO (eV)	-1.56	-	-	-1.45	-	-
Band gap (eV)	3.71		-	3.59	-	-
Dipole moment (D)	1.72	1.54	-	4.19	2.25	-
$\Sigma_{(C\text{-}B\text{-}C)}$ (°)	359.9	359.9	359.8	360	359.7	360
$\Sigma_{(C\text{-}N\text{-}C)}$ (°)	343.5	357.4	343.2	358.1	360	359.7
B-C (Å)	1.570	1.633	1.553	1.561	1.623	1.559
N-C (Å)	1.418	1.374	1.409	1.386	1.365	1.371
$\theta_{D\text{-}A}$ (°)	79.6	88.5	57.4	28.4	73.9	32.2
$\theta_{S\text{-}A}$ (°)	35.8	59.8	37	22.8	73.7	32.1
$\theta_{D\text{-}S}$ (°)	61.3	40.7	61.1	12.9	0.3	3.2

Table S4: Summary of computed singlet vertical transitions involved in **1** through TD-DFT calculation using 6-31G (d,p)/B3LYP level of theory.

Transitions	E (eV)	λ (nm)	*f*	Dominant transitions (%)
$S_0 \rightarrow S_1$	3.2191	385.16	0.3005	HOMO →LUMO (47.6)
$S_0 \rightarrow S_2$	3.5704	347.26	0.0820	HOMO →LUMO+1 (47.8)
$S_0 \rightarrow S_3$	3.8018	326.12	0.0041	HOMO-3 →LUMO (5.4) HOMO-2 →LUMO (42.9)
$S_0 \rightarrow S_4$	3.8787	319.65	0.0112	HOMO-4 →LUMO (47.8)
$S_0 \rightarrow S_5$	3.8918	318.58	0.0090	HOMO-3 →LUMO (41.9) HOMO-2 →LUMO (4.7)

Table S5: Summary of computed singlet vertical transitions involved in **2** through TD-DFT calculation using 6-31G (d,p)/B3LYP level of theory.

Transitions	E (eV)	λ (nm)	*f*	Dominant transitions (%)
$S_0 \rightarrow S_1$	3.2191	385.15	0.4676	HOMO →LUMO (47.9)
$S_0 \rightarrow S_2$	3.5930	345.07	0.0730	HOMO-1 →LUMO (48.6)
$S_0 \rightarrow S_3$	3.7116	334.05	0.0143	HOMO-3 →LUMO (12.4) HOMO-2 →LUMO (17.9) HOMO →LUMO+1 (17.4)
$S_0 \rightarrow S_4$	3.7720	328.69	0.0020	HOMO-3 →LUMO (14.6) HOMO-2 →LUMO (28.7) HOMO →LUMO+1 (3.9)
$S_0 \rightarrow S_5$	3.8650	320.79	0.0217	HOMO-4 →LUMO (45.7) HOMO →LUMO+1 (1.6)

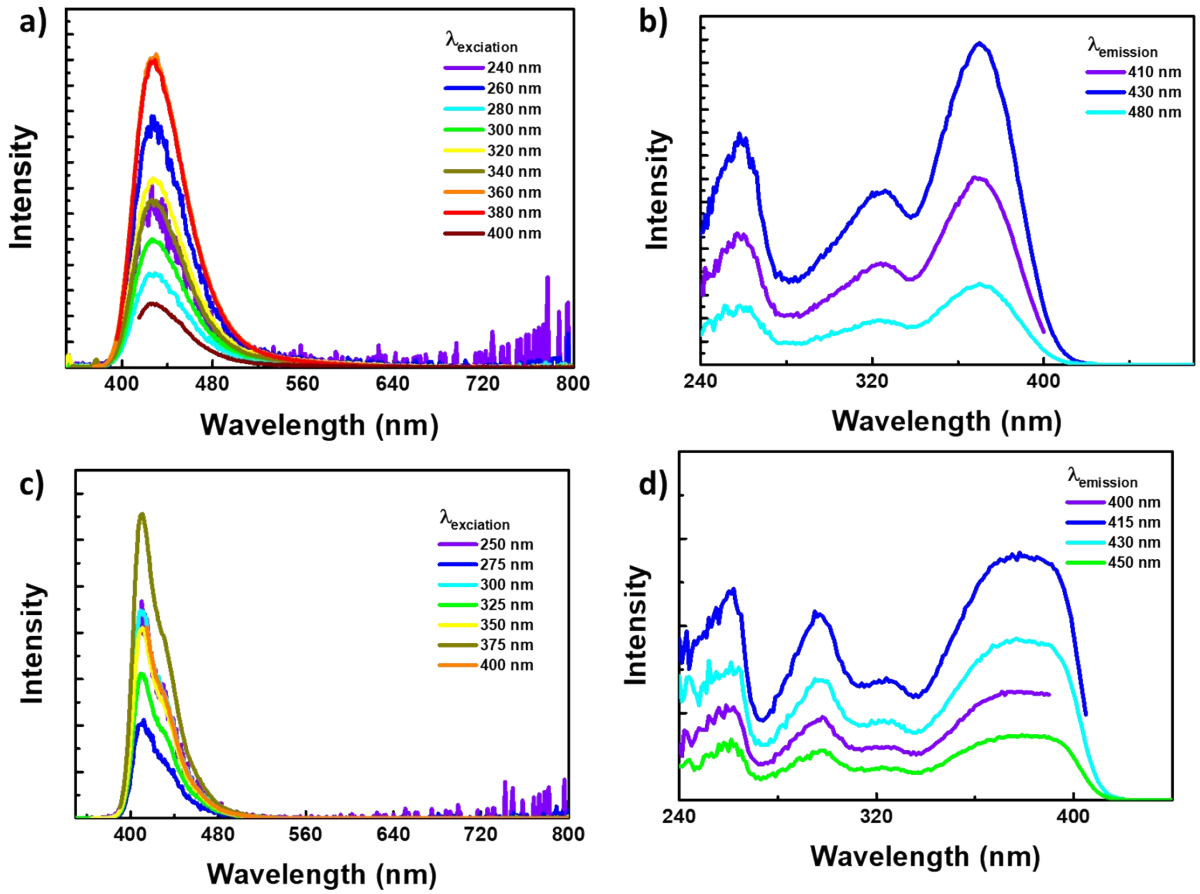

Figure S18. (a,c) PL spectra at different excitation (b,d) Excitation spectra at different emission wavelengths for **1** (a,b) and **2** (c,d) (as prepared solid) at 298K under ambient conditions.

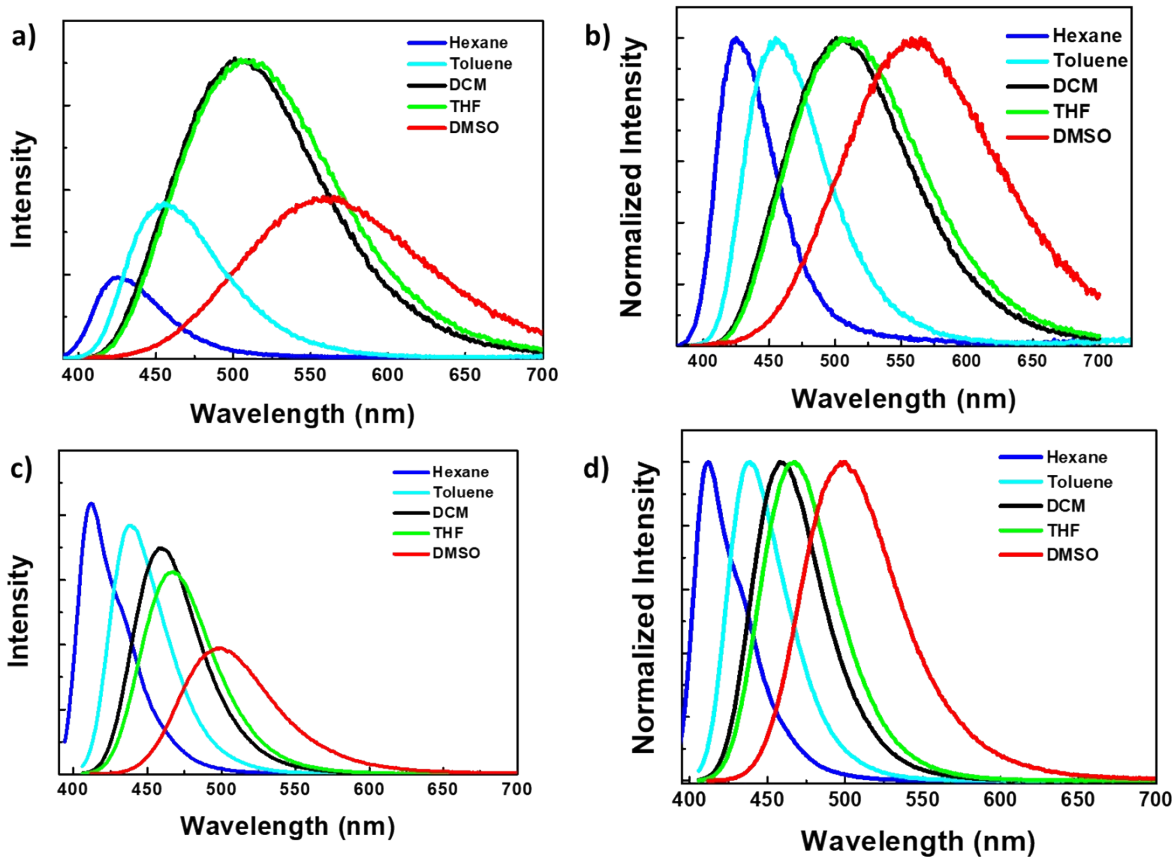

Figure S19. Photoluminescence spectra (PL) of compound (a, b) **1** and **2** (c, d) in different solvents (conc. 10^{-5} M) at λ_{ex}= 380 nm respectively.[b,d are normalized PL spectra; the normalization is done to **1**]. Photoluminescence spectra of **1** and **2** in hexane (conc. 10^{-5} M)

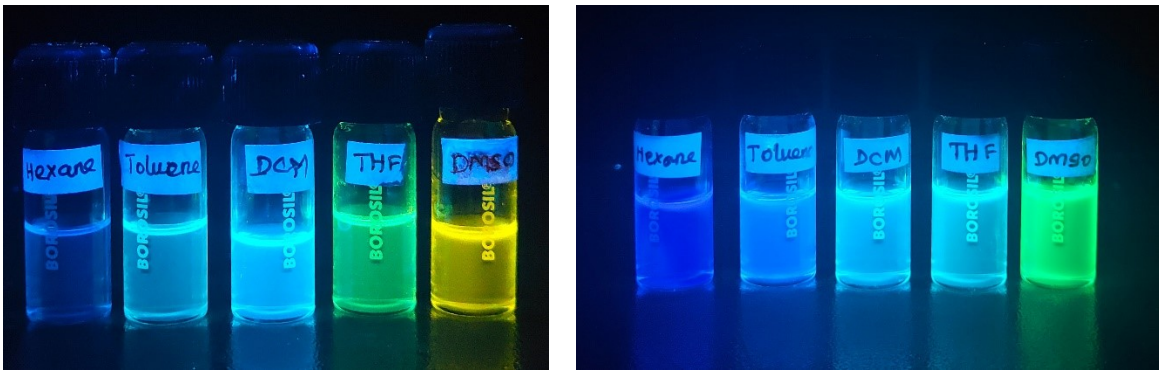

Figure S20. Images of compounds **1** (left) and **2** (right) under UV light in different solvents (λ_{ex}= 365 nm)

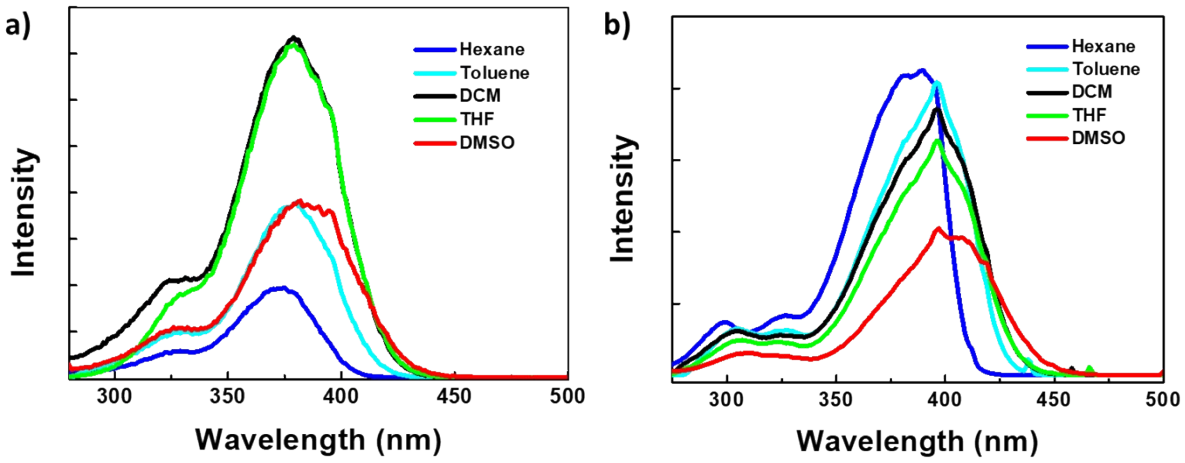

Figure S21. Excitation spectra of compound (a) **1**, (b) **2** at corresponding emission maxima in different solvents (conc. 10^{-5} M).

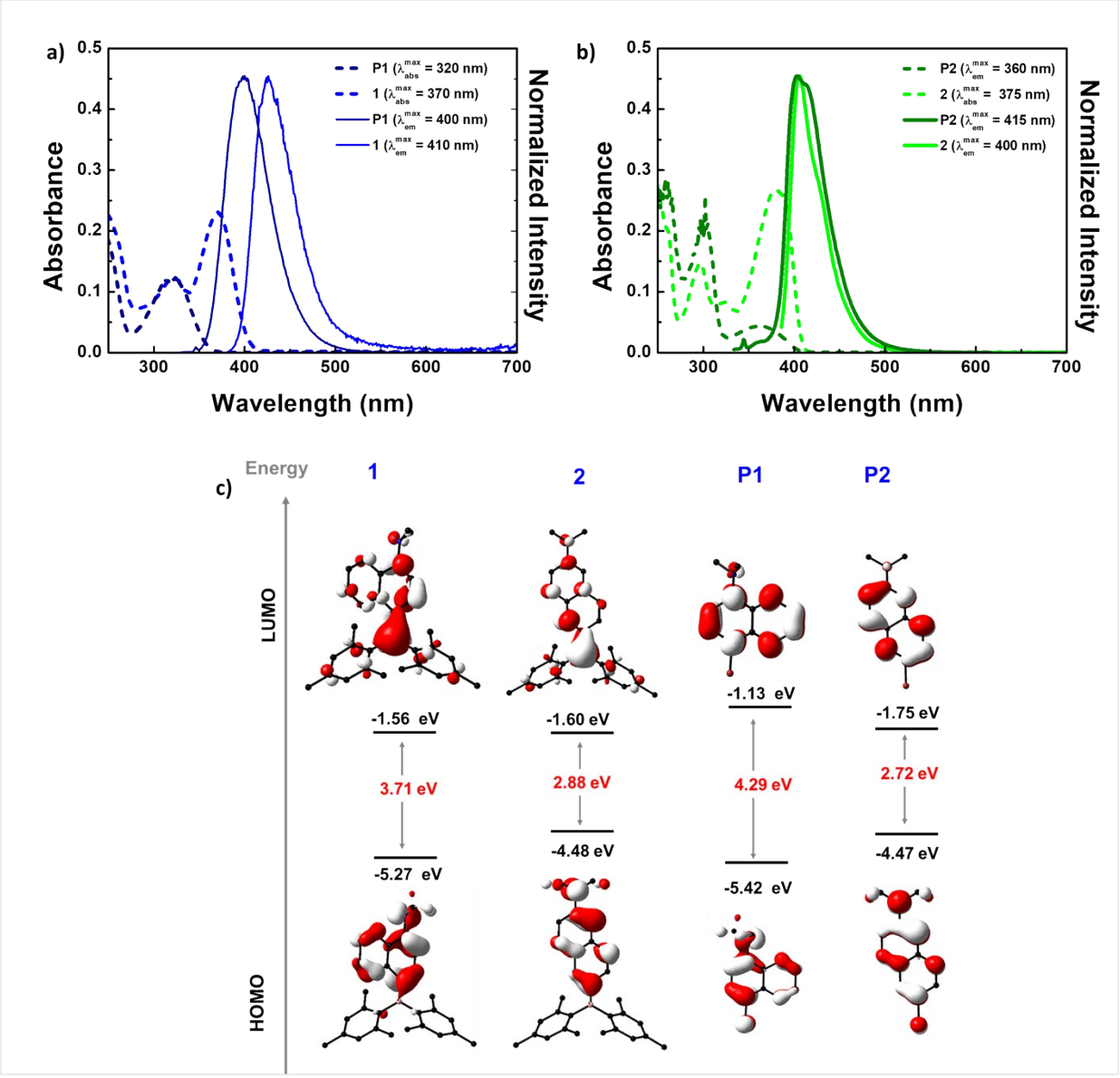

Figure S22. (a) UV-visible absorption and PL spectra [λ_{ex} = 320 nm for **P1**, 300 nm for **P2**, and 380 nm for **1** and **2** in DCM (conc.10^{-5} M) (b)UV-visible absorption and PL spectra [λ_{ex} = 320 nm for **P1**, 300 nm for **P2**, and 380 nm for **1** and **2** respectively] in hexane (conc.10^{-5} M) and (c) frontier molecular orbitals (iso value = 0.04) generated from the ground state S_0 geometries using the B3LYP/6-31G (d, p) level of theory for **P1, P2, 1,** and **2**.

Table S6: Important absorption, and emission parameters along with lifetime and photoluminescence quantum yield (PLQY) data for **1** and **2** in different solvents (conc. 10^{-5} M).

	Solvent	λ_{abs} [nm] (ϵ) [mol^{-1} L cm^{-1}]	λ_{em} [nm]	PL lifetime [ns] λ_{ex} = 375 nm		PLQY [%]
				τ_1 (A_1 in %)	τ_2 (A_2 in %)	
1	Hexane	320 (12000) 370 (23000)	423	0.44 (86.54)	2.66 (13.46)	6.9
	Toluene	323 (12000) 376 (26000)	455	3.89 (100)		44.4
	DCM	320 (10000) 375 (19000)	504	9.36 (100)	-	49.2
	THF	316 (7000) 376 (13000)	510	9.31 (100)	-	50.5
	DMSO	320 (6000) 379 (14000)	558	10.01 (100)		33.2
2	Hexane	297 (14000) 380 (26000)	412	2.94 (100)	-	71.6
			430	2.93 (100)	-	
	Toluene	301 (15000) 392 (27000)	440	3.27 (100)		82.9
	DCM	301 (12000) 392 (24000)	459	3.46 (100)		94.4
	THF	301 (13000) 393 (24000)	467	3.81 (100)		92.3
	DMSO	303 (10000) 401 (18000)	499	4.41 (100)		86.7

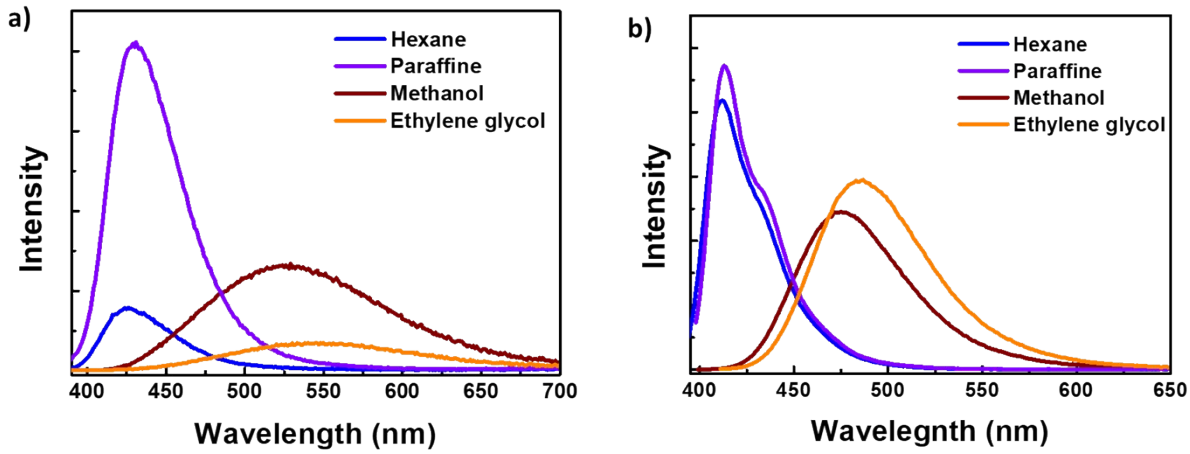

Figure S23. PL spectra of (a) **1** and (b) **2** in different viscous solvents [Hexane: nonpolar; non-viscous, Paraffine; nonpolar; viscous, Methanol; polar; non-viscous, and ethylene glycol; polar; viscous] at λ_{ex}= 380 nm.

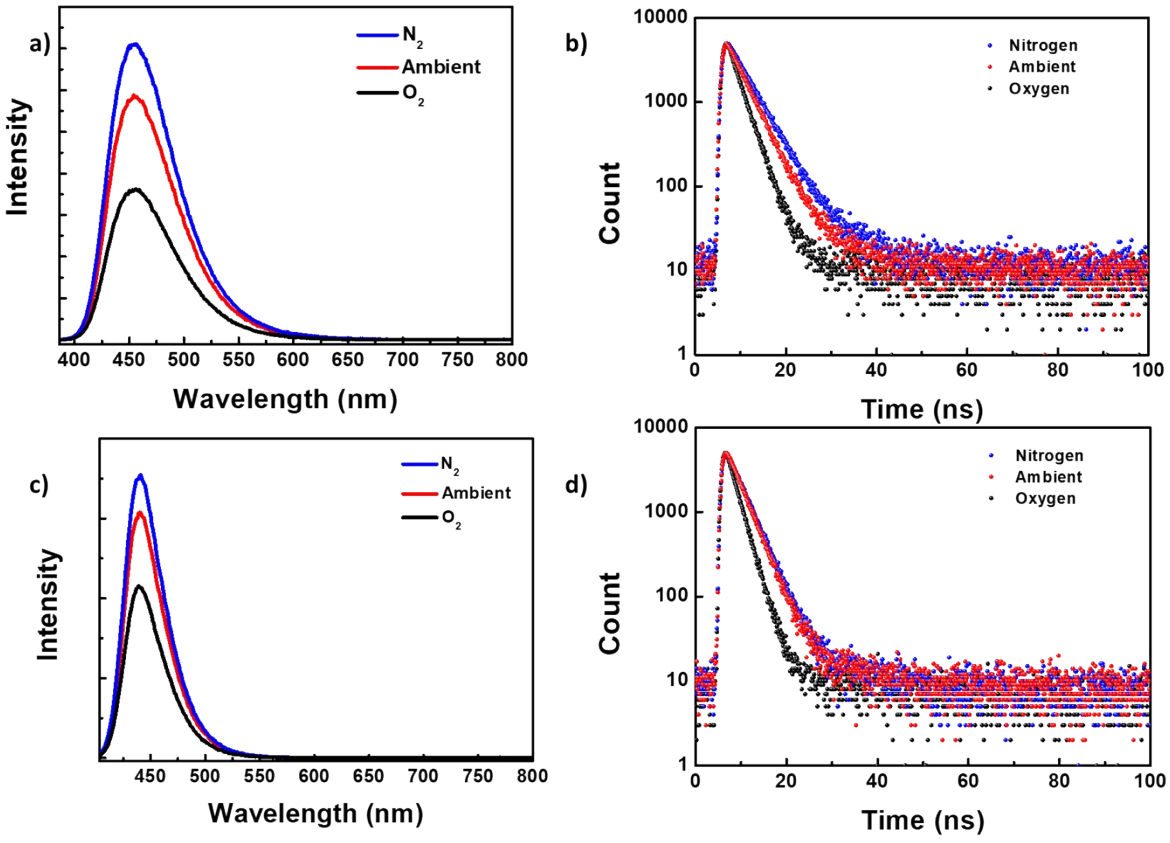

Figure S24. (a, c) PL spectra at λ_{ex}= 380 nm and (b, d) fluorescence decay for **1** (a,b) and **2** (c, d) in degassed toluene (conc. 10^{-5} M) under nitrogen, ambient, and oxygen atmospheric at λ_{ex}= 380 nm and λ_{em}= 455 nm (**1**), 440 nm (**2**).

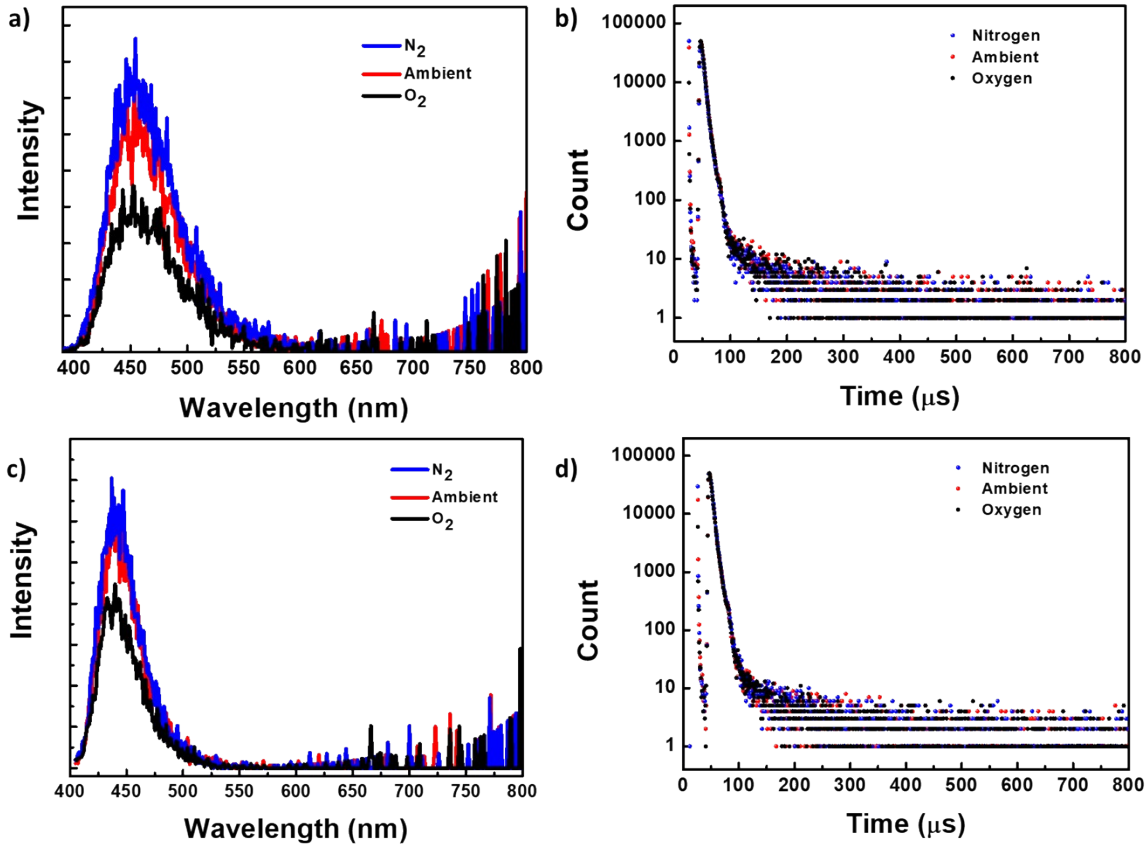

Figure S25. (a, c) Time-gated (delayed) (20 μs delay) PL spectra at λ_{ex}= 380 nm and (b, d) delayed fluorescence decay for **1** (a, b) and **2** (c, d) in degassed toluene (conc. 10^{-5} M) under nitrogen, ambient, and oxygen atmospheric at λ_{ex}= 380 nm and λ_{em}= 455 nm (**1**), 440 nm (**2**).

Supplementary information

The equation for Calculating Rate constance[7]

$$k_r^{PF} = \frac{\phi_{PF}}{\tau_{PF}}$$

$$k_r^{DF} = \frac{\phi_{DF}}{\tau_{DF}}$$

$$k_{Total}^{PF} = \frac{1}{\tau_{PF}}$$

$$k_{Total}^{DF} = \frac{1}{\tau_{DF}}$$

$$k_{nr}^{ISC} = \frac{\phi_{DF}\, k_{Total}^{PF}}{\phi_{total}}$$

$$k_{nr}^{rISC} = \frac{\phi_{DF}\, k_{Total}^{PF}\, k_{Total}^{DF}}{k_{nr}^{ISC}\, \phi_{PF}}$$

$$k_{nr}^{S} = \frac{1}{\tau_{PF}} - (k_r^{PF} + k_{nr}^{ISC})$$

$k_{Total}^{PF} = Total\ deacy\ Rate\ of\ \ prompt\ component$

$k_{Total}^{DF} = Total\ decay\ rate\ of\ \ delayed\ component$

$k_r^{PF} = Radiative\ decay\ rate\ of\ \ prompt\ component$

$k_r^{DF} = Radiative\ decay\ rate\ of\ \ delayed\ component$

$k_{nr}^{ISC} = Rate\ of\ \ intersystem\ crossing$

$k_{nr}^{rISC} = Rate\ of\ \ reverse\ intersystem\ crossing$

$k_{nr}^{S} = Non\ radiative\ decay\ rate\ \ from\ S_1$

$\tau_{PF} = Lifetime\ of\ \ Prompt\ component$

$\tau_{DF} = Lifetime\ of\ \ Prompt\ component$

$\phi_{total} = Total\ photoluminscence\ quantum\ yield$

$\phi_{PF} = Prompt\ \ fluorescence\ quantum\ yield$

$\phi_{DF} = Deleyed\ \ fluorescence\ quantum\ yield$

Table S7. Fluorescence, delayed fluorescence lifetime, and total PLQY for **1** and **2** in toluene (conc. 10^{-5} M) under nitrogen, ambient, and oxygen atmospheric conditions.

Environment	λ_{ex}(nm)	λ_{em}(nm)	Fluorescence lifetime (ns)	Delayed fluorescence (µs)		PLQY [%]
			τ_1 (%)	τ_1 (A_1 in %)	τ_2 (A_2 in %)	
1						
Nitrogen	375	455	4.57 (100)	4.03 (80.53)	10.18 (19.47)	47.9
Ambient	375	455	3.89 (100)	4.07 (84.21)	11.06 (15.79)	44.3
Oxygen	375	455	2.66 (100)	4.00 (80.56)	9.97 (19.44)	24.0
2						
Nitrogen	395	440	3.52 (100)	4.15 (77.37)	10.05 (22.63)	93.4
Ambient	395	440	3.27 (100)	4.16 (79.95)	9.94 (20.05)	82.9
Oxygen	395	440	2.29 (100)	3.91 (72.71)	9.52 (27.29)	53.3

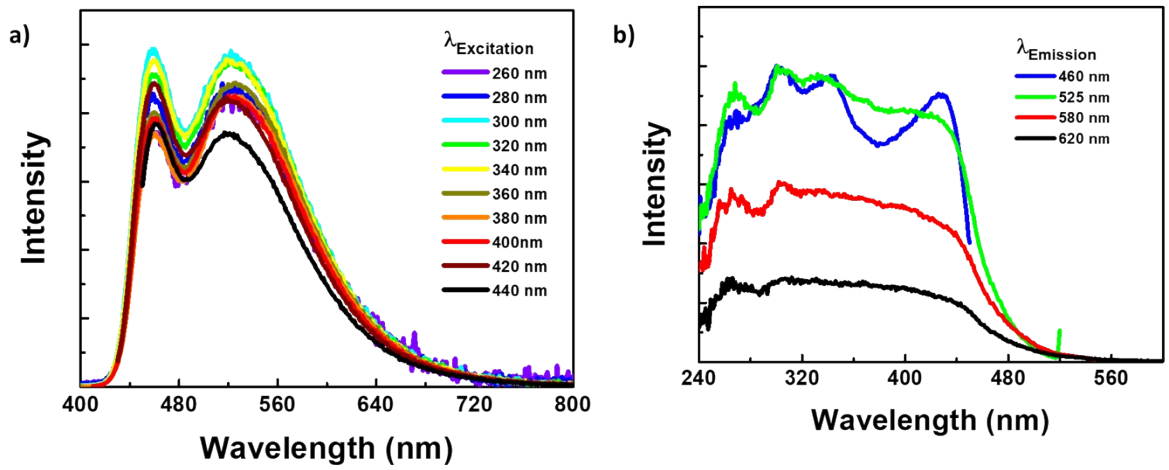

Figure S26. (a) PL spectra at different excitation (b) excitation spectra at different emission wavelengths for **1** (as prepared solid) at 298K under ambient conditions.

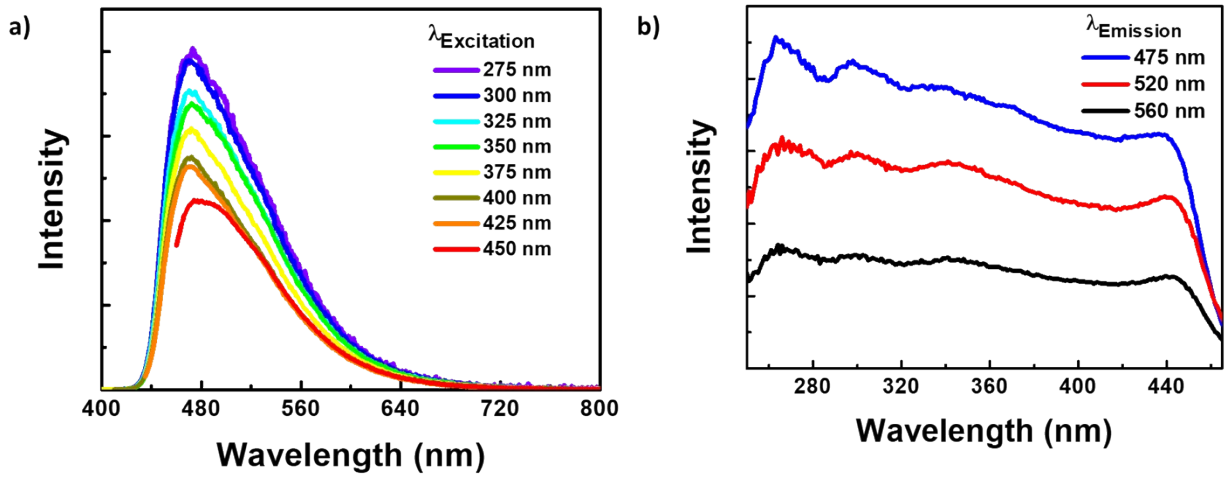

Figure S27. (a) PL spectra at different excitation (b) excitation spectra at different emission wavelengths for **2** (as prepared crystals) at 298K under ambient conditions.

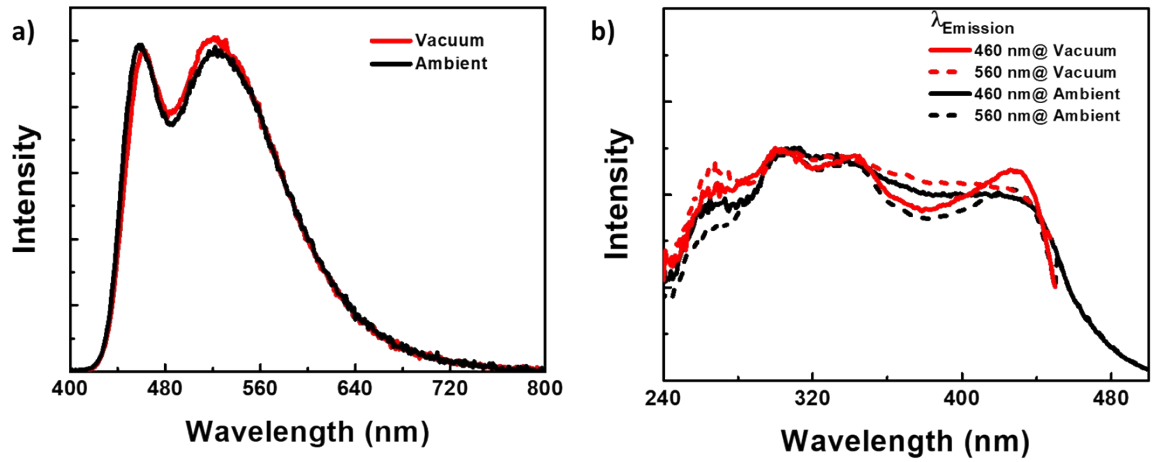

Figure S28. (a) PL spectra at λ_{ex} = 380 nm (b) excitation spectra at different emission wavelength for **1** (as prepared crystals) at 298K under vacuum (absence of oxygen) and ambient conditions (presence of oxygen).

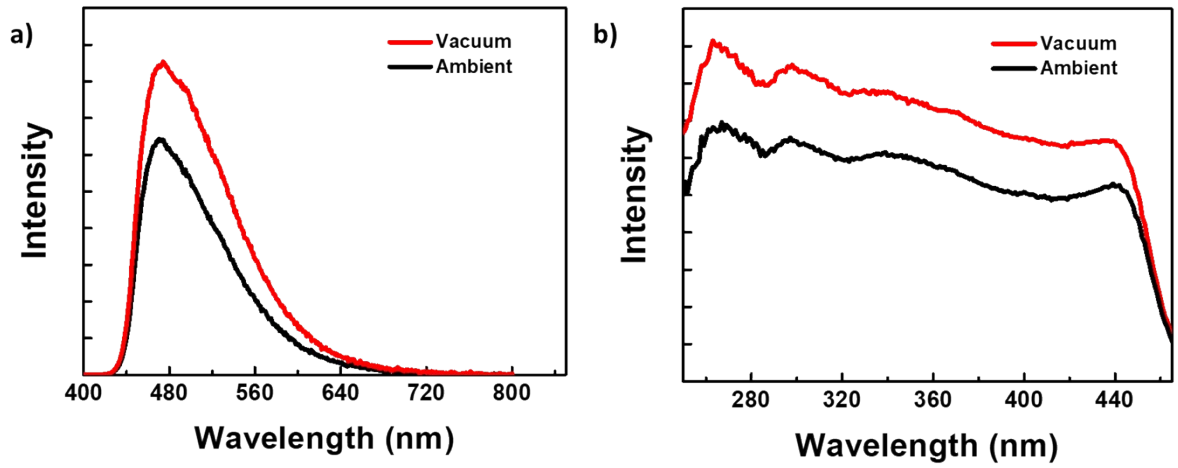

Figure S29. (a) PL spectra at λ_{ex} = 380 nm (b) excitation spectra at λ_{em} = 475 nm for **2** (as prepared solid) at 298K under vacuum (absence of oxygen) and ambient conditions (presence of oxygen).

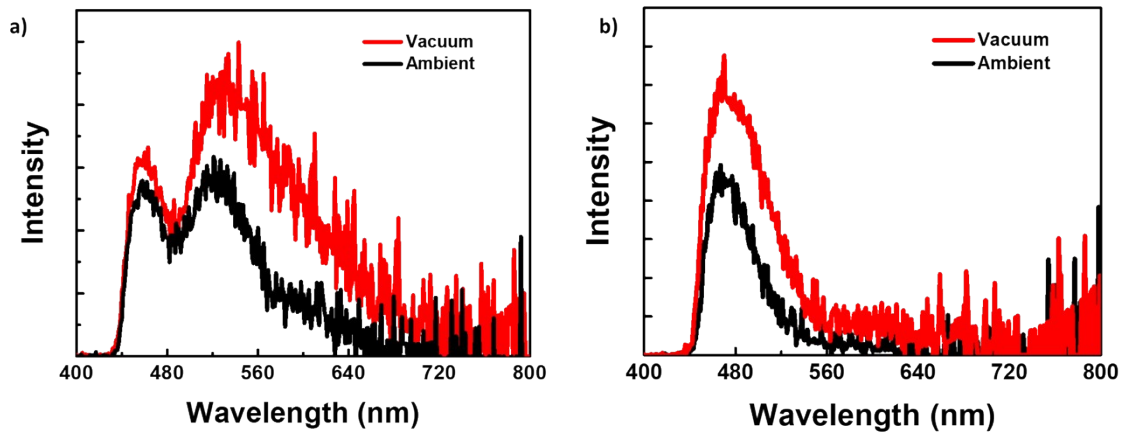

Figure S30. (a) Time-gated PL spectra (50 µs delay) at λ_{ex} = 380 nm for (a) **1** and (b) **2** (as prepared crystals) at 298K under vacuum (absence of oxygen) and ambient conditions (presence of oxygen).

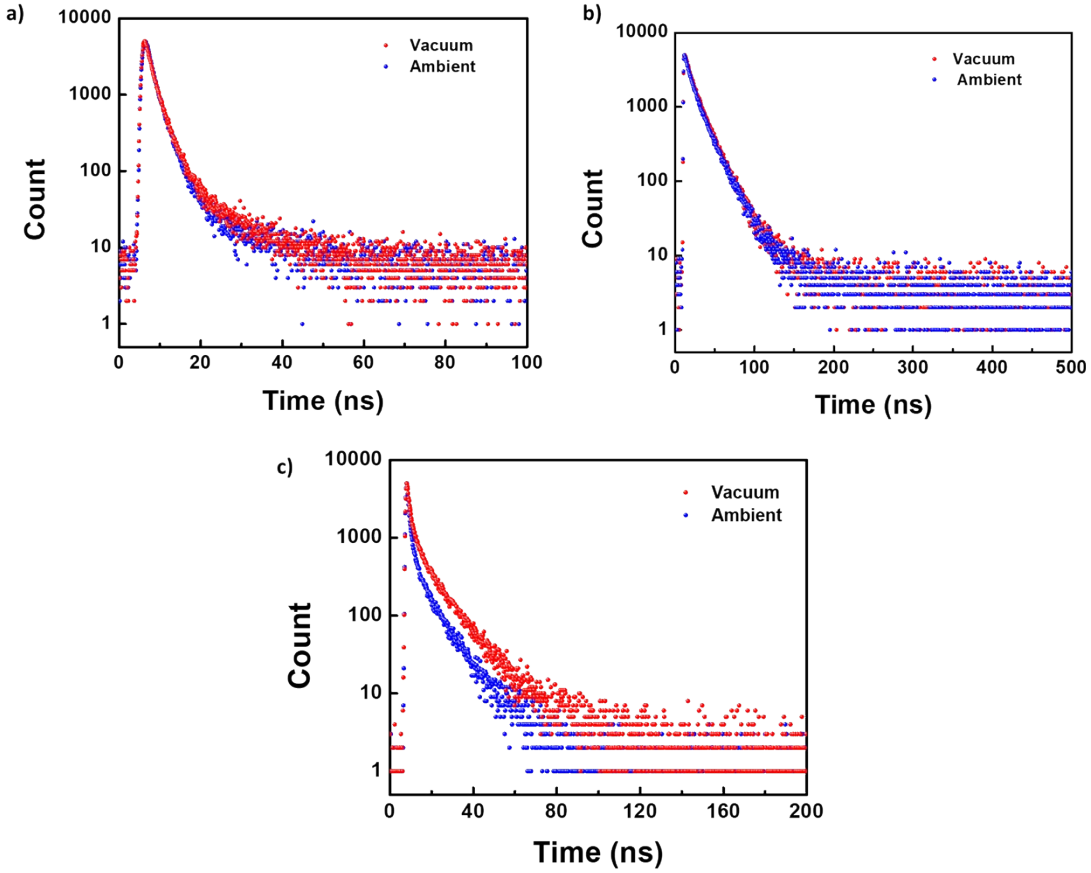

Figure S31. Fluorescence lifetime decay at λ_{ex} = 375 nm for **1** (a) λ_{em} = 460 nm (b) λ_{em} = 520 nm (c) fluorescence lifetime decay for **2** at λ_{ex} = 375 nm, λ_{em} = 475 nm] (as prepared solid) at 298K under vacuum (absence of oxygen) and ambient conditions (presence of oxygen).

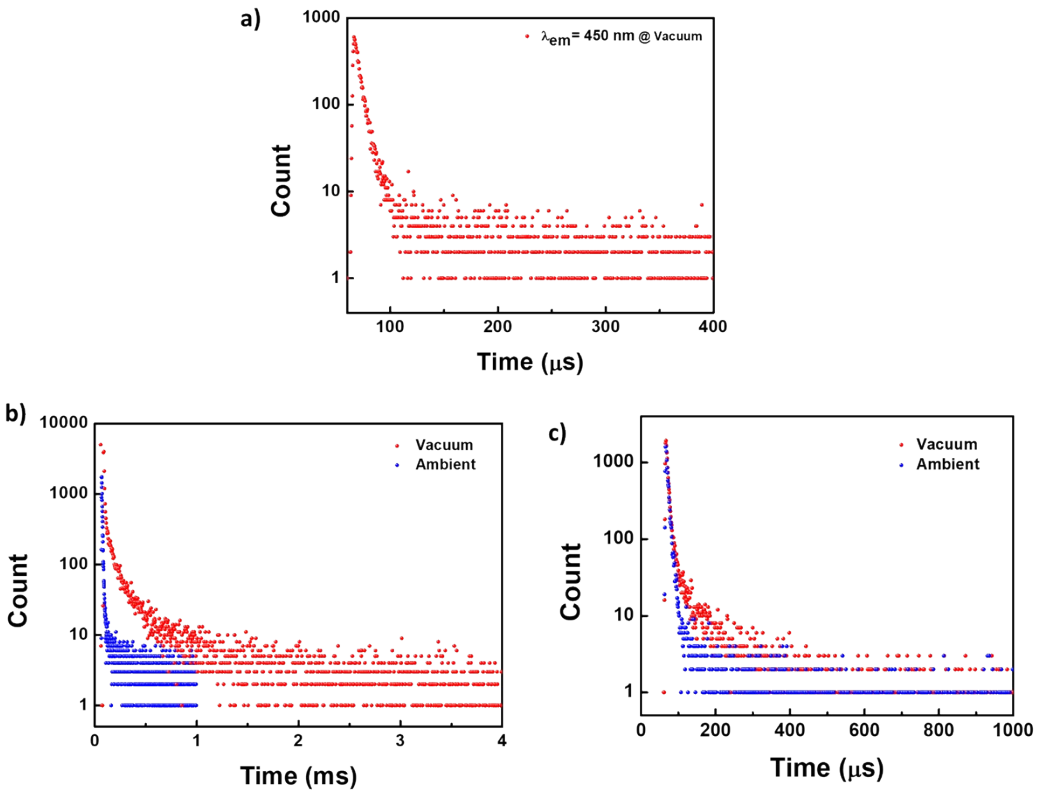

Figure S32. Delayed fluorescence lifetime decay for **1** (a) λ_{ex} =300 nm, λ_{em} = 460 nm at 298 K under vacuum (b) λ_{ex} =300 nm, λ_{em} = 520 nm at 298K under vacuum (absence of oxygen) and ambient conditions (presence of oxygen) (c) delayed fluorescence lifetime decay for **2** [λ_{ex} =300 nm, λ_{em} = 475 nm] (as prepared crystals) at 298K under vacuum (absence of oxygen) and ambient conditions (presence of oxygen).

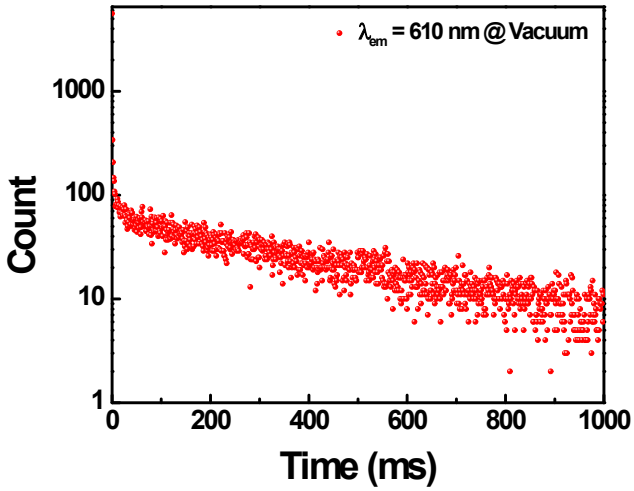

Figure S33. Phosphorescence decay for **2** [λ_{ex} = 300 nm, λ_{em} = 610 nm], at 298K under vacuum (absence of oxygen) and ambient conditions.

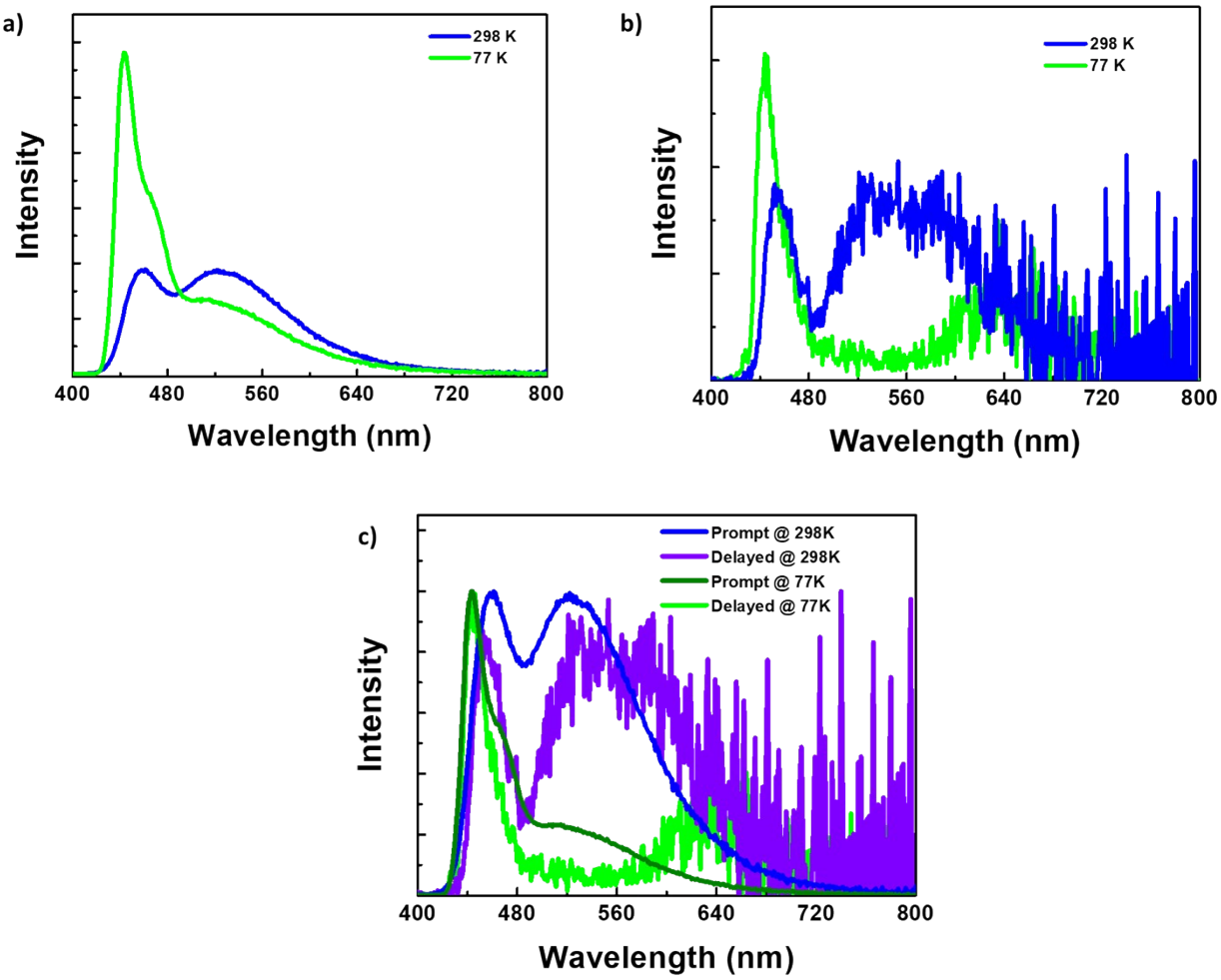

Figure S34. (a) Fluorescence spectra (b) time-gated spectra [50 μs delay] (c) normalized fluorescence and delayed spectra [50 μs delay] under vacuum atmosphere at 298 K and 77 K for **1** upon λ_{ex} = 380 nm.

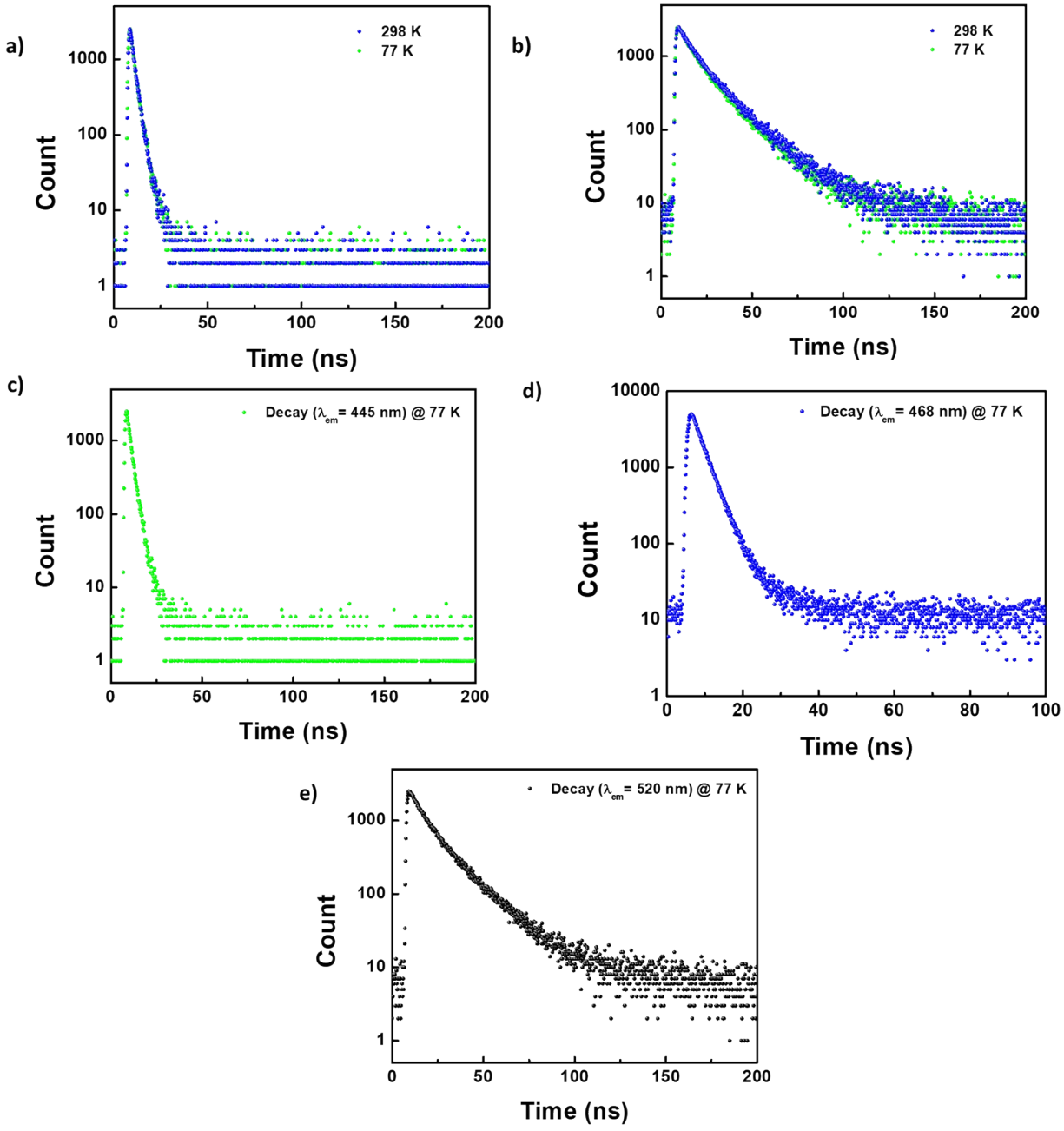

Figure S35. (a, b) Fluorescence lifetime decay under vacuum at 298 K and 77 K for **1** upon λ_{ex} = 375 nm, λ_{em} = 450 nm, and λ_{em} = 520 nm respectively. (c,d,e) fluorescence lifetime decay under vacuum at 77 K for **1** upon λ_{ex} = 375 nm, λ_{em} = 445 nm, λ_{em} = 468 nm, and λ_{em} = 520 nm respectively.

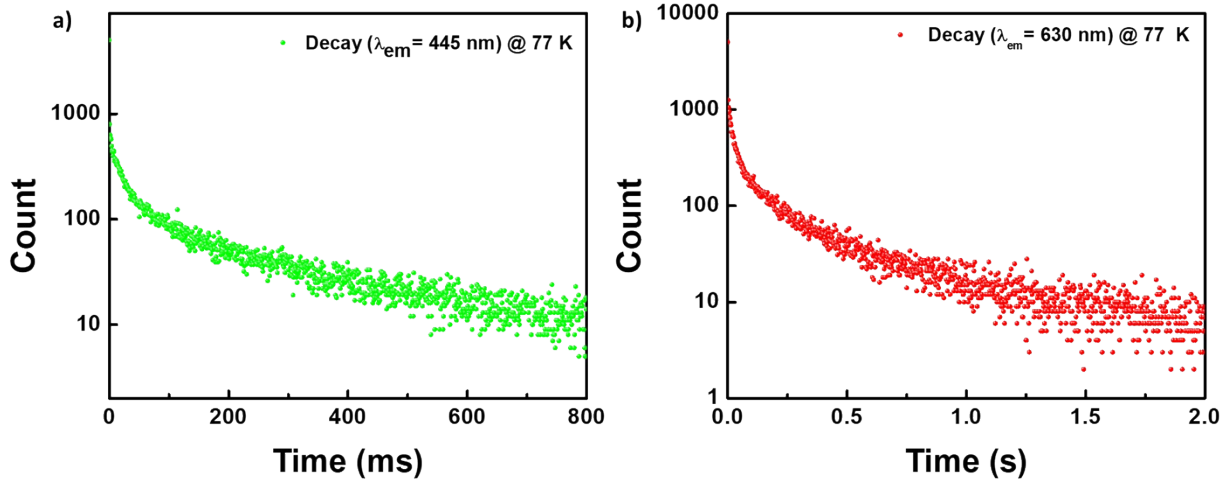

Figure S36. (a) Delayed Fluorescence decay [λ_{em} = 445 nm] (b) phosphorescence [λ_{em} = 620] decay under vacuum at 77 K for **1** upon λ_{ex} = 300 nm.

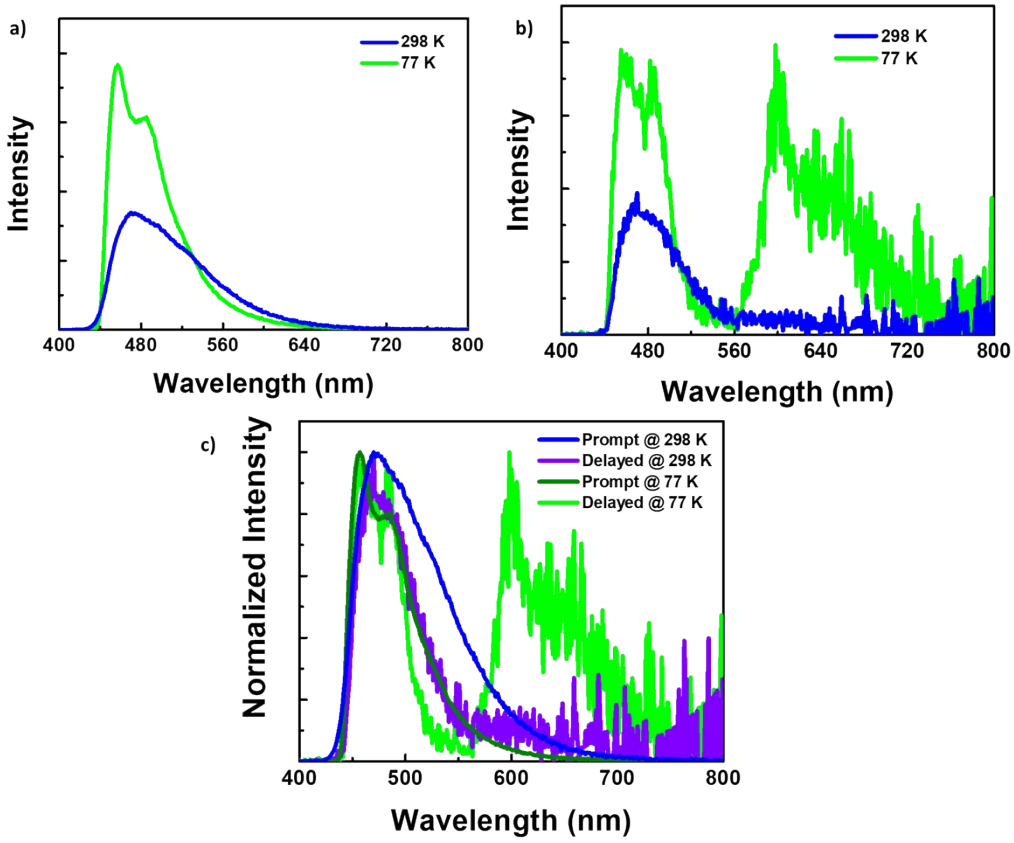

Figure S37. (a) Fluorescence spectra (b) time-gated spectra [50 μs delay] (c) normalized fluorescence and delayed spectra [50 μs delay] under vacuum atmosphere at 298 K and 77 K for **2** upon λ_{ex} = 380 nm.

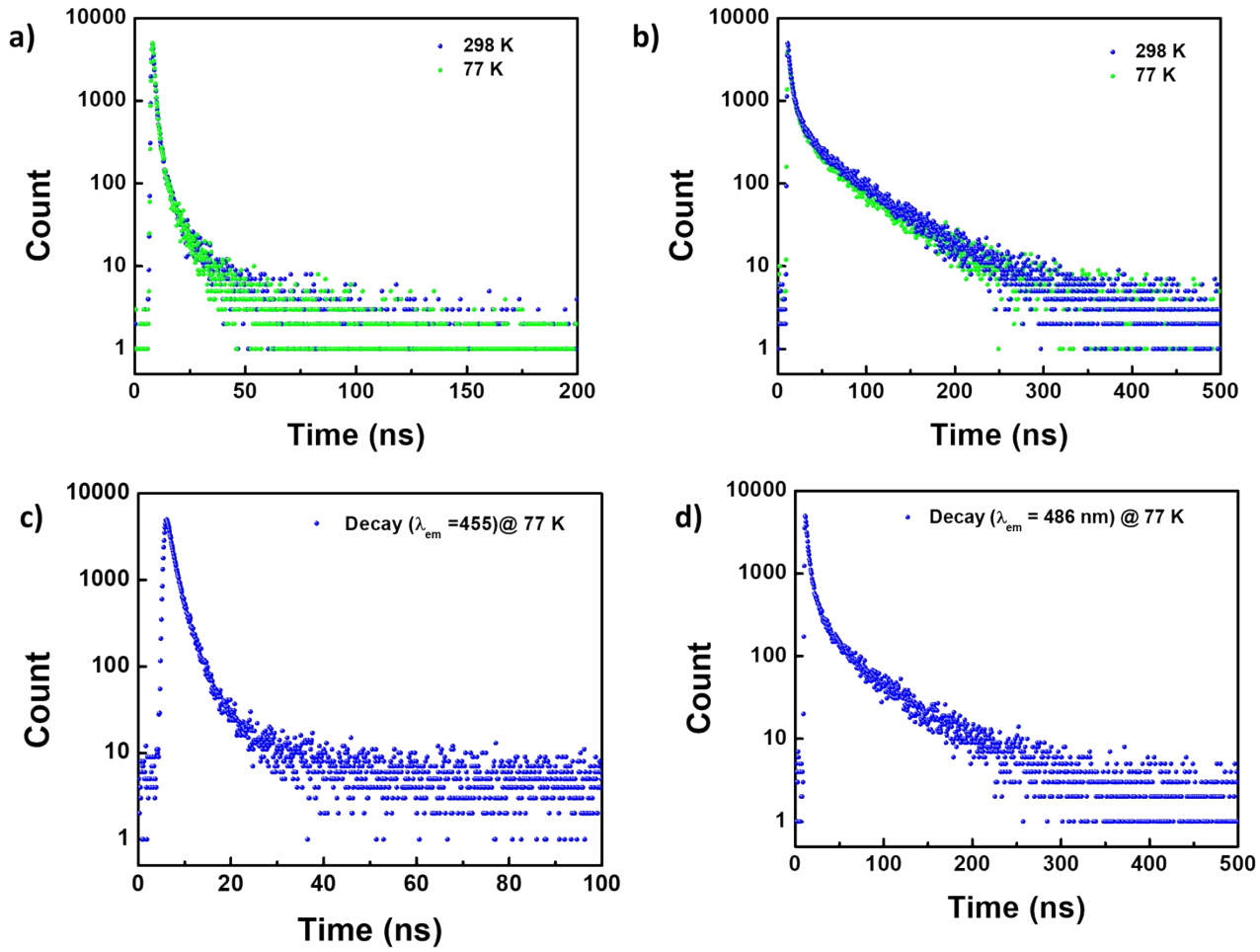

Figure S38. (a, b) Fluorescence lifetime decay under vacuum at 298 K and 77 K for **2** upon λ_{ex} = 375 nm, λ_{em} = 475 nm, and λ_{em} = 520 nm respectively. (c,d) fluorescence lifetime decay under vacuum at 77 K for **2** upon λ_{ex} = 375 nm, λ_{em} = 455 nm, and λ_{em} = 486 nm, respectively.

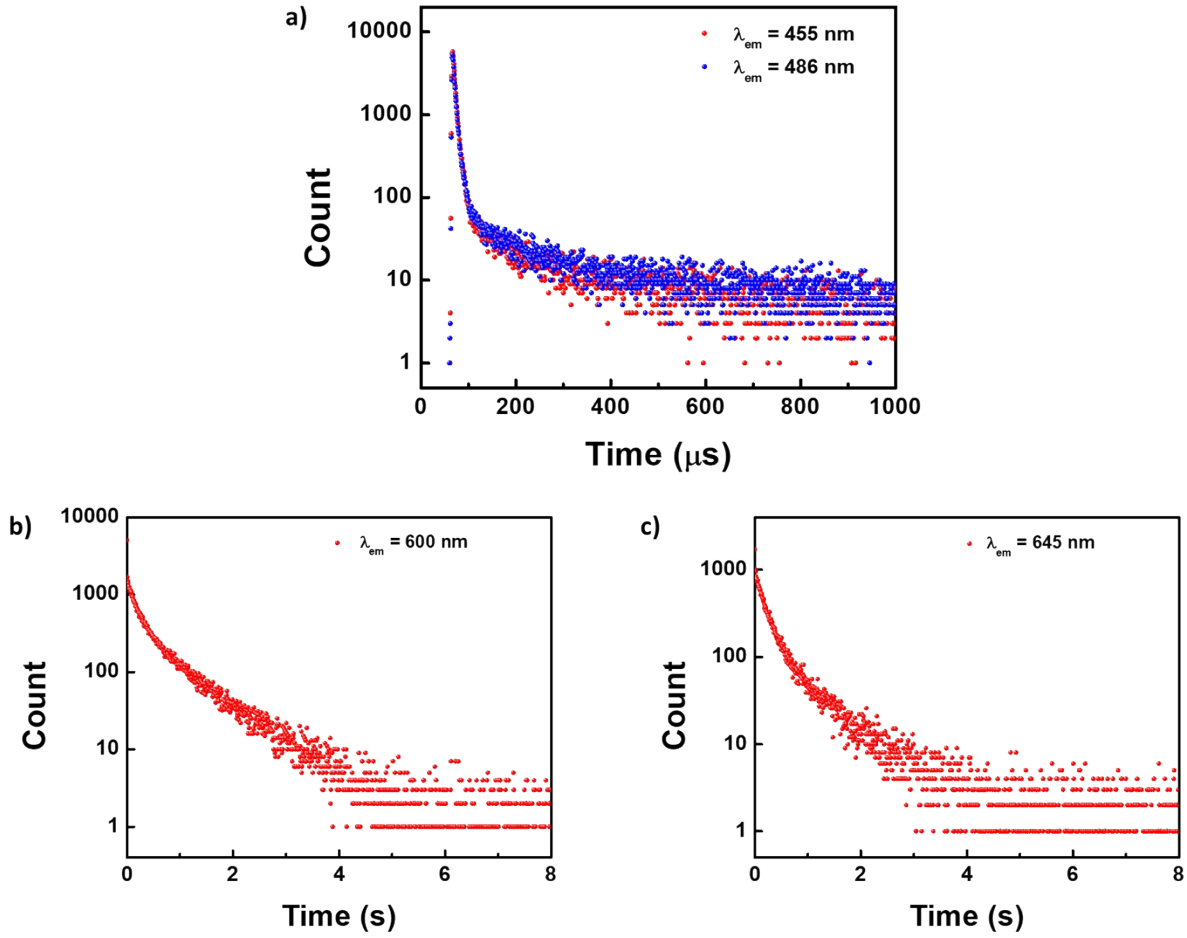

Figure S39. (a) Delayed Fluorescence decay at [λ_{em} = 455 nm and 486 nm] (b,c) phosphorescence decay [λ_{em} = 600 nm and 645 nm] under vacuum at 77 K for **2** upon λ_{ex} = 300 nm.

Table S8: Fluorescence lifetime for **1** and **2** under different atmospheric conditions and different temperatures along with total PLQY under ambient conditions at 298 K.

	Fluorescence lifetime (ns)												PLQY [%]
	77 K (Vacuum)				298 K (Vacuum)				298 K (Ambient)				
	λ_{ex} (nm)	λ_{em} (nm)	τ_1 (A_1 %) (ns)	τ_2 (A_2 %) (ns)	λ_{ex} (nm)	λ_{em} (nm)	τ_1 (A_1 %) (ns)	τ_2 (A_2 %) (ns)	λ_{ex} (nm)	λ_{em} (nm)	τ_1 (A_1 %) (ns)	τ_2 (A_2 %) (ns)	
1													
Solid	375	445	2.52 (100)	-	-	-	-	-	-	-	-	-	39.2
	375	450	2.45 (100)	-	375	450	2.03 (83.95)	9.14 (16.05)	375	450	2.09 (83.99)	10.01 (16.01)	
	375	468	3.08 (95.28)	11.02 (4.72)	-	-	-	-	-	-	-	-	
	375	520	7.74 (42.13)	19.74 (57.87)	375	520	10.02 (45.12)	21.95 (54.88)	375	520	9.39 (44.63)	21.91 (55.37)	
2													
Solid	375	455	1.51 (74.86)	5.43 (25.14)	-	-	-	-	-	-	-	-	56.2
	-	-	-	-	375	470	2.69 (29.89)	12.90 (70.11)	375	470	1.19 (54.25)	9.76 (45.75)	
	375	486	7.16 (35.99)	52.64 (64.01)	375	-	-	-	-	-	-	-	
	375	520 (br Tail)	8.14 (36.66)	53.67 (63.34)	375	520	6.48 (45.83)	18.72 (54.17)	375	520	5.40 (43.05)	16.28 (56.95)	

Table S9: Delayed fluorescence and phosphorescence lifetime for **1** and **2** under different atmospheric conditions.

	Delayed fluorescence (μs)/Phosphorescence lifetime (ms)		
	77 K (Vacuum)	298 K (Vacuum)	298 K (Ambient)

Supplementary information

	λ_{ex} (nm)	λ_{em} (nm)	τ_1 (A_1 %)	τ_2 (A_2 %)	λ_{ex} (nm)	λ_{em} (nm)	τ_1 (A_1 %)	τ_2 (A_2 %)	λ_{ex} (nm)	λ_{em} (nm)	τ_1 (A_1 %)	τ_2 (A_2 %)
1												
Solid	300	445	21.73 µs (25.12)	202.98 µs (74.88)	-	-	-	-	-	-	-	-
	-	-	-	-	300	450	6.09 µs (93.24)	53.92 µs (6.76)	-	-	-	-
	-	-	-	-	300	520	64.44 µs (52.87)	365.87 µs (47.13)	300	520	5.63 µs (87.57)	91.99 µs (12.43)
	300	620	35.50 ms (27.74)	323.45 ms (72.26)	-	-	-	-	-	-	-	-
2												
Solid	300	455	6.09 µs (76.62)	125.26 µs (23.28)	-	-	-	-	-	-	-	-
	300	486	6.03 µs (72.71)	125.10 µs (27.29)	300	470	5.43 µs (71.49)	47.41 µs (28.51)	300	450	5.93 µs (100)	-
	300	600	172.67 ms (35.95)	840.03 ms (64.05)					-	-	-	-
	300	645	182.94 ms (49.59)	783.21 ms (50.41)	300	610	2.72 ms (3.92)	378.19 ms (96.08)	-	-	-	-

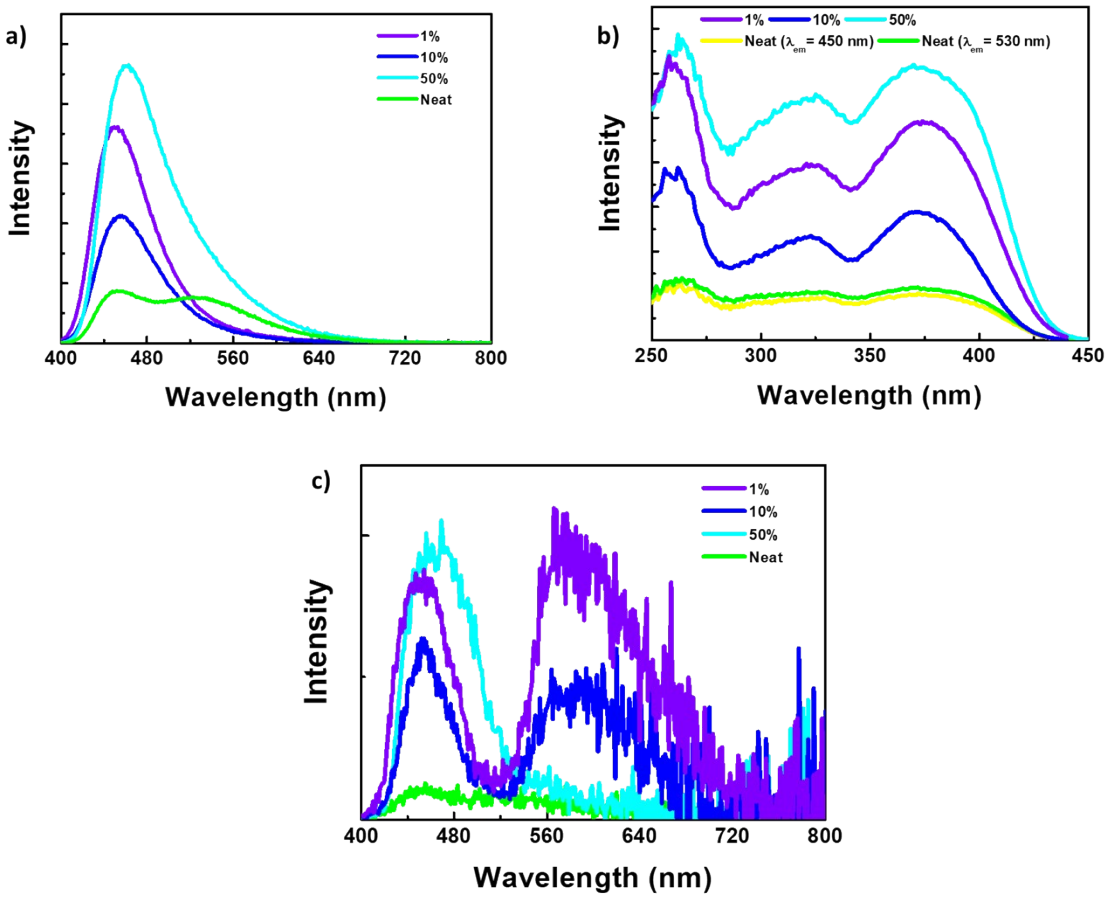

Figure S40. (a) Fluorescence spectra (b) excitation spectra corresponding to emission maxima (c) delayed fluorescence spectra [50 μs delay] under vacuum atmosphere at 298 K for **1** as neat film and doped film on PMMA matrix (λ_{ex} = 380 nm).

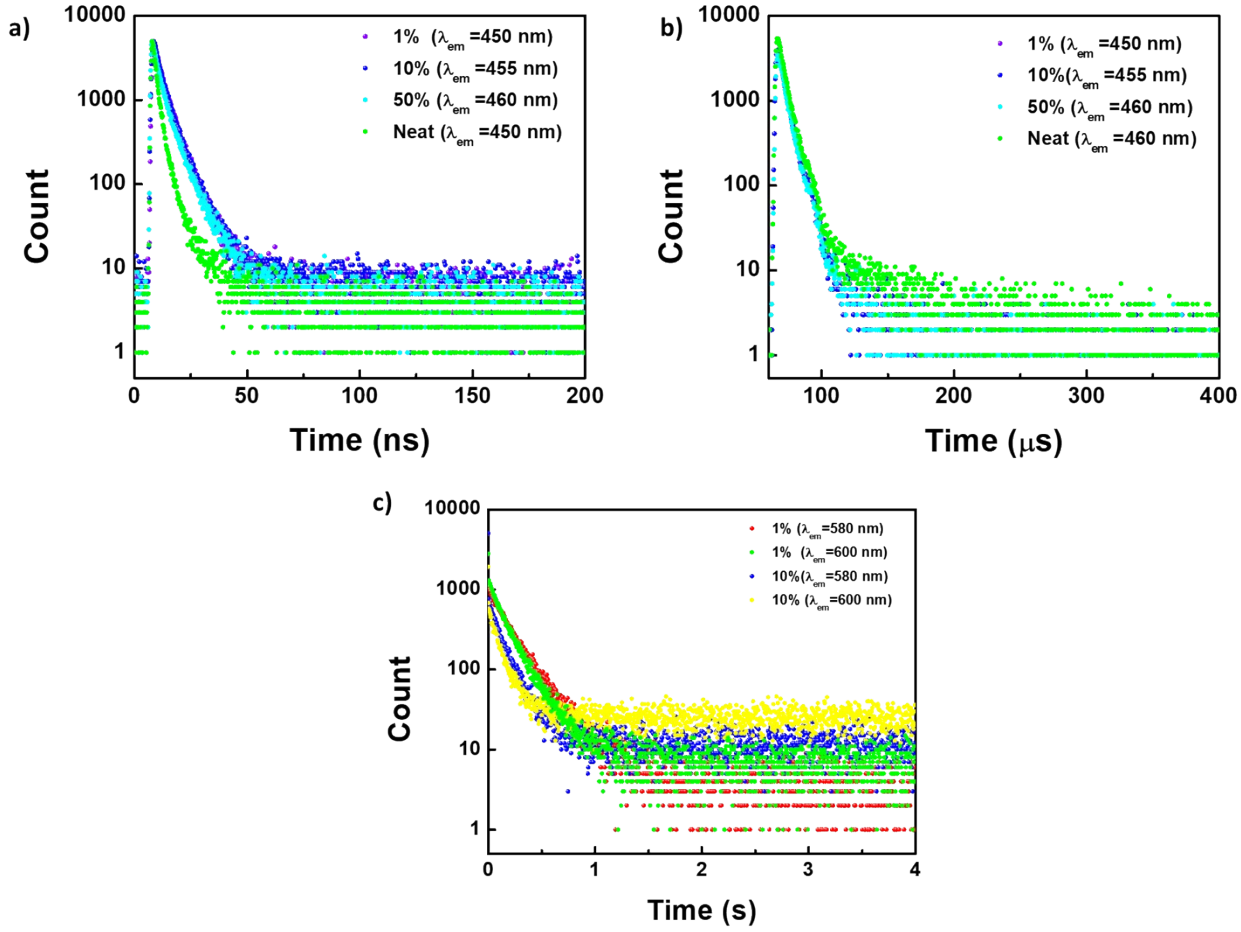

Figure S41. (a) Fluorescence lifetime deacy at λ_{ex} = 375 nm (b) delayed fluorescence lifetime decay at λ_{ex} = 375 nm for **1** as neat film and doped film on PMMA matrix at different wt% .(c) phosphorescence lifetime decay for **1** as doped film on PMMA matrix (1 wt%, 10 wt%) at λ_{ex} = 380 nm.

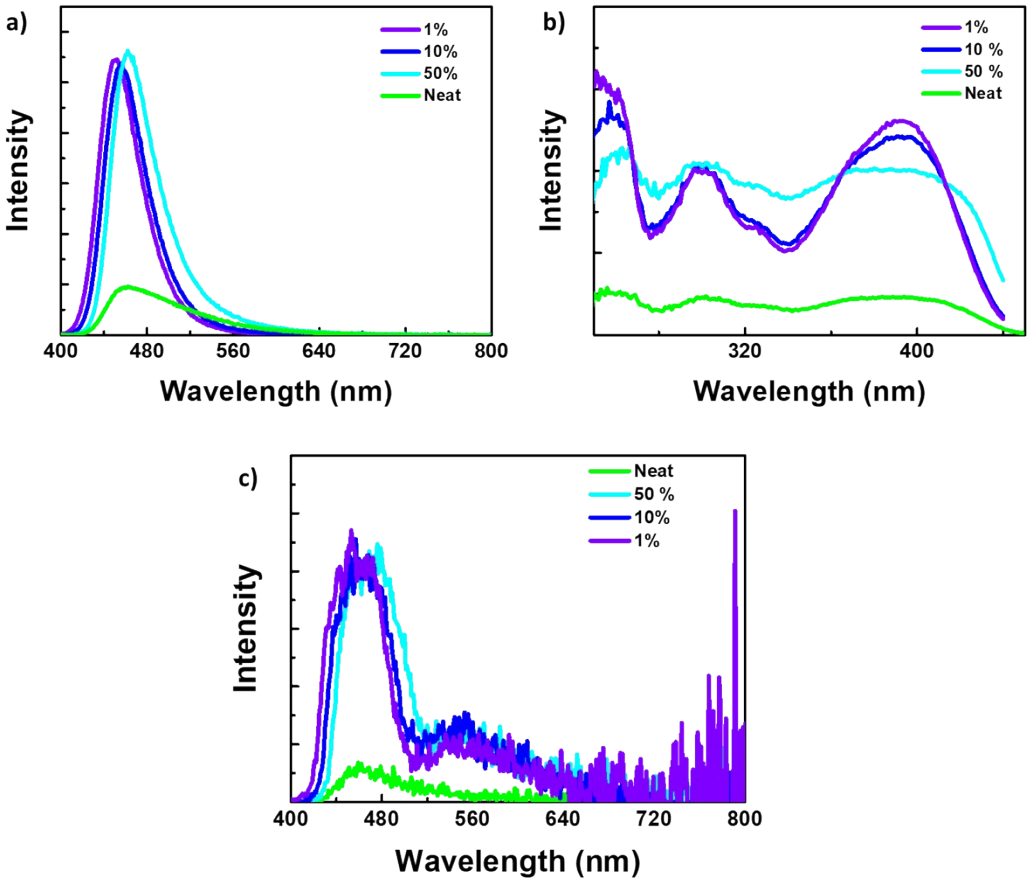

Figure S42. (a) Fluorescence spectra for **2** as doped film on PMMA matrix (λ_{ex} = 380 nm) (b) excitation spectra corresponding to emission maxima, (c) delayed fluorescence spectra [50 μs delay] under vacuum atmosphere at 298 K for **2** as neat film and doped film on PMMA matrix (λ_{ex} = 380 nm).

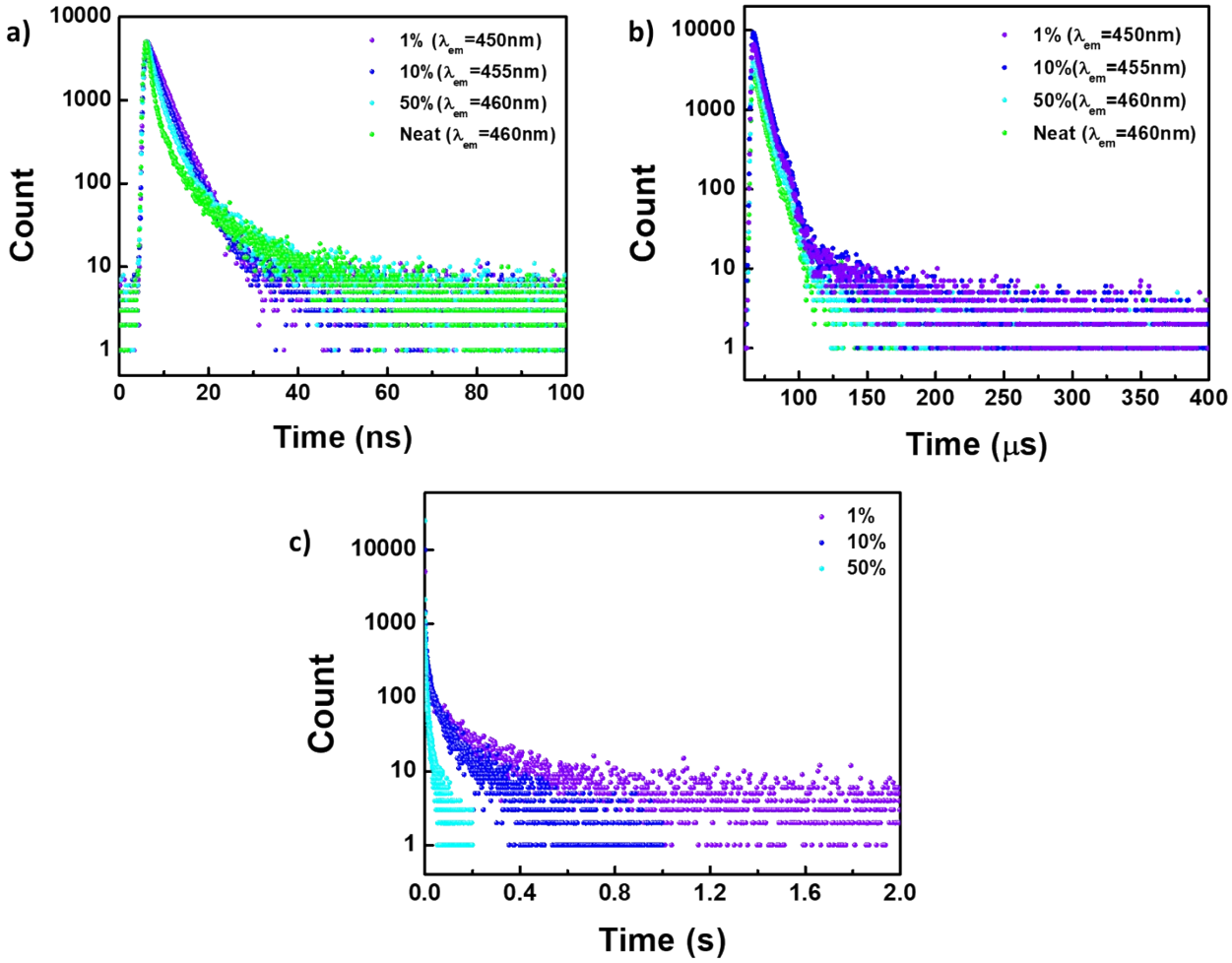

Figure S43. (a) Fluorescence lifetime deacy at λ_{ex} = 375 nm (b) delayed fluorescence lifetime decay at λ_{ex} = 375 nm for **2** as neat film and doped film on PMMA matrix at different wt%. (c) phosphorescence lifetime decay for **2** as doped film on PMMA matrix (1 wt%, 10 wt%, and 50 wt%) under vacuum atmosphere at 298 K upon λ_{ex} = 380 nm, λ_{em} = 540 nm.

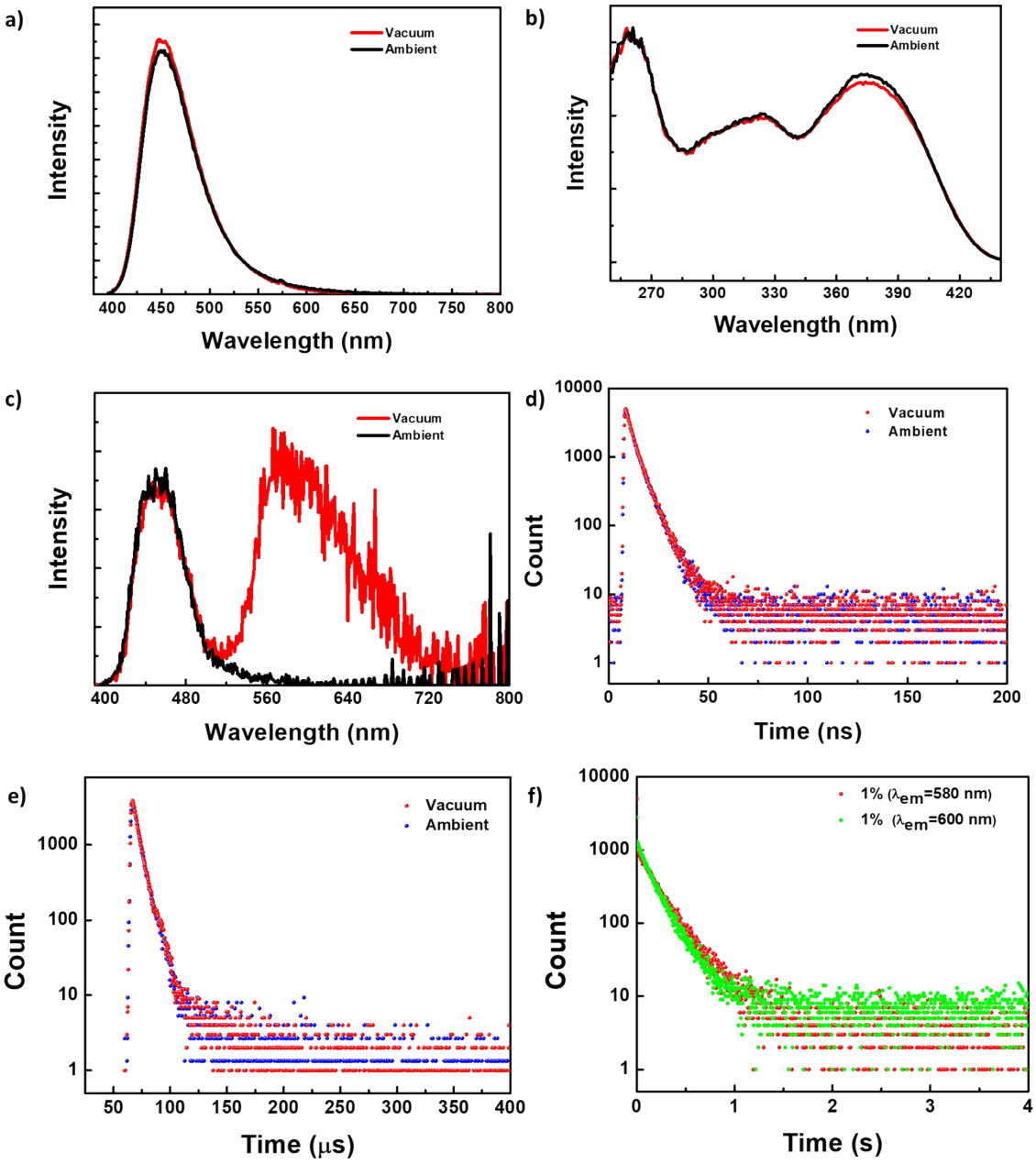

Figure S44. (a) Fluorescence spectra (b) excitation spectra corresponding to emission maxima (c) delayed fluorescence spectra [50 μs delay] (d) fluorescence lifetime decay [λ_{ex} = 375 nm and λ_{ex} = 450 nm], (e) delayed fluorescence lifetime decay [λ_{ex} = 380 nm and λ_{ex} = 450 nm] and phosphorescence lifetime decay [λ_{ex} = 375 nm and λ_{ex} = 580 nm, 600 nm] under vacuum [absence of oxygen] and ambient atmosphere [presence of oxygen] at 298 K for **1** doped in PMMA matrix (1 wt%) [λ_{ex} = 380 nm].

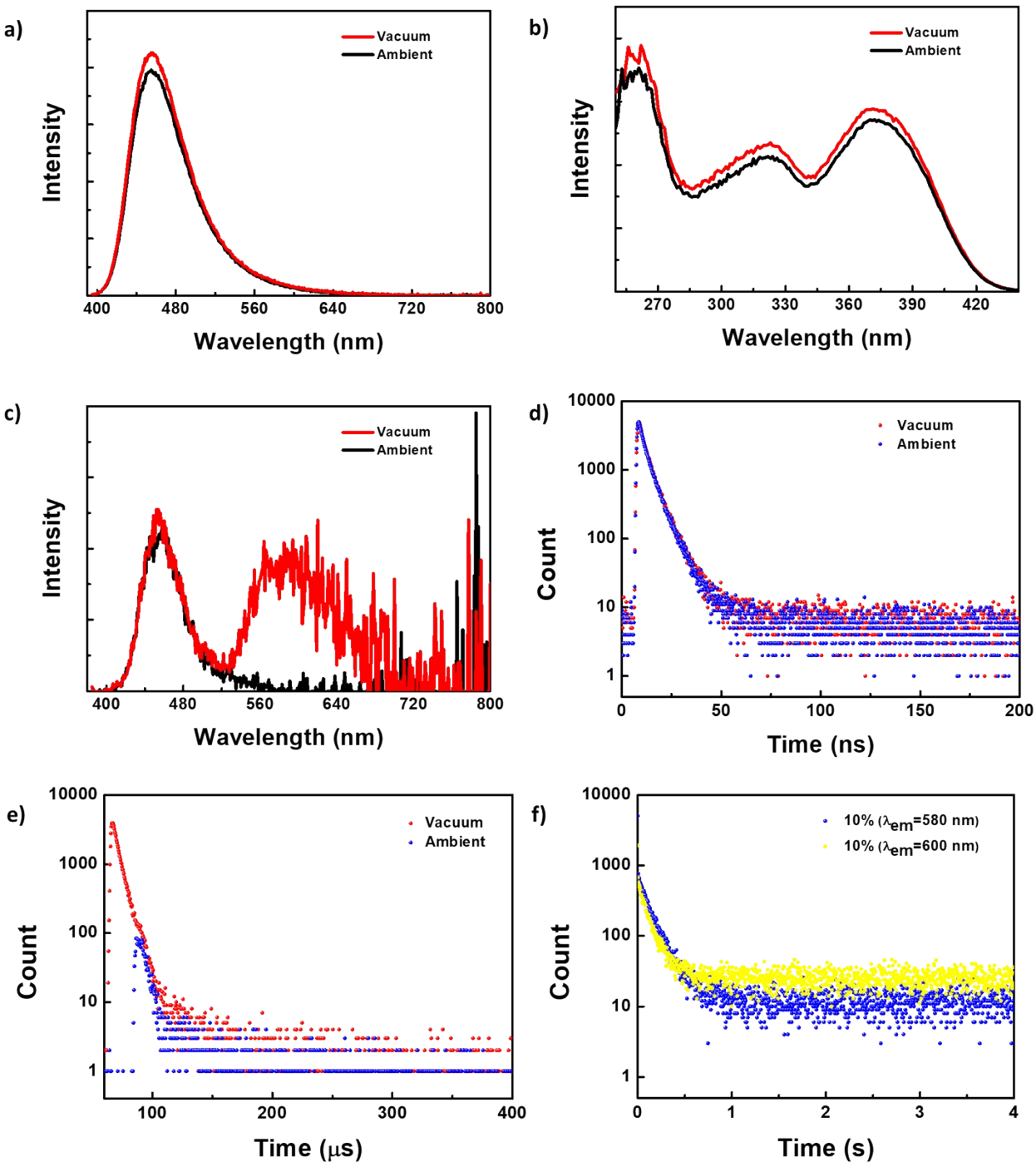

Figure S45. (a) Fluorescence spectra (b) excitation spectra corresponding to emission maxima (c) delayed fluorescence spectra [50 μs delay] (d) fluorescence lifetime decay [λ_{ex} = 375 nm and λ_{ex} = 455 nm] (e) delayed fluorescence lifetime decay [λ_{ex} = 380 nm and λ_{ex} = 455 nm] and (f) phosphorescence lifetime decay [λ_{ex} = 375 nm and λ_{ex} = 580 nm, 600 nm] under vacuum [absence of oxygen] and ambient atmosphere [presence of oxygen] at 298 K for **1** doped in PMMA matrix (10 wt%) [λ_{ex} = 380 nm].

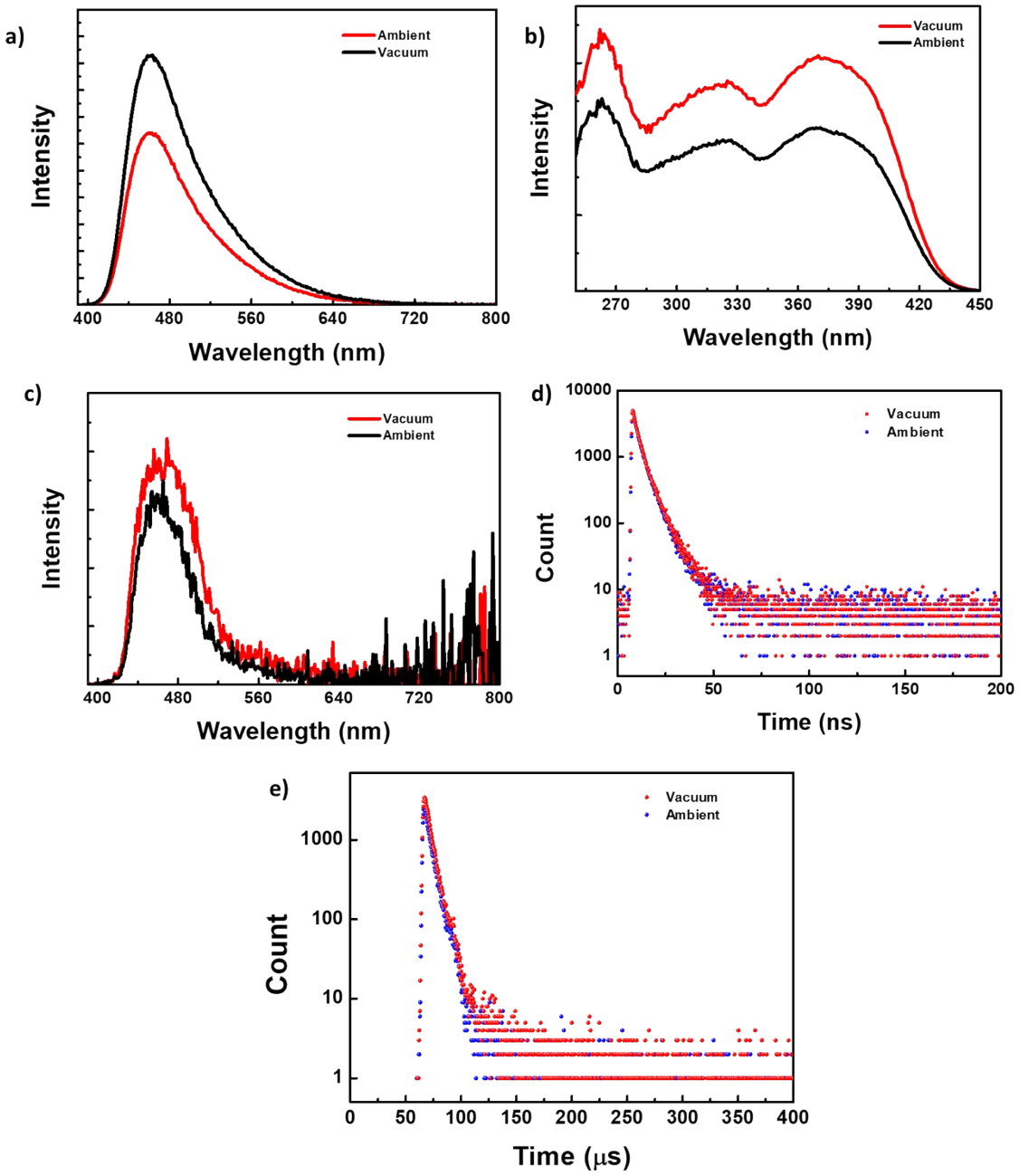

Figure S46. (a) Fluorescence spectra (b) excitation spectra corresponding to emission maxima (c) delayed fluorescence spectra [50 μs delay] (d) fluorescence lifetime decay [λ_{ex} = 375 nm and λ_{ex} = 460 nm] (e) delayed fluorescence lifetime decay [λ_{ex} = 380 nm and λ_{ex} = 460 nm] under vacuum [absence of oxygen] and ambient atmosphere [presence of oxygen] at 298 K for **1** doped in PMMA matrix (50 wt%) [λ_{ex} = 380 nm].

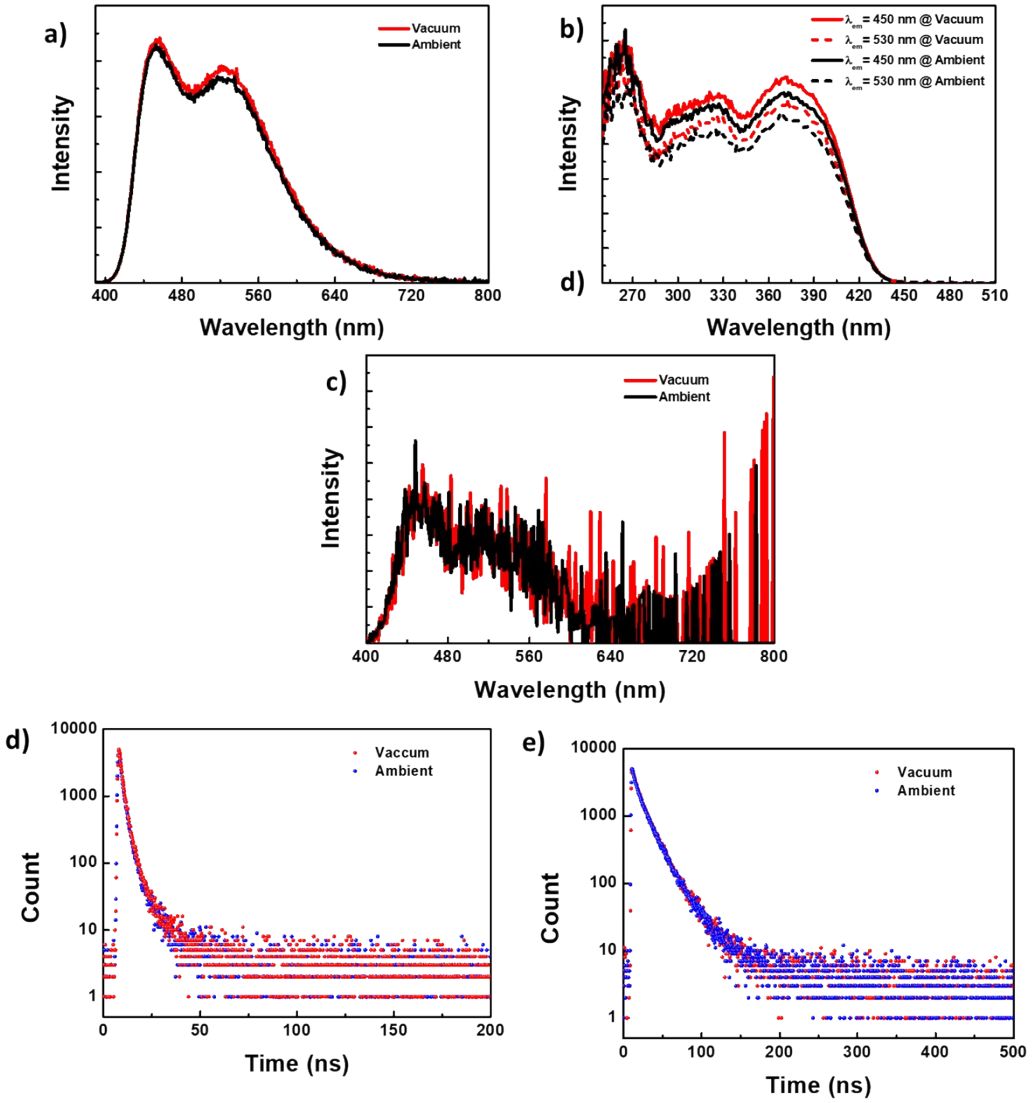

Figure S47. (a) Fluorescence spectra (b) excitation spectra corresponding to emission maxima, (c) delayed fluorescence spectra [50 μs delay] (d) fluorescence lifetime decay [λ_{ex} = 375 nm and λ_{ex} = 460 nm] (e) fluorescence lifetime decay [λ_{ex} = 375 nm and λ_{ex} = 530 nm] under vacuum [absence of oxygen] and ambient atmosphere [presence of oxygen] at 298 K for **1** as neat film [λ_{ex} = 380 nm]. Delayed fluorescence emission is weak in neat film, so we could not record the lifetime.

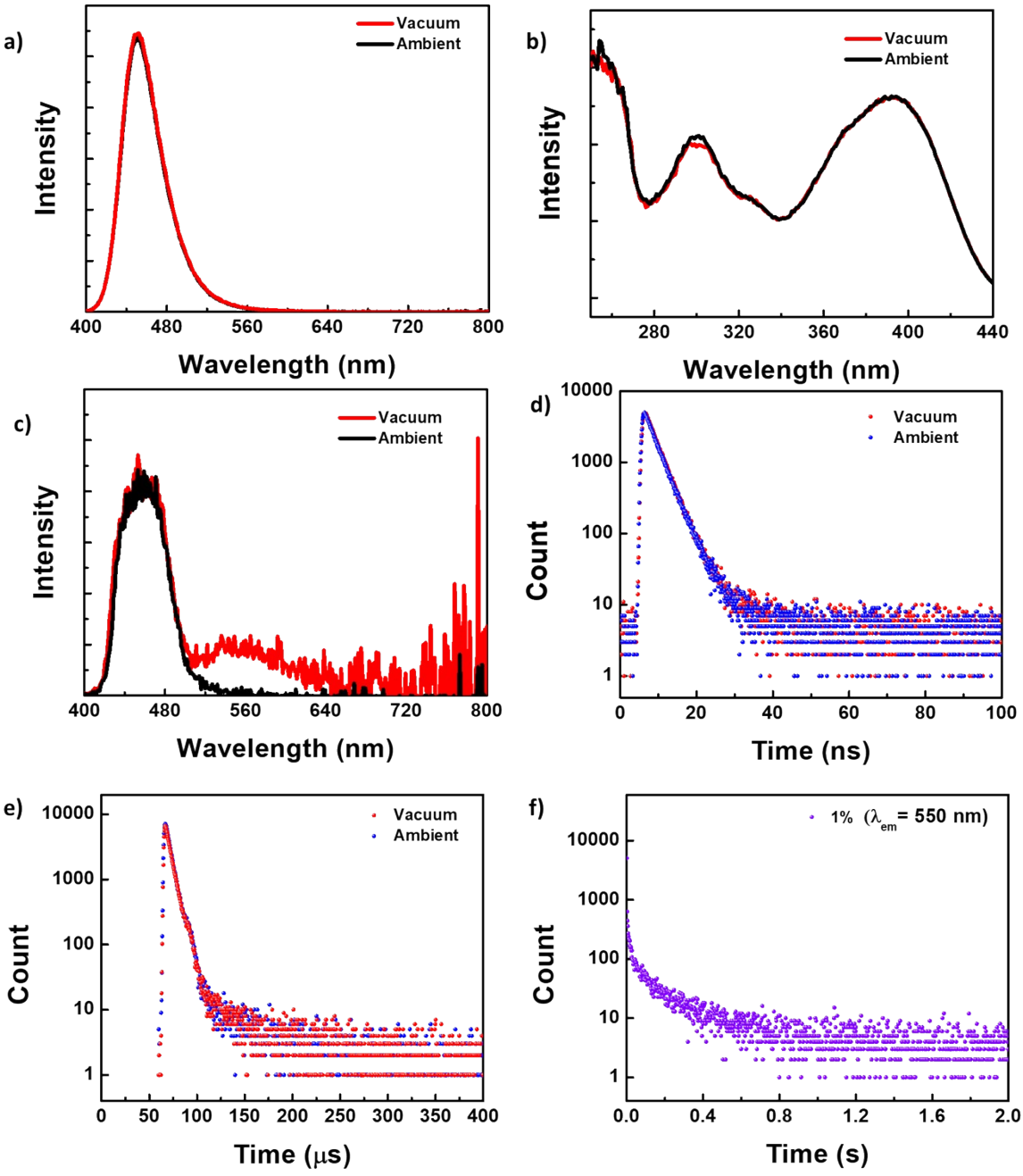

Figure S48. (a) Fluorescence spectra (b) excitation spectra corresponding to emission maxima (c) delayed fluorescence spectra [50 μs delay] (d) fluorescence lifetime decay [λ_{ex} = 375 nm and λ_{ex} = 450 nm] (e) delayed fluorescence lifetime decay [λ_{ex} = 380 nm and λ_{ex} = 450 nm] and phosphorescence lifetime decay [λ_{ex} = 380 nm and λ_{ex} = 550 nm] under vacuum [absence of oxygen] and ambient atmosphere [presence of oxygen] at 298 K for **2** doped in PMMA matrix (1 wt%) [λ_{ex} = 380 nm].

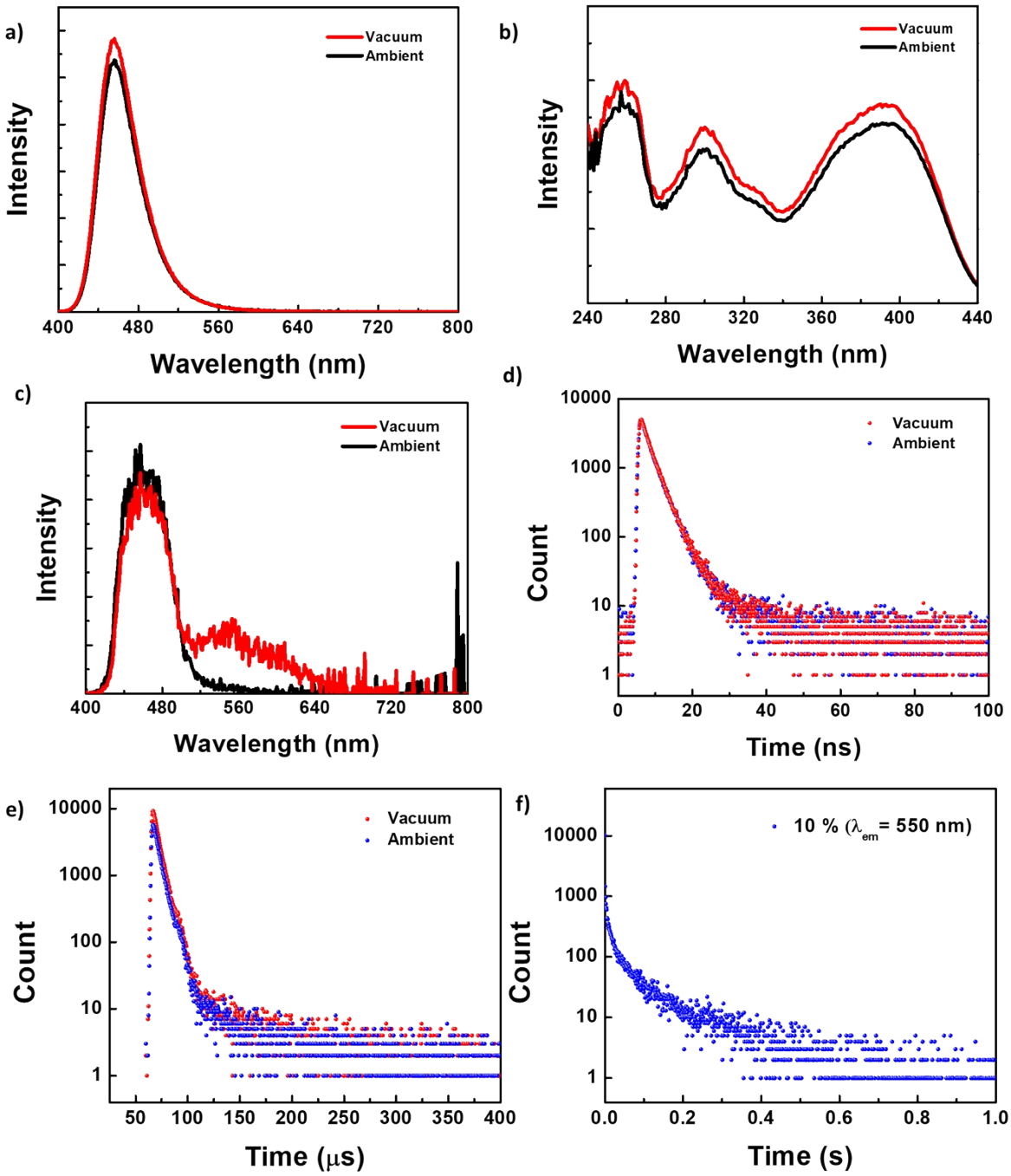

Figure S49. (a) Fluorescence spectra (b) excitation spectra corresponding to emission maxima (c) delayed fluorescence spectra [50 μs delay] (d) fluorescence lifetime decay [λ_{ex} = 375 nm and λ_{ex} = 455 nm] (e) delayed fluorescence lifetime decay [λ_{ex} = 380 nm and λ_{ex} = 455 nm] and (f) phosphorescence lifetime decay [λ_{ex} = 380 nm and λ_{ex} = 550 nm] under vacuum [absence of oxygen] and ambient atmosphere [presence of oxygen] at 298 K for **2** doped in PMMA matrix (10 wt%) [λ_{ex} = 380 nm].

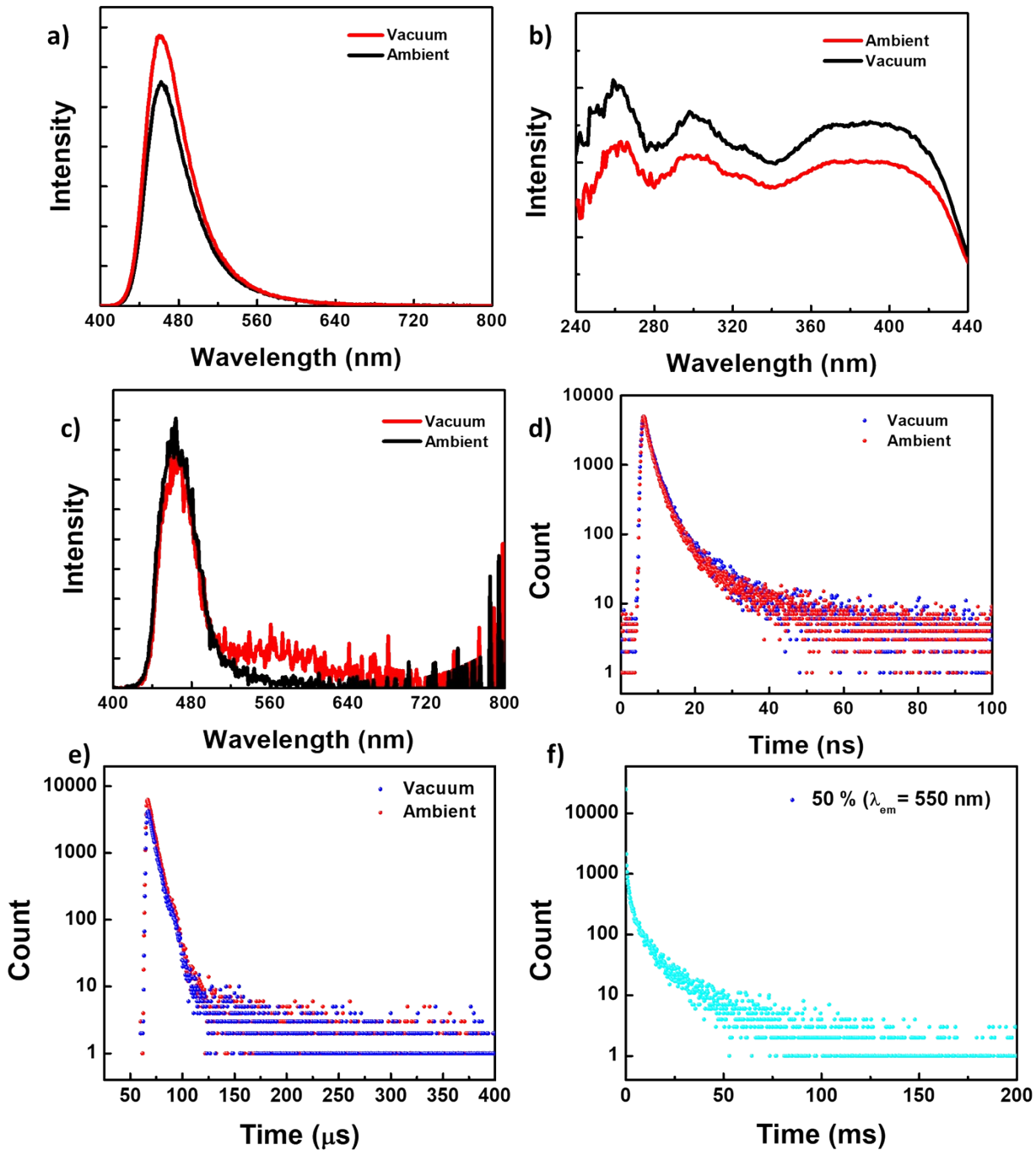

Figure S50. (a) Fluorescence spectra (b) excitation spectra corresponding to emission maxima (c) delayed fluorescence spectra [50 μs delay] (d) fluorescence lifetime decay [λ_{ex} = 375 nm and λ_{ex} = 460 nm] (e) delayed fluorescence lifetime decay [λ_{ex} = 380 nm and λ_{ex} = 460 nm] under vacuum [absence of oxygen] and ambient atmosphere [presence of oxygen] at 298 K for **2** doped in PMMA matrix (50 wt%) [λ_{ex} = 380 nm].

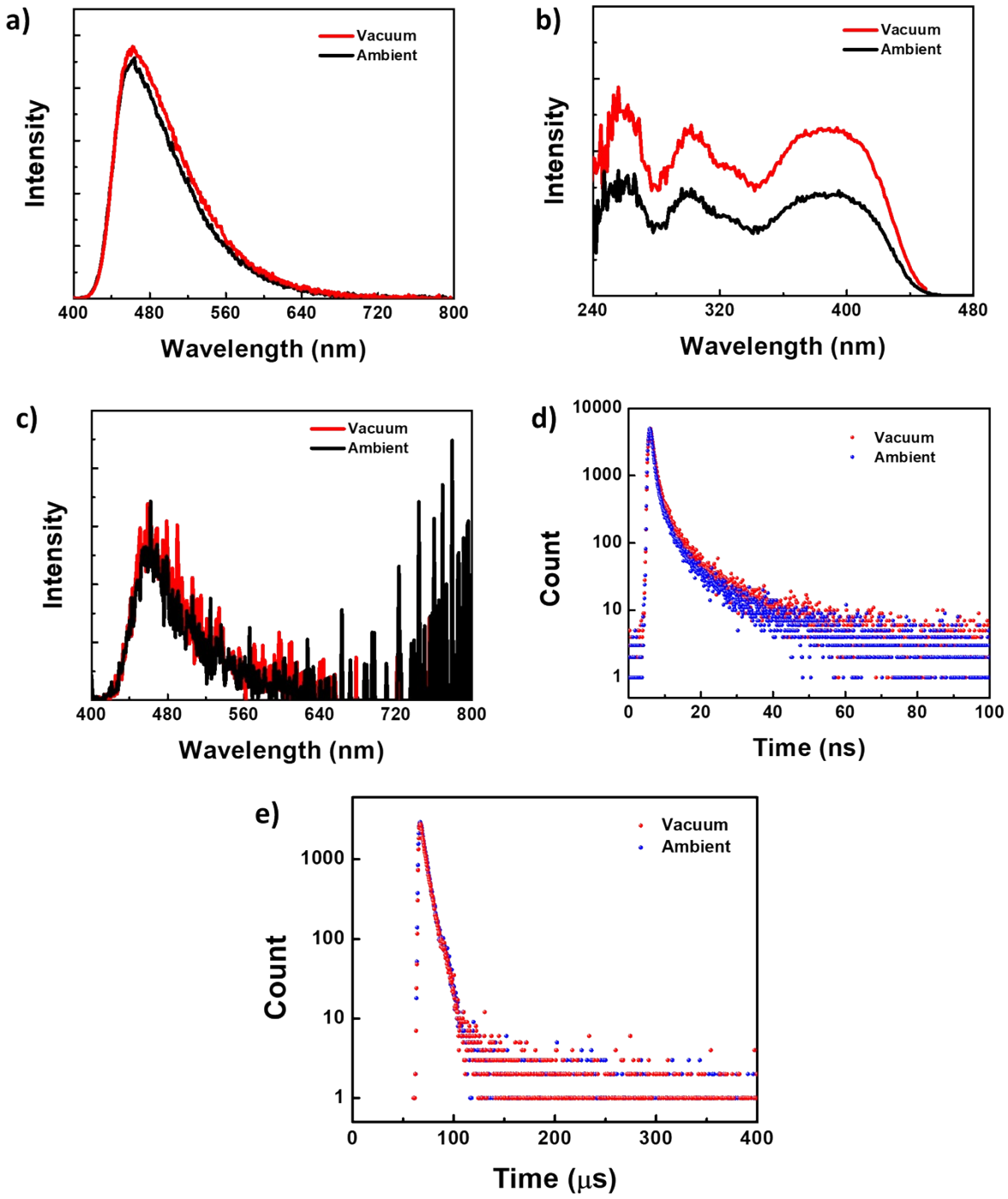

Figure S51. (a) Fluorescence spectra (b) excitation spectra corresponding to emission maxima (c) delayed fluorescence spectra [50 μs delay] (d) fluorescence lifetime decay [λ_{ex} = 375 nm and λ_{ex} = 460 nm] (e) delayed fluorescence lifetime decay [λ_{ex} = 375 nm and λ_{ex} = 460 nm] under vacuum [absence of oxygen] and ambient atmosphere [presence of oxygen] at 298 K for **2** as neat film [λ_{ex} = 380 nm]. Delayed fluorescence emission is weak in neat film, so we could not record the lifetime.

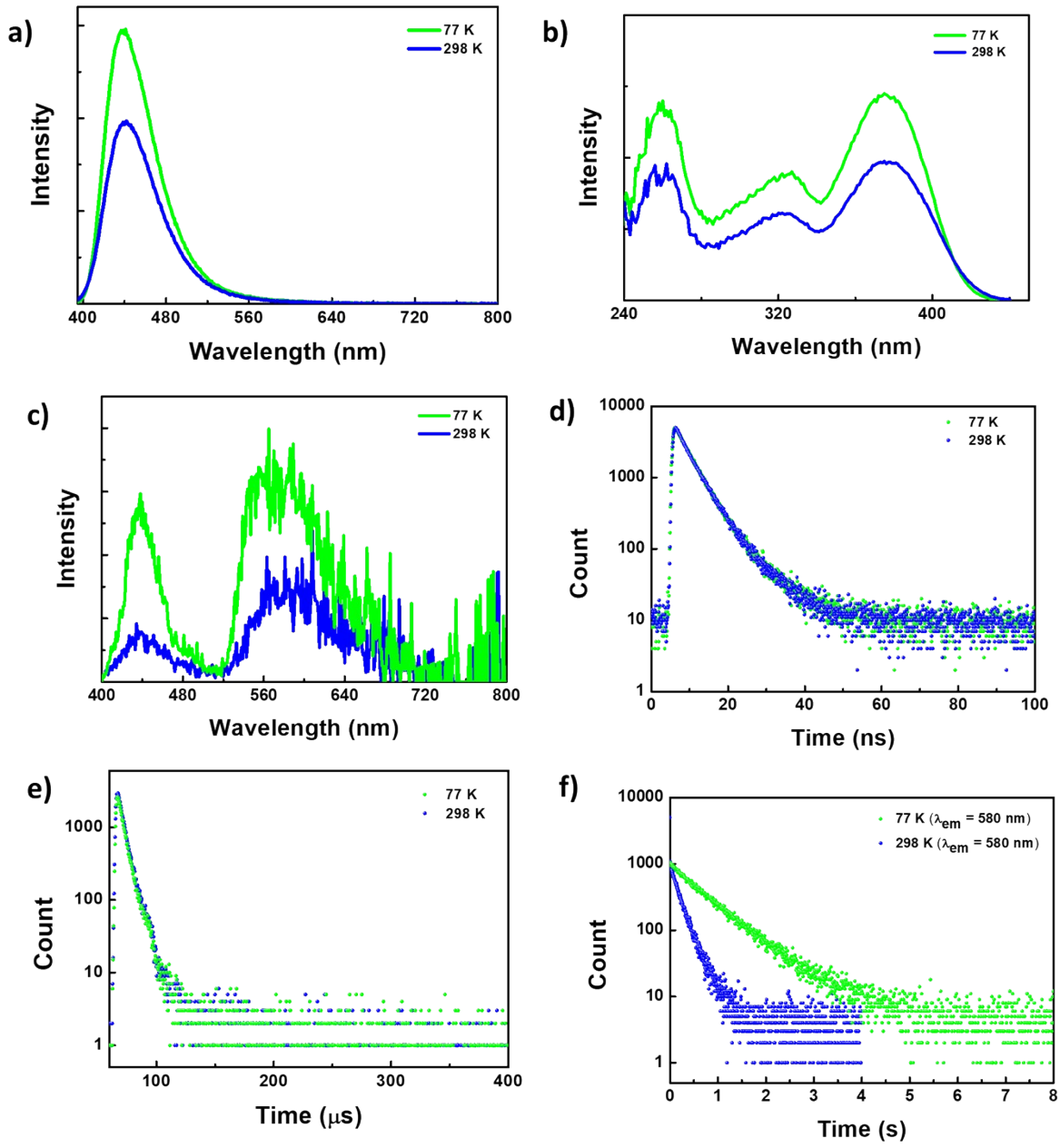

Figure S52. (a) Fluorescence spectra (b) excitation spectra at λ_{em} = 450 nm (c) delayed fluorescence spectra [50 μs delay] (d) fluorescence lifetime decay [λ_{ex} = 375 nm and λ_{em} = 450 nm] (e) delayed fluorescence lifetime decay [λ_{ex} = 380 nm and λ_{em} = 450 nm] and phosphorescence lifetime decay [λ_{ex} = 380 nm and λ_{ex} = 580 nm] at 298 K and 77 K under vacuum for **1** doped in PMMA matrix (1 wt%) [λ_{ex} = 380 nm].

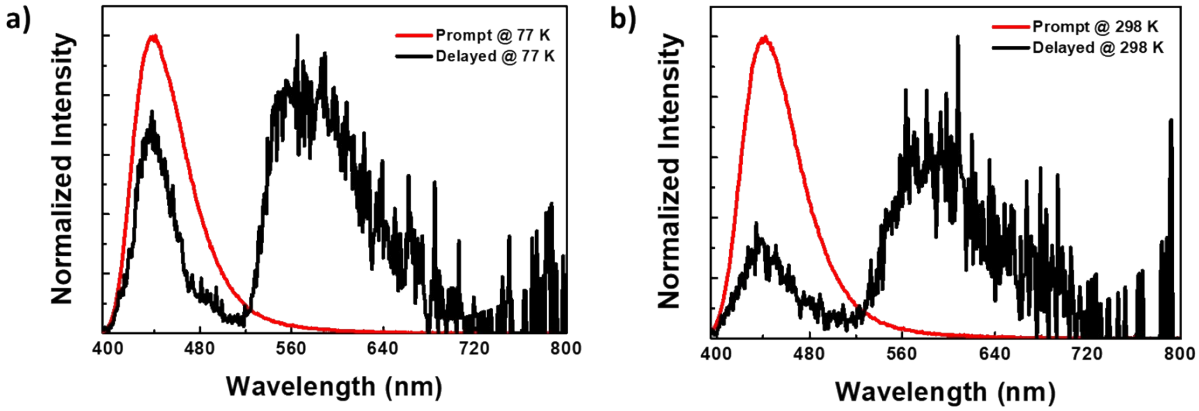

Figure S53. Prompt fluorescence spectra and delayed spectra [50 μs delay] at (a) 77 K and (b) 298 K under vacuum for **1** doped in PMMA matrix (1 wt%) [λ_{ex} = 380 nm].

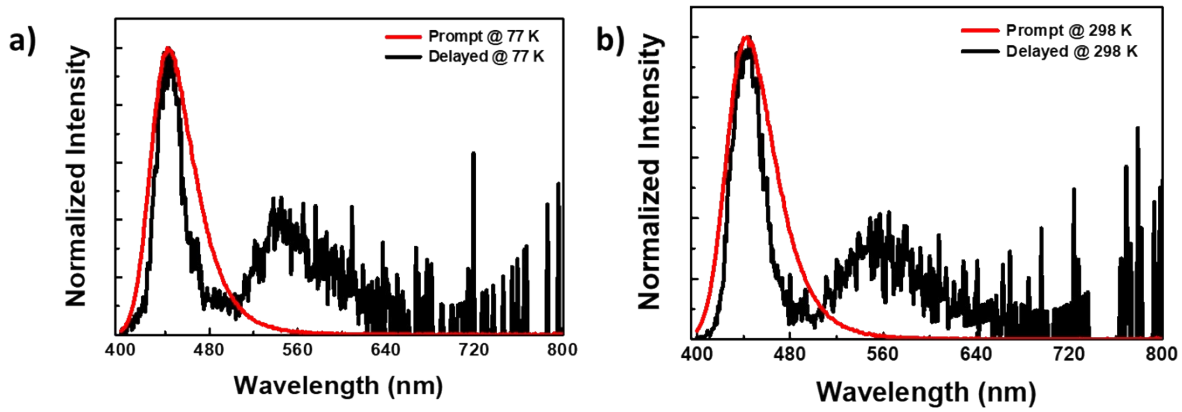

Figure S54. Prompt fluorescence spectra and delayed spectra [50 μs delay] at (a) 77 K and (b) 298 K under vacuum for **2** doped in PMMA matrix (1 wt%) [λ_{ex} = 380 nm].

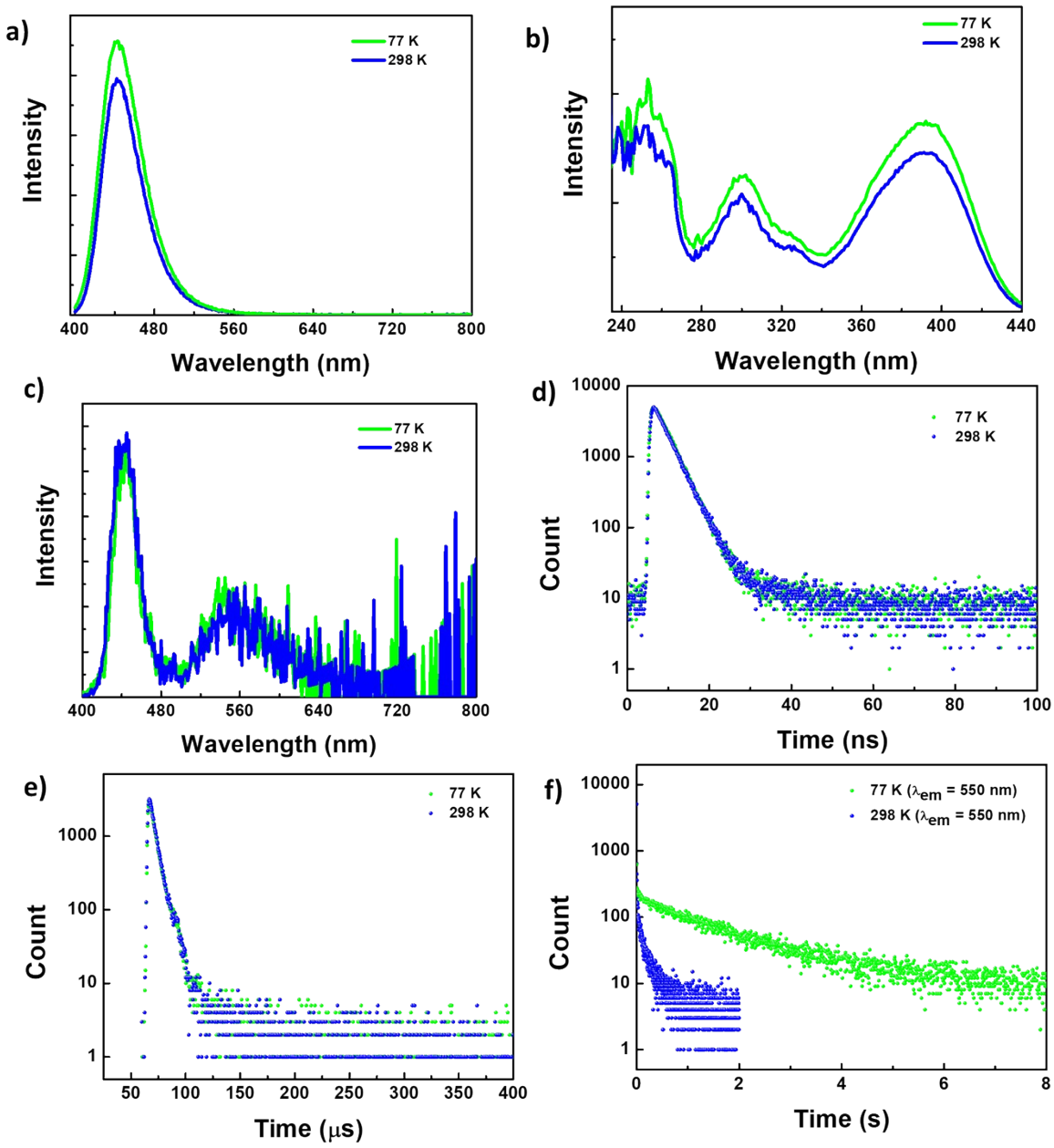

Figure S55. (a) Fluorescence spectra (b) excitation spectra at λ_{em} = 450 nm (c) delayed fluorescence spectra [50 μs delay] (d) fluorescence lifetime decay [λ_{ex} = 375 nm and λ_{em} = 450 nm] (e) delayed fluorescence lifetime decay [λ_{ex} = 380 nm and λ_{em} = 450 nm] and phosphorescence lifetime decay [λ_{ex} = 375 nm and λ_{ex} = 550 nm] at 298 K and 77 K under vacuum for **2** doped in PMMA matrix (1 wt%) [λ_{ex} = 380 nm].

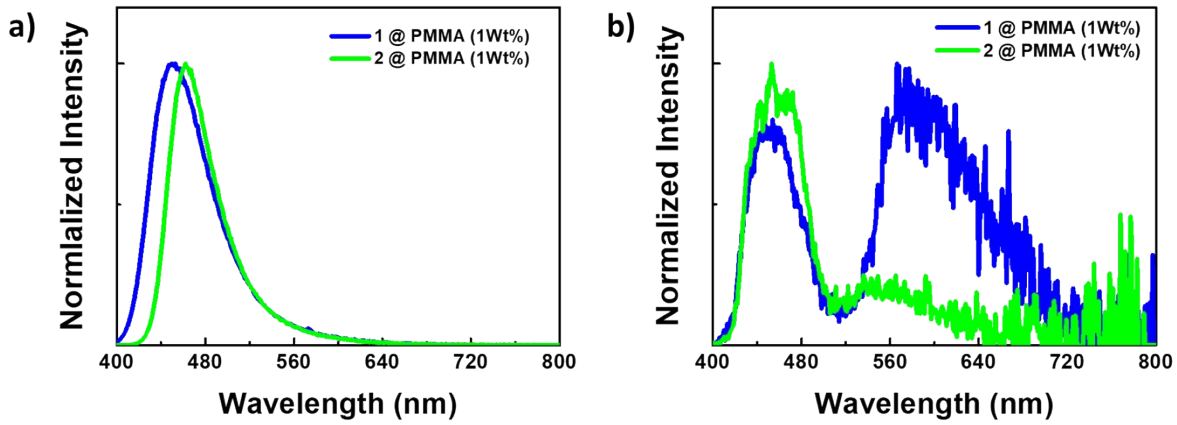

Figure S56. (a) Fluorescence spectra (b) delayed fluorescence spectra [50 μs delay] at 298 K and 77 K under vacuum for **1** and **2** doped in PMMA matrix (1 wt%) [λ_{ex} = 380 nm].

Supplementary information

Table S10: Fluorescence lifetime for **1** under different atmospheric conditions along with total PLQY under ambient conditions at 298 K

	Fluorescence lifetime (ns)												**PLQY** [%]
	77 K (Vacuum)				**298 K (Vacuum)**				**298 K (Ambient)**				
	λ_{ex} (nm)	λ_{em} (nm)	τ_1 (A_1[%]) (ns)	τ_2 (A_2[%]) (ns)	λ_{ex} (nm)	λ_{em} (nm)	τ_1 (A_1[%]) (ns)	τ_2 (A_2[%]) (ns)	λ_{ex} (nm)	λ_{em} (nm)	τ_1 (A_1[%]) (ns)	τ_2 (A_2[%]) (ns)	
Neat					375	450	1.72 (78.02)	6.22 (21.98)	375	450	1.59 (78.13)	6.22 (21.87)	51.1
					375	525	9.22 (47.28)	23.67 (52.72)	375	525	8.24 (41.07)	22.53 (58.93)	
50 wt%@ PMMA					375	460	2.81 (51.07)	7.43 (48.93)	375	460	2.82 (51.87)	7.35 (48.13)	57.4
10 wt% @PMMA					375	450	2.77 (43.19)	6.93 (56.81)	375	450	2.83 (46.45)	6.97 (53.55)	72.6
1 wt% @PMMA	375	450	4.00 (81.53)	9.22 (18.47)	375	450	3.20 (46.29)	7.18 (53.71)	375	450	3.29 (48.66)	7.23 (51.34)	76.7

Supplementary information

Table S11: Delayed fluorescence and phosphorescence lifetime for **1** under different atmospheric conditions.

	Delayed Fluorescence lifetime / Phosphorescence lifetime											
	77 K (Vacuum)				**298 K (Vacuum)**				**298 K (Ambient)**			
	λ_{ex} (nm)	λ_{em} (nm)	τ_1 (A_1 [%])	τ_2 (A_2 [%])	λ_{ex} (nm)	λ_{em} (nm)	τ_1 (A_1[%])	τ_2 (A_2[%])	λ_{ex} (nm)	λ_{em} (nm)	τ_1 (A_1 [%])	τ_2 (A_2 [%])
Neat	-	-	-	-	Emission was very weak so we could not record lifetime with our source							
50 wt%@ PMMA					375	460	5.28 µs (88.97)	14.15 µs (11.03)	375	460	5.99 µs (100)	-
10 wt% @PMMA					375	450	4.98 µs (79.93)	10.92 µs (20.07)	-	-	-	-
					375	580	8.57 ms (1.03)	134.40 ms (98.97)	-	-	-	-
					375	630	18.06 ms (7.69)	109.36 ms (92.31)	-	-	-	-
1 wt% @PMMA	375	450	5.21 µs (90.16)	12.96 µs (9.84)	375	450	4.75 µs (76.15)	10.73 µs (23.85)	375	450	5.57 µs (94.01)	15.02 µs (5.99)
	375	540	735.52 ms (100)		375	540	153.25 ms (55.87)	290.30 ms (44.13)	-	-	-	-
	375	580	560.34 ms (50.36)	952.45 ms (49.94)	375	580	92.12 ms (31.86)	203.80 ms (68.14)	-	-	-	-

Table S12: Fluorescence lifetime for **2** under different atmospheric conditions along with total PLQY under ambient conditions at 298 K

	Fluorescence lifetime (ns)													PLQY [%]
	77 K (Vacuum)				298 K (Vacuum)					298 K (Ambient)				
	λ_{ex} (nm)	λ_{em} (nm)	τ_1 (A_1 [%]) (ns)	τ_2 (A_2 [%]) (ns)	λ_{ex} (nm)	λ_{em} (nm)	τ_1 (A_1 [%]) (ns)	τ_2 (A_2[%]) (ns)	τ_3 (A_3[%]) (ns)	λ_{ex} (nm)	λ_{em} (nm)	τ_1 (A_1[%]) (ns)	τ_2 (A_2[%]) (ns)	τ_3 (A_3[%]) (ns)	
Neat					390	450	0.82 (42.32)	3.22 (39.19)	13.51 (18.49)	390	450	0.70 (45.18)	2.88 (37.23)	13.21 (17.58)	26.8
					390	500	5.12 (58.93)	30.11 (41.07)	-	390	500	4.66 (58.56)	27.42 (41.44)	-	
50 wt% @PMMA					375	450	1.24 (33.02)	3.05 (55.54)	12.66 (11.43)	375	450	1.11 (33.17)	2.89 (55.34)	12.38 (11.49)	46.6
10 wt% @PMMA					375	450	2.58 (86.52)	6.65 (13.48)		375	450	2.53 (83.05)	6.10 (16.95)		78.1
1 wt% @PMMA	375	450	3.47 (98.26)	37.65 (1.74)	375	450	3.15 (97.77)	11.42 (2.23)		375	450	3.15 (97.15)	10.12 (2.85)		88.5

Table S13: Delayed fluorescence and phosphorescence lifetime for **2** under different atmospheric conditions.

	Delayed Fluorescence lifetime (μs)/ Phosphorescence lifetime (ms)											
	77 K (Vacuum)				**298 K (Vacuum)**				**298 K (Ambient)**			
	λ_{ex} (nm)	λ_{em} (nm)	τ_1 (A_1[%])	τ_2 (A_2[%])	λ_{ex} (nm)	λ_{em} (nm)	τ_1 (A_1[%])	τ_2 (A_2[%])	λ_{ex} (nm)	λ_{em} (nm)	τ_1 (A_1[%])	τ_2 (A_2[%])
Neat	-	-	-	-	390	450	6.06 μs (100)	-	390	450	5.14 μs (79.18)	10.49 μs (20.82)
50 wt%@ PMMA	-	-	-	-	390	450	4.13 μs (50.09)	8.50 μs (49.91)	390	450	4.31 μs (55.58)	8.77 μs (44.42)
	-	-	-	-	390	550	1.78 ms (44.58)	14.4 ms (55.42)	-	-	-	-
10 wt% @PMMA	-	-	-	-	390	450	5.14 μs (82.03)	11.85 μs (17.97)	390	450	4.30 μs (59.10)	9.13 μs (40.90)
	-	-	-	-	390	550	12.65 ms (39.60)	103.90 ms (60.40)	-	-	-	-
1 wt% @PMMA	390	450	4.65 μs (80.29)	11.17 μs (19.71)	390	450	6.29 μs (94.65)	42.24 μs (5.35)	390	450	4.36 μs (61.19)	9.41 μs (38.81)
	390	550	241.84 ms (5.18)	1583.23 ms (94.82)	390	550	10.92 ms (29.60)	179.98 ms (70.40)	-	-	-	-

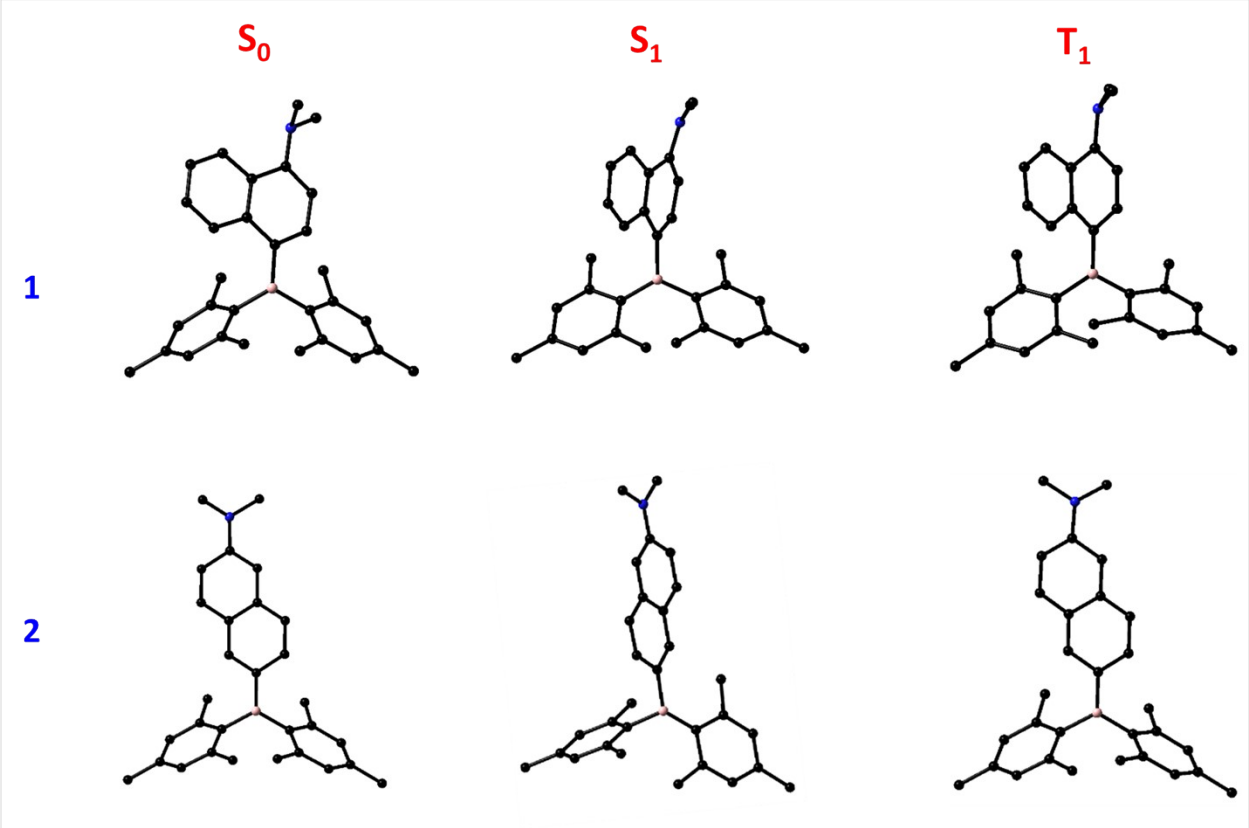

Figure S57. Optimized geometry of S_0, S_1, and T_1 states for **1** and **2** from DFT/TD-DFT calculations using B3LYP functional and 6-31G(d) basis set.

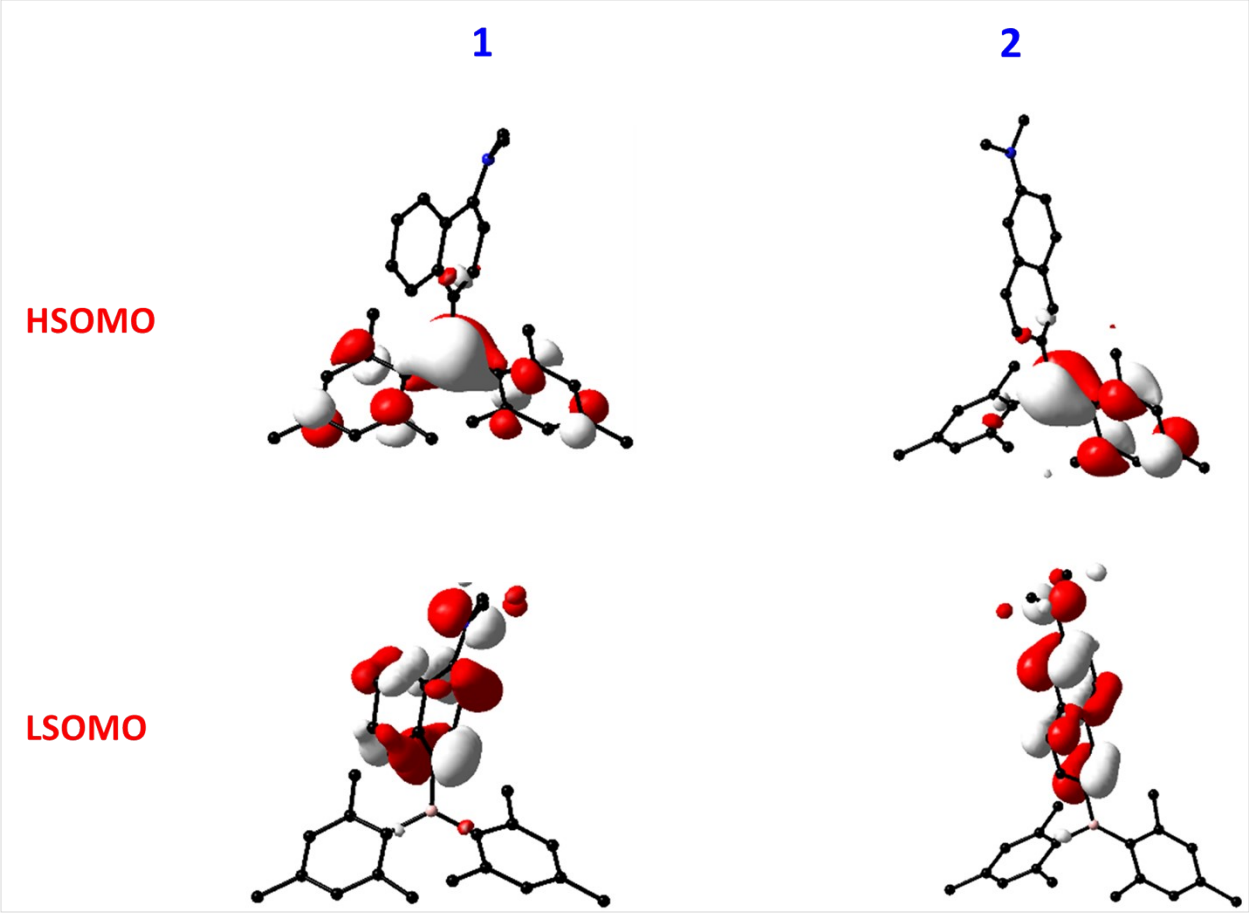

Figure S58. MO's from the optimized geometry of S_1 state for **1** and **2** from DFT/TD-DFT calculations using B3LYP functional and 6-31G (d, p) basis set.

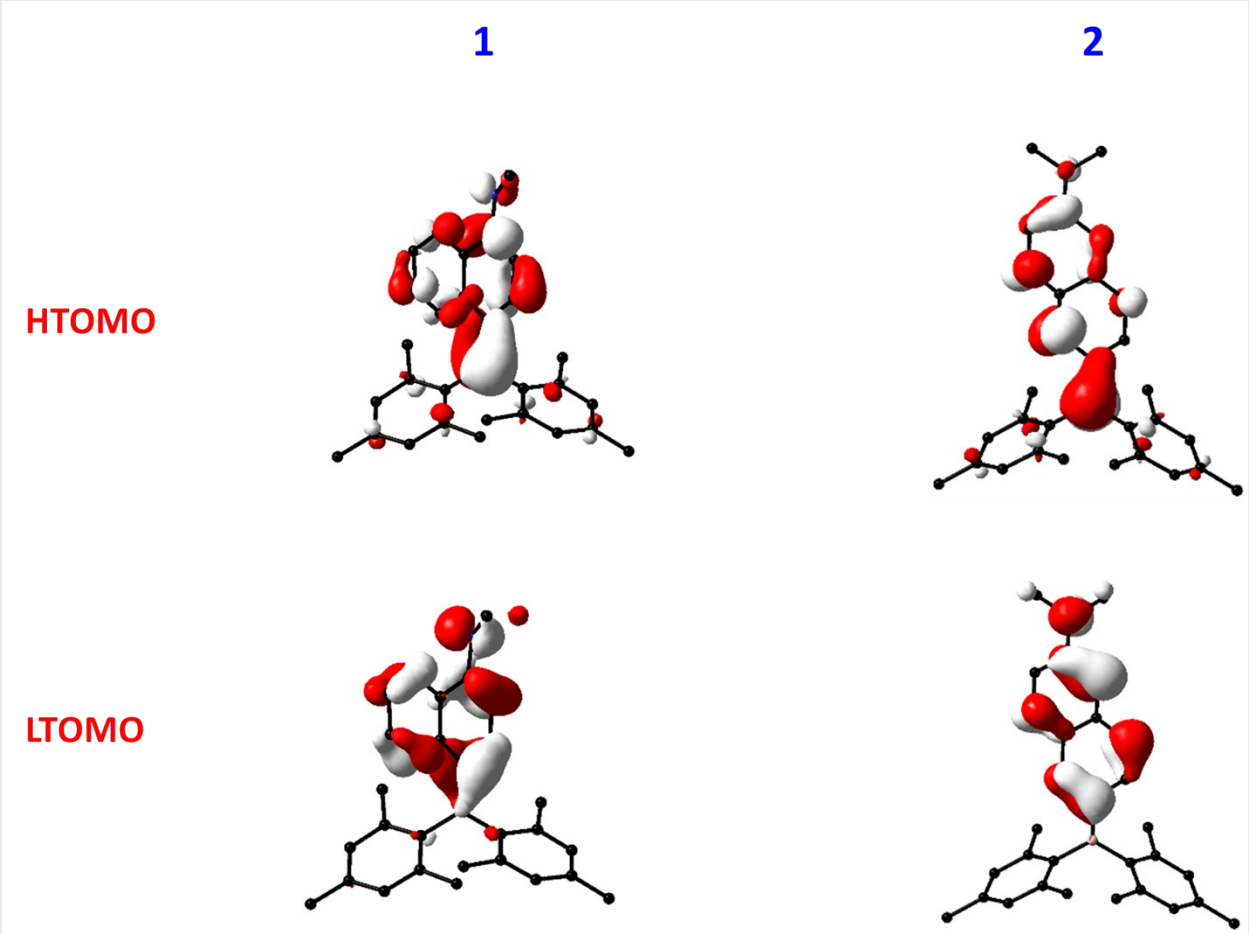

Figure S59. MO's from the optimized geometry of T_1 for **1** and **2** from DFT/TD-DFT calculations using B3LYP functional and 6-31G (d, p) basis set.

Table S14: Comparison of different structural and geometrical parameters of **1** and **2** in S_0, S_1, and T_1 obtained from DFT/TD-DFT calculations using B3LYP functional and 6-31G(d, p) basis set.

Parameter	1			2		
	Ground State	S_1 State	T_1 State	Ground State	S_1 State	T_1 State
Dipole moment (D)	1.72	1.54	2.76	4.19	2.25	3.64
$\Sigma_{(C\text{-}B\text{-}C)}$ (°)	359.9	359.9	359.9	360	359.8	360
$\Sigma_{(C\text{-}N\text{-}C)}$(°)	343.5	357.4	350.3	358.1	360	350.8
B-C (Å)	1.570	1.633	1.558	1.561	1.623	1.558
N-C (Å)	1.418	1.374	1.403	1.386	1.365	1.398
$\theta_{B\text{-}N}$ (°)	79.6	88.5	73.6	28.4	73.9	22.3
$\theta_{B\text{-}Nap}$ (°)	35.8	59.8	33.3	22.8	73.7	22.9
$\theta_{N\text{-}Nap}$ (°)	61.3	40.7	56.2	12.9	0.3	36.2

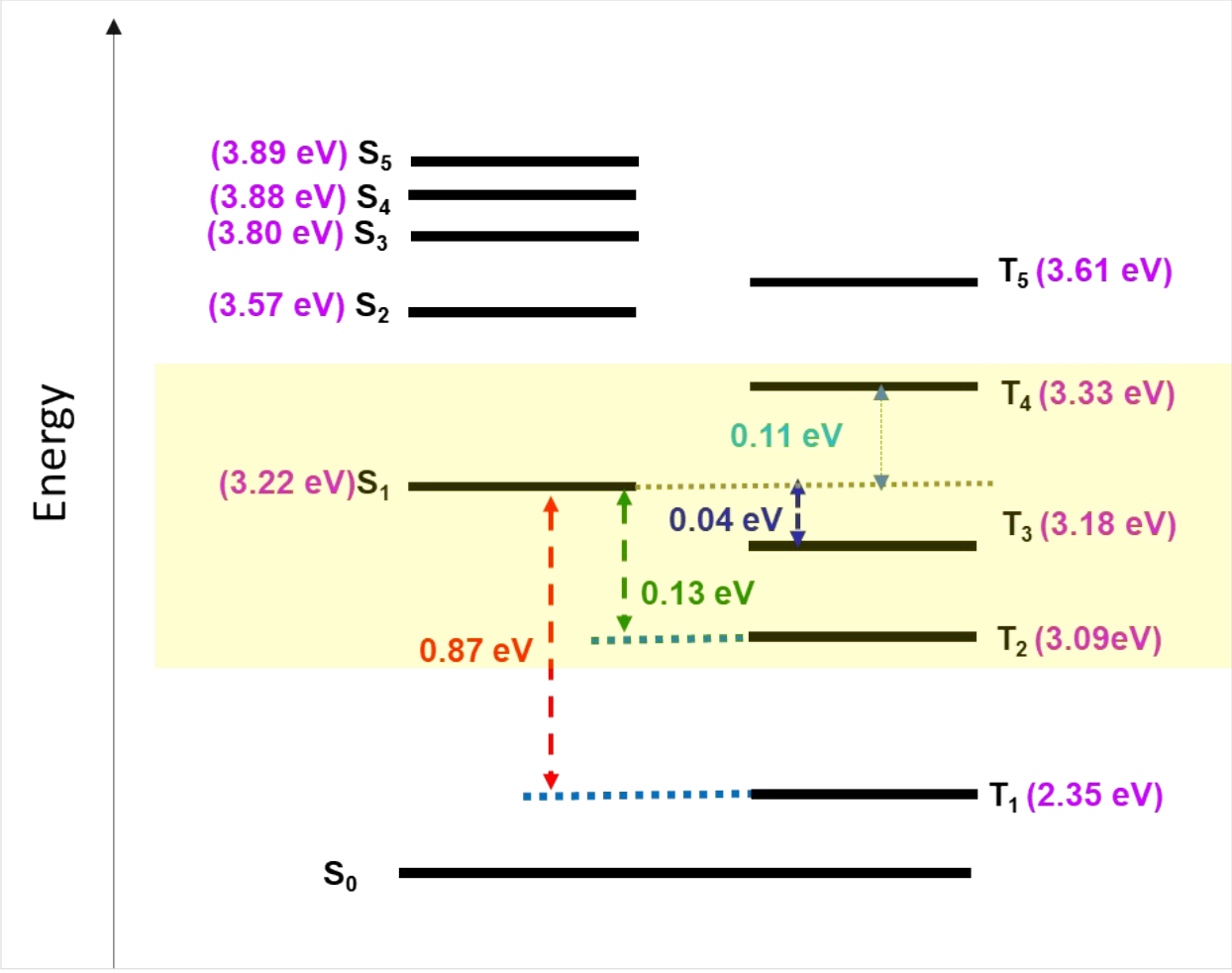

Figure S60. Energy level diagram showing singlet-triplet energy gap, and possible ISC channel for **1** [energy levels in the diagram are not up-to-scale, most possible T_n state involved in for spin-crossover according to the energy difference are highlighted in yellow box] (Energy levels are calculated from singlet and triplet vertical transitions through TD-DFT using 6-31G (d, p)/B3LYP level of theory).

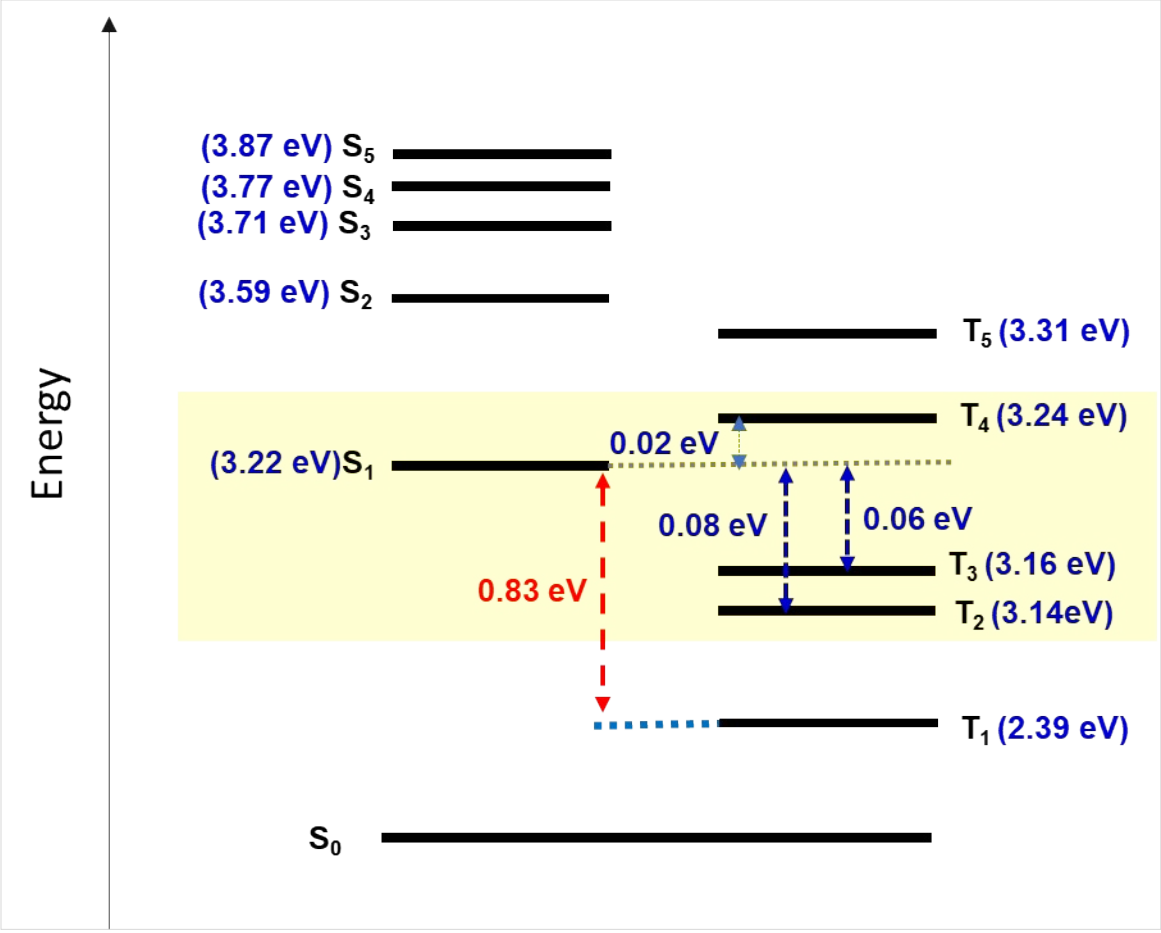

Figure S61. Energy level diagram showing singlet-triplet energy gap, and possible ISC channel for **2** [energy levels in the diagram are not up-to-scale, most possible T_n state involved in for spin-crossover according to the energy difference are highlighted in yellow box] (Energy levels are calculated from singlet and triplet vertical transitions through TD-DFT using 6-31G (d, p)/B3LYP level of theory).

Table S15: List of spin-orbital coupling values for **1** and **2** between different singlet and triplet energy levels obtained theoretically using B3LYP/6-31G(d,p) level of theory.

Transition	SOC (cm^{-1})	
	1	**2**
$S_0 \rightarrow T_1$	0.1574	0.0781
$S_0 \rightarrow T_2$	0.2707	0.1612
$S_0 \rightarrow T_3$	0.8062	0.6622
$S_1 \rightarrow T_1$	0.4859	0.1574
$S_1 \rightarrow T_2$	1.2284	0.2707
$S_1 \rightarrow T_3$	0.4940	0.8062
$S_1 \rightarrow T_4$	0.3472	0.0547
$S_1 \rightarrow T_5$	0.1652	0.1994

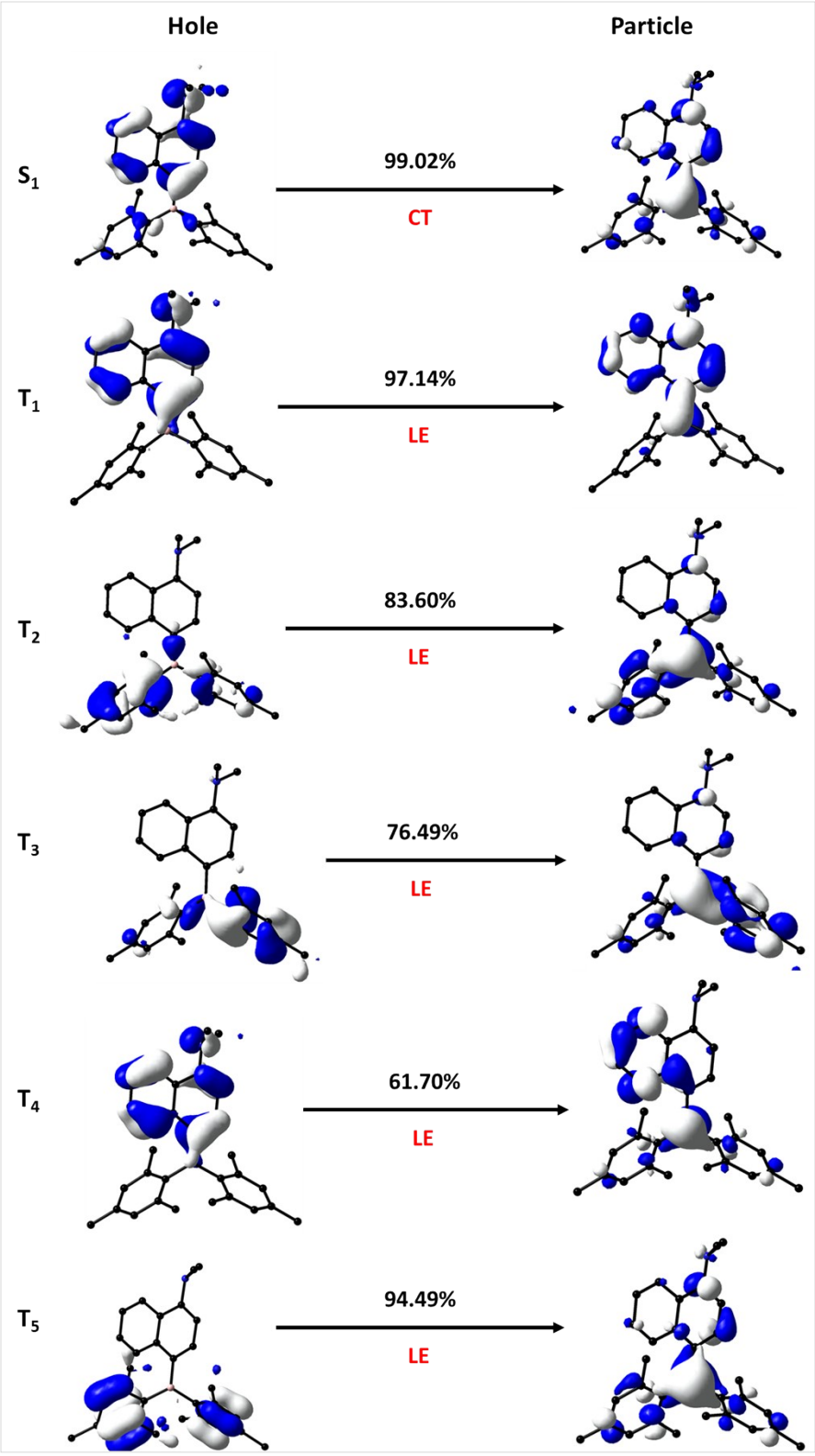

Figure S62. Natural transition orbitals (NTOs) for **1** calculated for S_1 and T_1-T_5 using B3LYP functional and 6-31G (d) basis set.

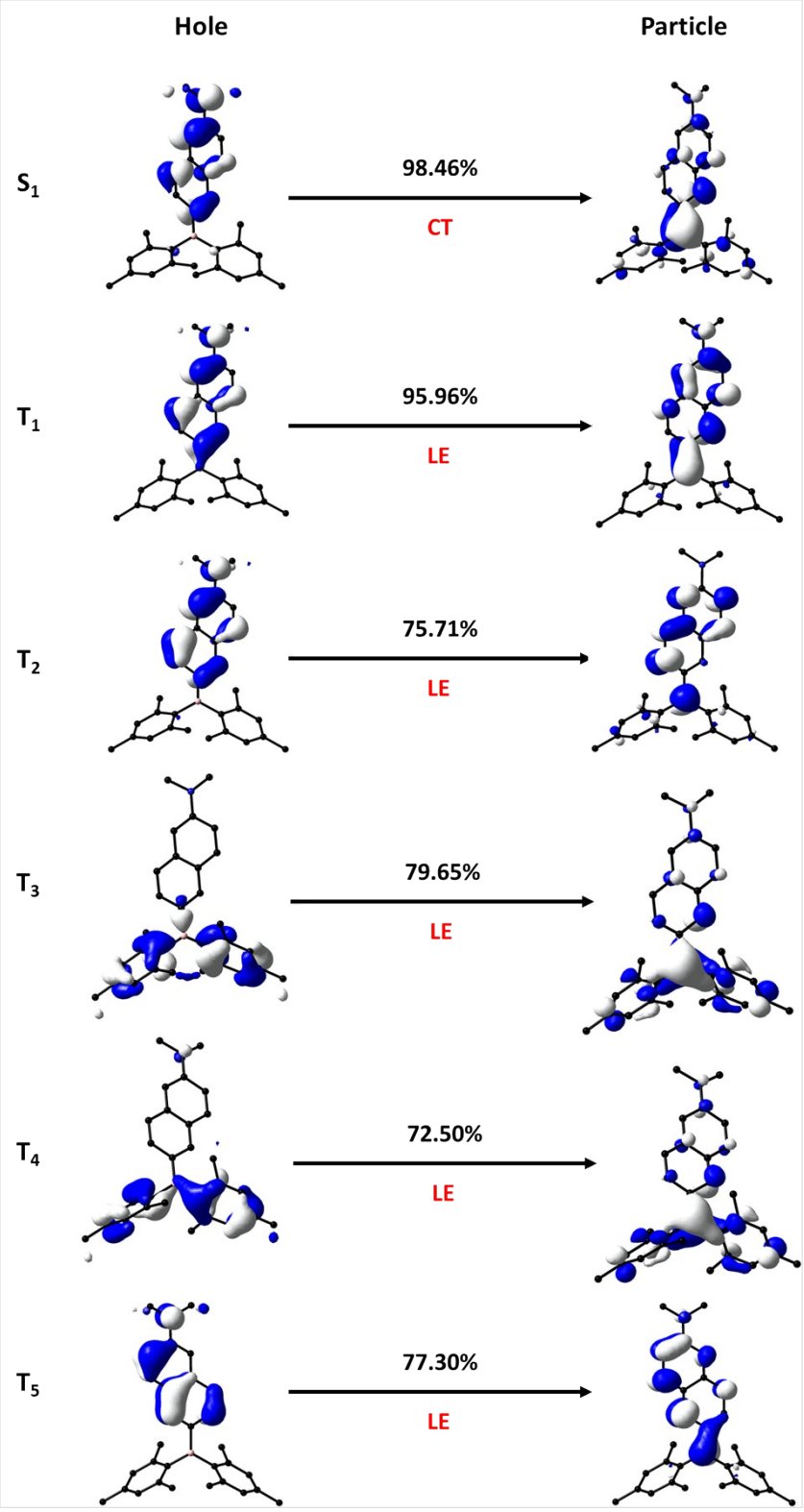

Figure S63. Natural transition orbitals (NTOs) for **2** calculated for S_1 and T_1-T_5 using B3LYP functional and 6-31G (d) basis set.

Table S16: Computed triplet vertical transitions involved in **1** calculated through TD-DFT calculation are done using 6-31G (d, p) basis set B3LYP functional in Gaussian09 in the gas phase.

Excited State	E (eV)	E (nm)	Dominant transitions (%)	ΔE_{S1-Tn}
T_1	2.3453	528.65	HOMO →LUMO (40.3) HOMO →LUMO+1 (5.9)	0.8738
T_2	3.0891	401.36	HOMO-2 →LUMO+3 (2.5) HOMO-1 →LUMO (32.9) HOMO-1 →LUMO+1 (3.7)	0.4813
T_3	3.1769	390.27	HOMO-3 →LUMO (9.7) HOMO-2→LUMO (15.2) HOMO-1→LUMO+3 (4.6)	0.6249
T_4	3.3295	372.38	HOMO-5 →LUMO (4.5) HOMO→LUMO (5.3) HOMO →LUMO+1 (17.7)	0.5492
T_5	3.6077	343.66	HOMO-4 →LUMO+3 (1.5) HOMO-3→LUMO (24.8)	0.2841

Table S17: Computed triplet vertical transitions involved in **2** calculated through TD-DFT calculation are done using 6-31G (d) basis set B3LYP functional in Gaussian09 in the gas phase.

Excited State	E (eV)	E (nm)	Dominant transitions (%)	ΔE_{S1-Tn}
T_1	2.3885	519.08	HOMO →LUMO (38.9) HOMO →LUMO +1 (4.4)	0.8306
T_2	3.1377	395.15	HOMO-3→LUMO+1 (7) HOMO-2 →LUMO (2.2) HOMO →LUMO+1 (25.4)	0.4553
T_3	3.1614	392.18	HOMO-2→LUMO +2 (2.8) HOMO-1→LUMO (34.4)	0.5502
T_4	3.2362	383.11	HOMO-4 →LUMO (10.8) HOMO-2→LUMO (13.9) HOMO -1→LUMO+2 (6.1)	0.5358
T_5	3.3113	374.42	HOMO-3 →LUMO (22.6) HOMO-3→LUMO+1 (3.7) HOMO-2→LUMO (7.1)	0.5537

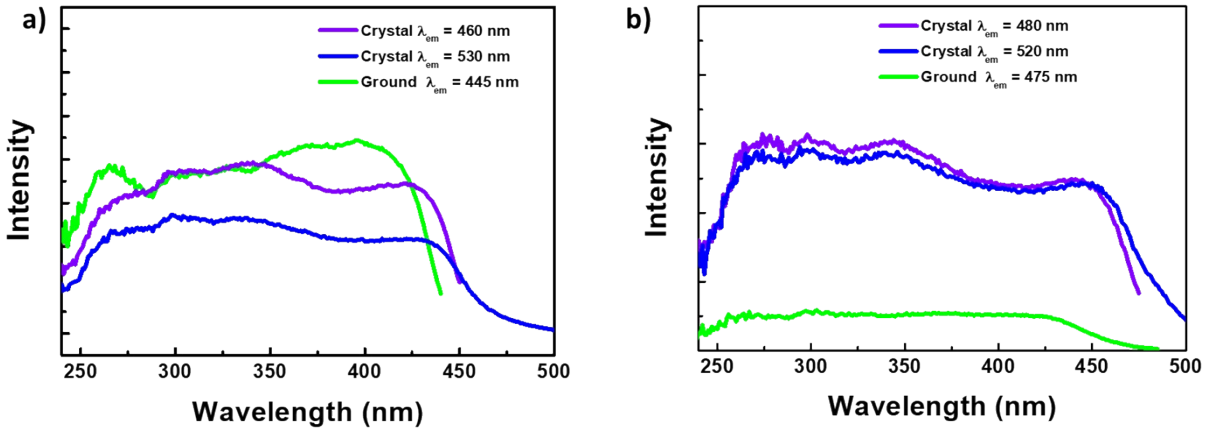

Figure S64. Excitation spectra correspond to crystal and ground emission maxima for (a) **1** and (b) **2** at 298 K under ambient conditions.

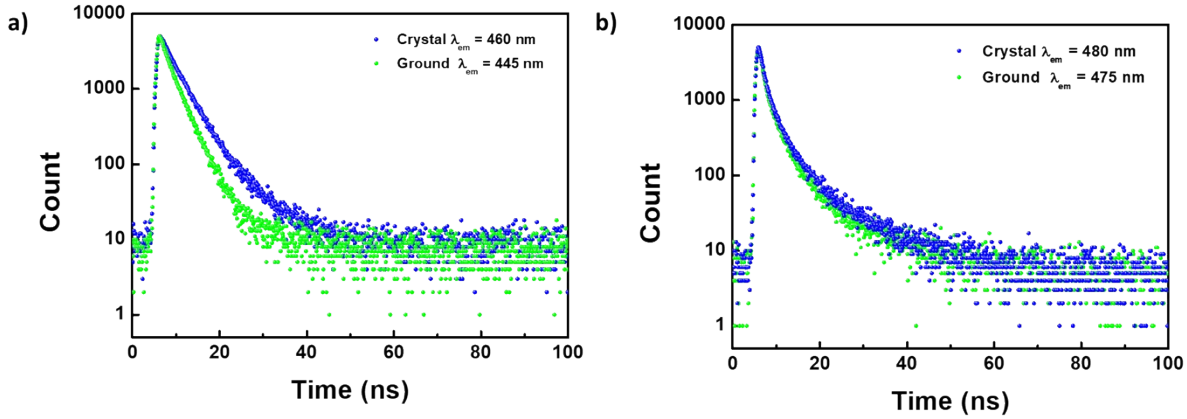

Figure S65. (a) Fluorescence lifetime decay for crystal and ground (a) **1** and (b) **2** at 298 K under ambient conditions at λ_{ex} = 375 nm

Table S18: Fluorescence lifetime of crystal and ground for **1** and **2** under ambient conditions upon λ_{ex} = 375 nm at 298 K.

	1				**2**			
	λ_{em} (nm)	τ_1 (A_1 [%]) (ns)	τ_2 (A_2[%]) (ns)	$\tau_{av,\ p}$ / ns [b]	λ_{em} (nm)	τ_1 (A_1[%]) (ns)	τ_2(A_2[%]) (ns)	$\tau_{av,\ p}$ / ns [b]
Crystal	460	2.33 (90.05)	10.10 (9.95)	3.11	490	1.73 (57.76)	8.34 (42.24)	4.51
	530	11.55 (64.31)	31.64 (35.69)	19.59	526	4.47 (57.50)	14.86 (42.50)	8.83
Ground	453	2.48 (73.76)	4.81 (26.24)	3.09	480	2.35 (62.96)	9.95 (37.04)	5.16

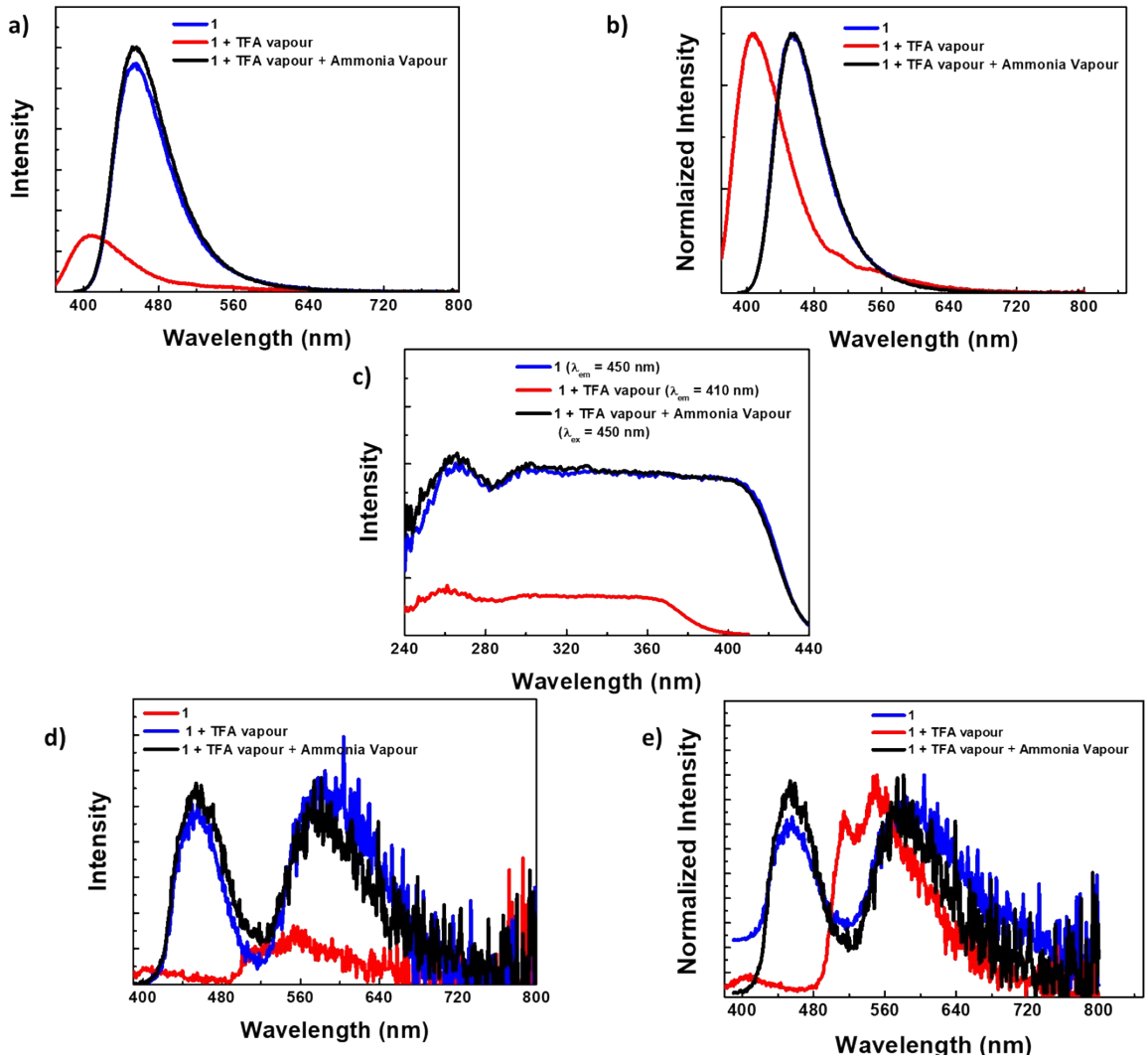

Figure S66. (a,b) Photoluminescence spectra at λ_{ex} = 380 nm (c) excitation spectra corresponding to emission maxima (d,e) Time gated spectra at λ_{ex} = 380 nm for doped film of **1 (**1 wt% in PMMA**)**, **1+ TFA Vapor** (1 after exposing to TFA Vapour) and **1+ TFA Vapour** + **Ammonia vapor** (1 after exposing to TFA Vapour flowed by exposing to ammonia vapor) under vacuum at 298 K.

Table S19: Fluorescence and Phosphorescence lifetime for **1**, **1+ TFA Vapour**, and **1+ TFA Vapour** + **Ammonia vapor** doped in PMMA film matrix (1 wt%) upon λ_{ex} = 375 nm at 298 K under vacuum.

	Fluorescence (ns)				**Phosphorescence (ms)**			
	λ_{em} (nm)	τ_1 (A_1[%]) (ns)	τ_2 (A_2[%]) (ns)	τ_{avg} ns	λ_{em} (nm)	τ_1 (A_1[%]) (ms)	τ_2 (A_2[%]) (ms)	τ_{avg} ms
1	450	3.20 (46.29)	7.18 ns (53.71)	5.35	580	92.12 (31.86)	203.80 (68.14)	168.06
1+TFA	400	2.50 (85.37)	2.50 (85.37)	3.09	550	16.7 (60.26)	79.90 (39.74)	41.98
					515	13.56 (57.83)	63.26 (42.17)	34.43
1+TFA + Ammonia	450	3.24 (46.21)	7.48 (53.79)	5.53	580	63.96 (25.78)	193.06 (74.22)	159.49

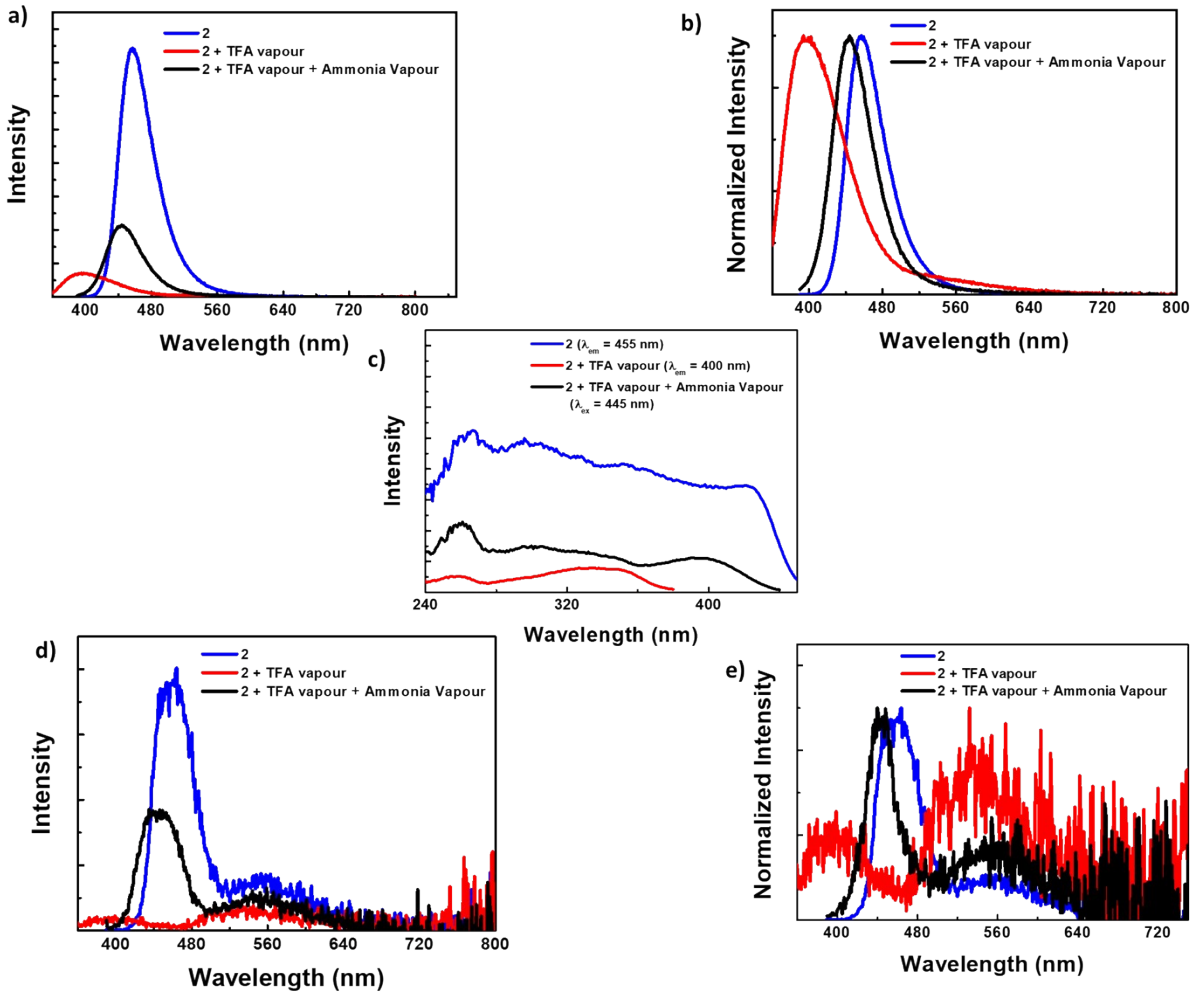

Figure S67. (a,b) Photoluminescence spectra at λ_{ex} = 380 nm (c) excitation spectra corresponding to emission maxima (d,e) time-gated spectra at λ_{ex} = 380 nm for doped film of **2 (**1 wt% in PMMA**)**, **2+ TFA Vapor** (1 after exposing to TFA Vapour) and **2+ TFA Vapour** + **Ammonia vapor** (1 after exposing to TFA Vapour flowed by exposing to ammonia vapor) under vacuum at 298 K.

Table S20: Fluorescence and Phosphorescence lifetime for **2**, **2+ TFA Vapour**, and **2+ TFA Vapour** + **Ammonia vapor** doped in PMMA film matrix (1 wt%) upon λ_{ex} = 375 nm at 298 K. at 298 K under vacuum.

	Fluorescence				**Phosphorescence**			
	λ_{em} (nm)	τ_1 (A_1[%]) (ns)	τ_2 (A_2[%]) (ns)	τ_{avg} ns	λ_{em} (nm)	τ_1 (A_1[%]) (ms)	τ_2 (A_2[%]) (ms)	τ_{avg} ms
2	455	3.88 (95.61)	13.98 (4.39)	4.32	550	10.92 (29.60)	179.98 (70.40)	129.93
2+TFA	400	2.37 (71.67)	7.77 (28.33)	3.88	550	2.40 (31.77)	17.44 (68.23)	12.66
2+TFA + Ammonia	455	3.51 (84.22)	12.50 (15.78)	4.93	550	3.16 (26.39)	40.29 ms (73.61)	30.49

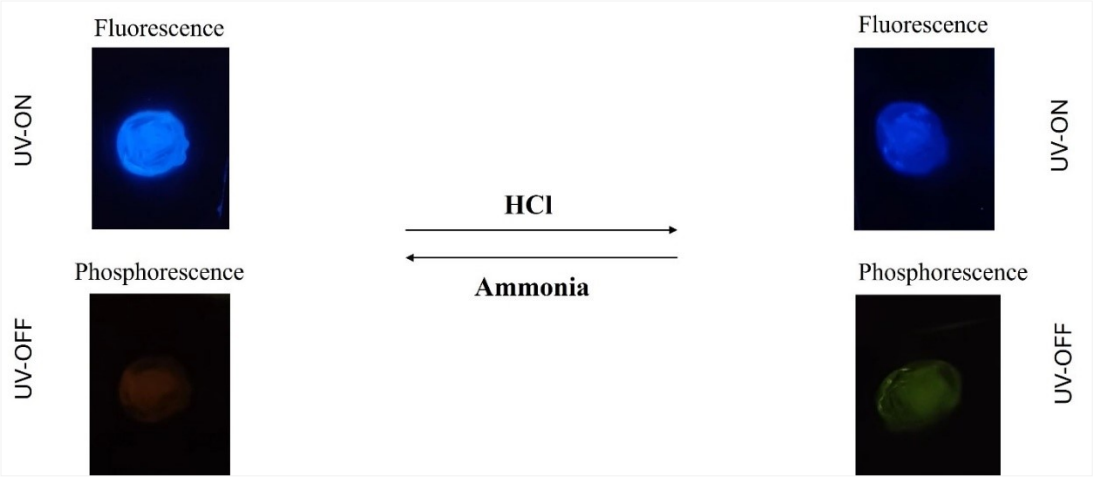

Figure S68. (a) Photographs of compounds before and after UV light (λ_{ex} = 365 nm) of **1** doped PMMA film (1 wt%).

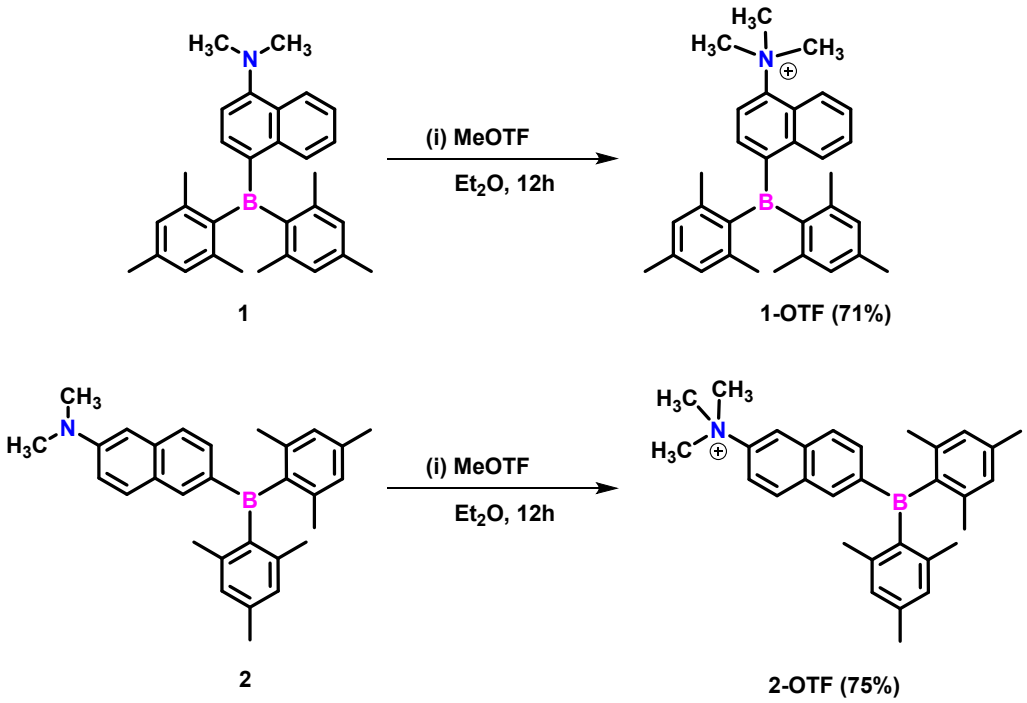

Scheme S2. Synthesis of precursor compounds **1-OTF** and **2-OTF**

General synthetic approach for 1-OTF and -2-OTF.

The MeOTf (0.894 mmol, in diethyl ether solvent) was added to a diethyl ether solution of **1** / **2** (0.596 mmol) at room temperature. The reaction mixture was allowed to stir for an additional 12h at the same temperature. The mother extract was decanted. The precipitate was dried up, and washed with *n*-pentane (20 mL) afforded the pure ammonium borane salts **1-OTF/2-OTF**. The X-ray quality crystals for **1-OTF** were obtained from the concentrated tetrahydrofuran solution kept at -30 ^{o}C.

Synthesis of 1-OTF.

1 (250 mg, 0.596 mmol), MeOTf (146.7 mg, 97.8 µL 0.894 mmol) Yield: 71 % (248 mg). ^{1}H NMR (300 MHz, $CDCl_3$): δ 8.34 (d, *J* = 8.25 Hz 1H), 8.11 (d, *J* = 8.14 Hz, 1H), 7.82-7.77 (m, 2H), 7.51-7.44 (m, 2H), 6.79 (s, 4H), 4.11(s,9H), 2.29 (s, 6H), 1.90 (s, 12H); ^{13}C NMR (75 MHz, $CDCl_3$): δ 143.14, 140.57, 140.21, 138.31, 131.44, 130.76, 128.53, 127.26, 123.16, 122.82, 122.55, 118.01, 58.21, 23.24, 21.29; ^{19}F NMR (282 MHz, $CDCl_3$): δ -78.39.

Synthesis of 2-OTF.

2 (250 mg, 0.596 mmol), MeOTf (146.7 mg, 97.8 µL 0.894 mmol). Yield: 75 % (262 mg). ^{1}H NMR (300 MHz, $CDCl_3$): δ 8.27 (s, 1H), 8.26-7.97 (m, 3H), 7.87 (d, *J* = 8.37, 1H), 7.72 (d, *J* = 7.20, 1H), 6.84 (s, 4H), 3.84 (s,9H), 2.33 (s, 6H), 1.97 (s, 12H); ^{13}C NMR (75 MHz, $CDCl_3$): δ 146.82, 144.99, 141.42, 140.87, 139.32, 136.51, 134.40, 134.17, 133.05, 132.74, 128.53, 128.43, 122.84, 118.60, 118.45, 116.45, 57.29, 23.47, 21.27; ^{19}F NMR (282 MHz, $CDCl_3$): δ -78.41.

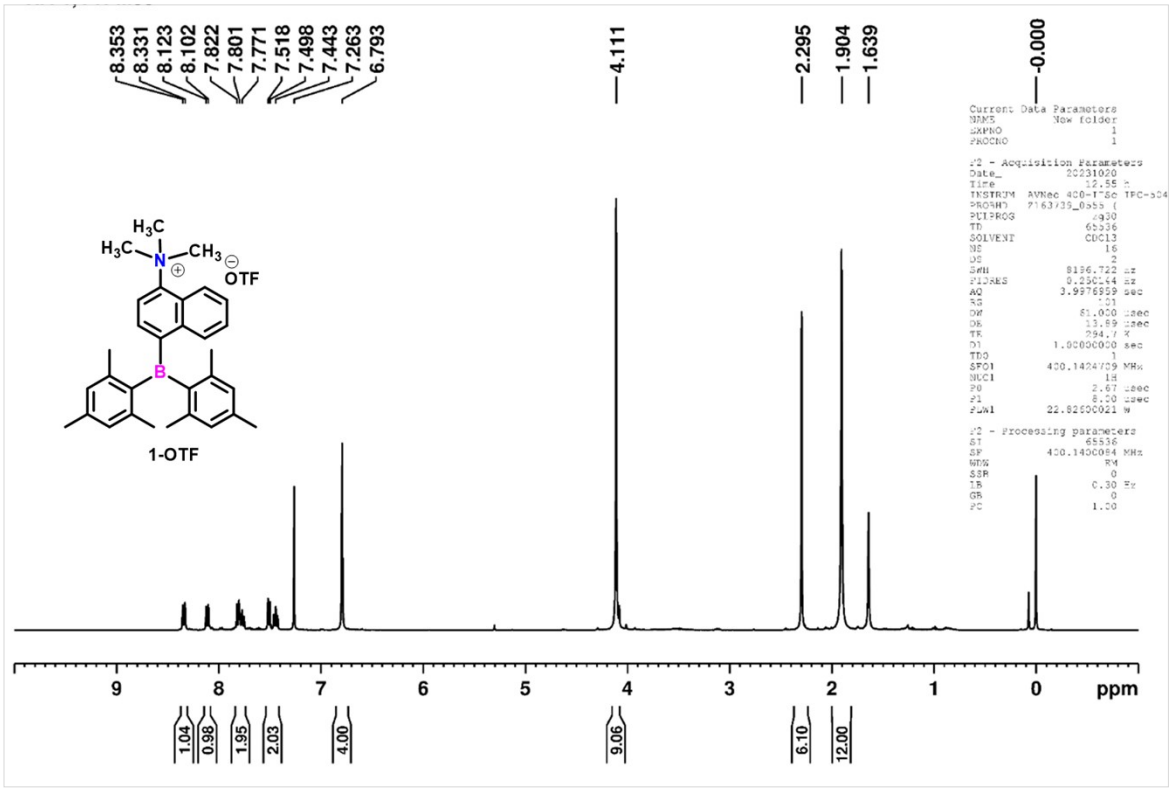

Figure S69. ^{1}H NMR spectrum of **1-OTF** in $CDCl_3$.

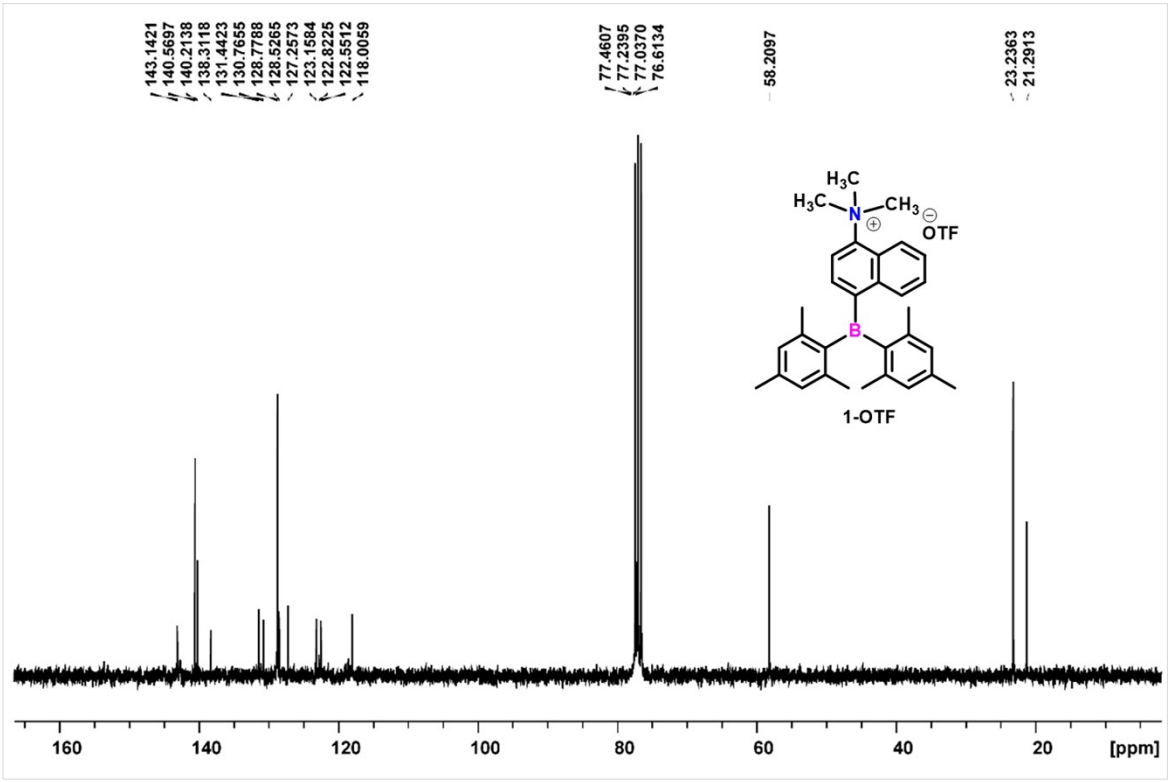

Figure. S70. ^{13}C NMR spectrum of **2-OTF** in $CDCl_3$.

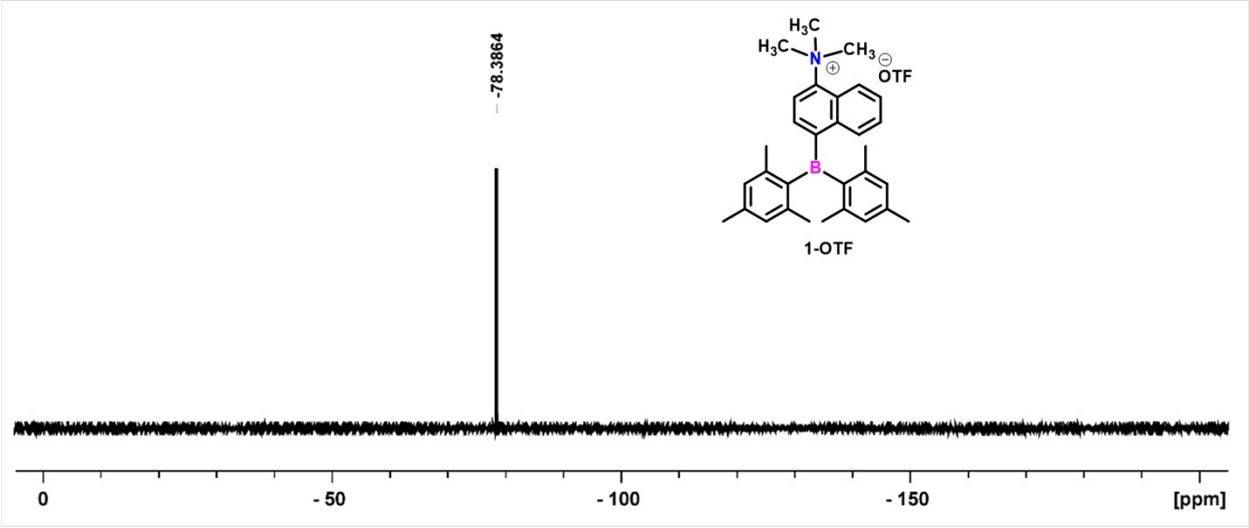

Figure S71. ^{19}F NMR spectrum of **1-OTF** in $CDCl_3$.

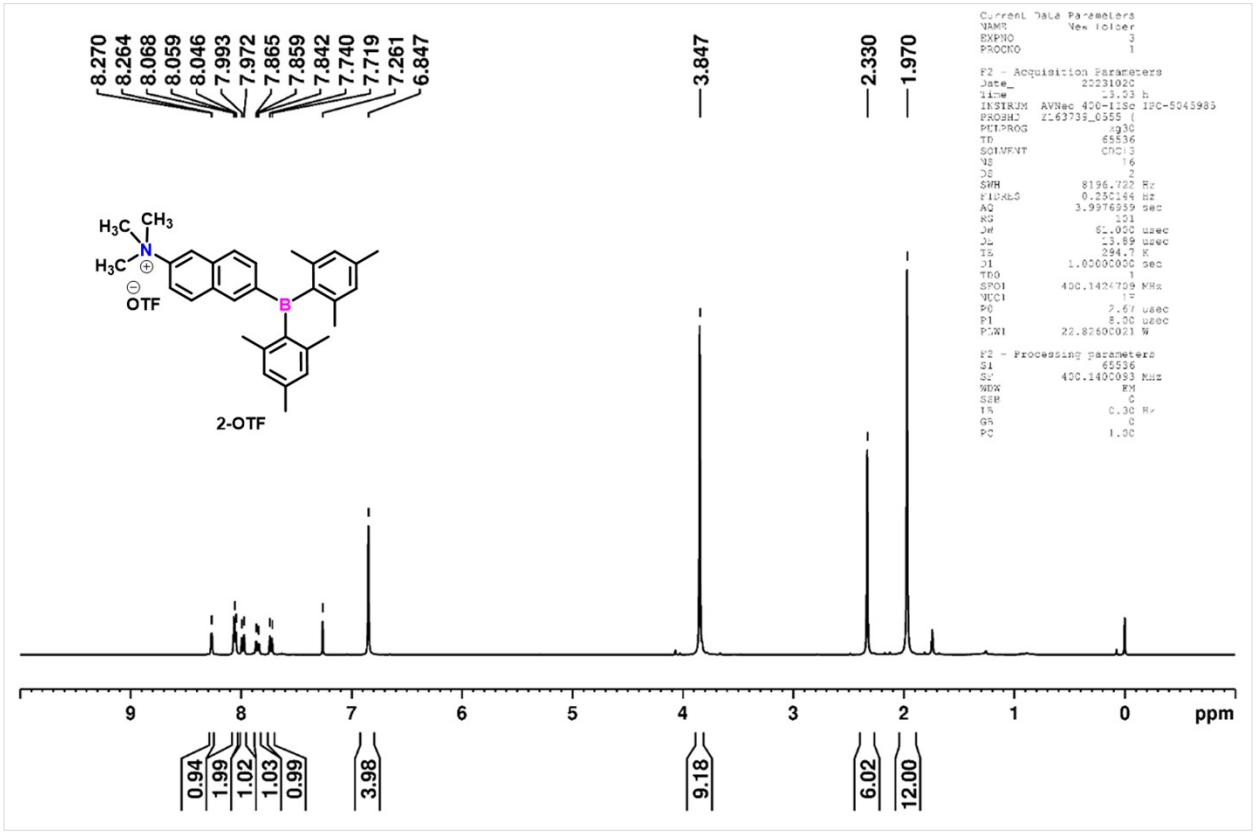

Figure S72. ^{1}H NMR spectrum of **2-OTF** in $CDCl_3$.

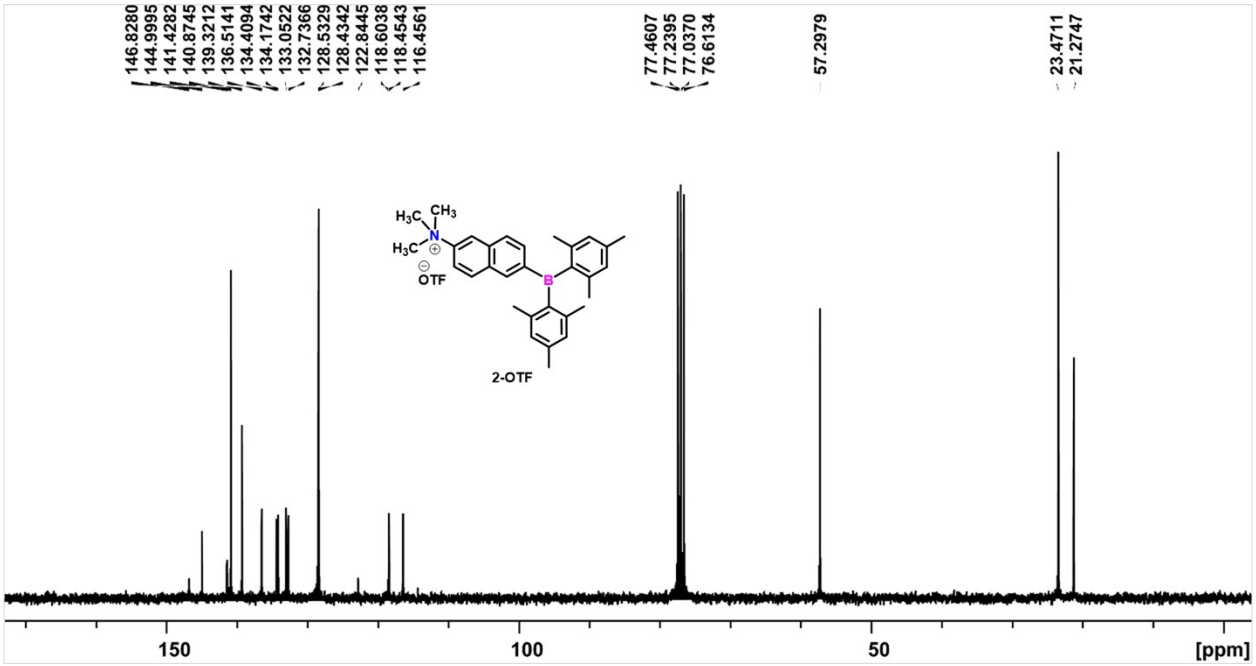

Figure S73. ^{13}C NMR spectrum of **2-OTF** in $CDCl_3$.

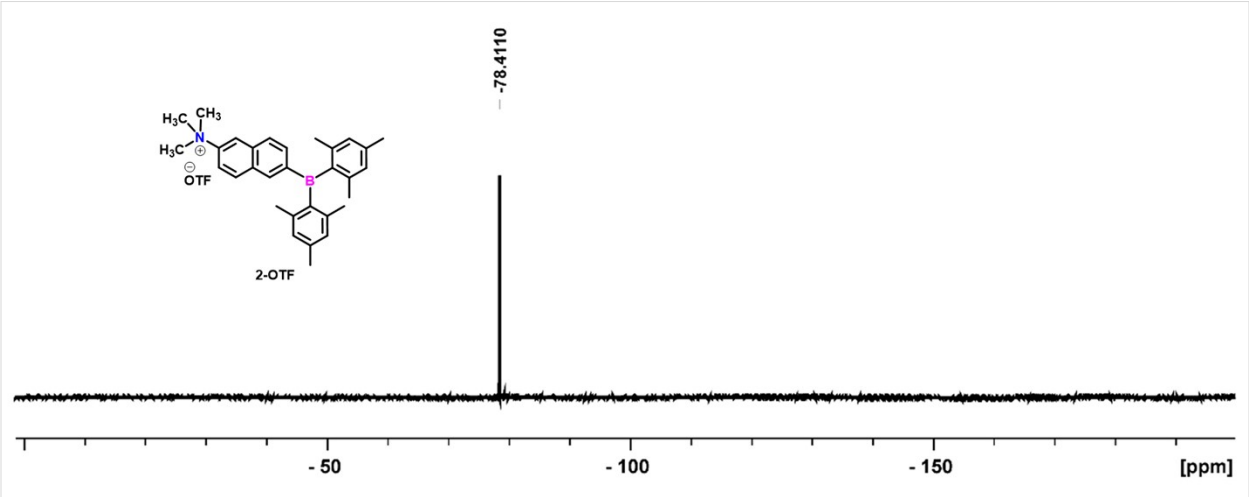

Figure S74. ^{19}F NMR spectrum of **2-OTF** in $CDCl_3$.

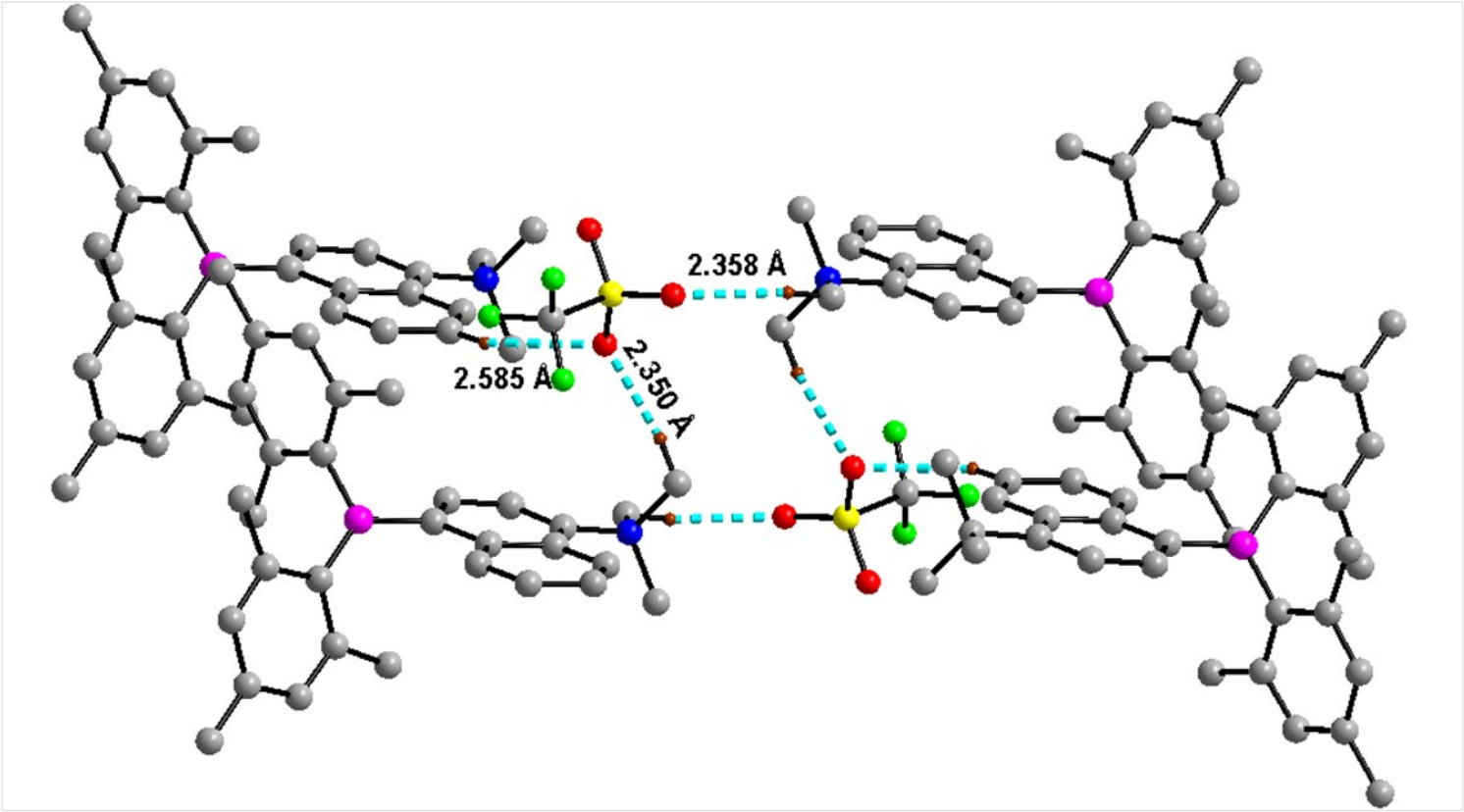

Figure S75. O···H (turquoise line) intermolecular interactions in **1-OTF** which extended in one direction and formed a 1D chain. Hydrogen atoms are omitted for clarity. Color code: carbon (gray 50), boron (magenta), nitrogen (blue), oxygen (red), sulfur (yellow) and fluorine (bright green)

Table S21. Crystallographic data and refinement parameters for **1-OTF**

	1-OTF
Empirical formula	$C_{34}\ H_{41}\ B\ Cl_4\ F_3\ N\ O_3\ S$
FW	753.35
T (K)	100 K
Crystal system	Monoclinic
Space group	*I 2/a*
a/Å	17.9022(7)
b/Å	8.3999(3)
c/Å	47.9410(16)
α/deg	90
β/deg	95
γ/deg	90
V/Å^3	7184.0 (5)
Z	4
ρ_{calcd} (gcm^{-3})	1.393
μ (Mo Kα) (mm^{-1})	0.439
λ/Å	0.71073
F (000)	3136
Collected reflections	10077
Unique reflections	7829
Goodness of Fit (GOF) [F2]	1.026
R1 [I>2σ(I)][a]	0.0764
wR2 [I>2σ(I)][b]	0.2146
CCDC Number	**2291487**

Table S22: Comparison of different parameters for **1-OTF** and **2-OTF** obtained from crystal data and ground state optimized geometry through DFT calculation using 6-31G (d)/B3LYP level of theory

Parameter	1-OTF		2-OTF	
	ground state (S_0)	Crystal	ground state (S_0)	Crystal
HOMO (eV)	-5.90	-	-5.96	-
LUMO (eV)	-2.32	-	-2.30	-
Bang gab (eV)	3.58	-	3.66	-
Dipole moment (D)	14.91	-	15.25	-
$\Sigma_{(C\text{-}B\text{-}C)}$ (°)	359.9	359.8	360	-
B-C (Å)	1.590	1.583(3)	1.578	-
N-C (Å)	1.521	1.511(3)	1.510	-
$\theta_{D\text{-}A}$ (°)	77.34	76.14	89.11	-
$\theta_{S\text{-}A}$ (°)	43.65	49.95	27.13	-
$\theta_{D\text{-}S}$ (°)	85.59	87.15	87.97	-

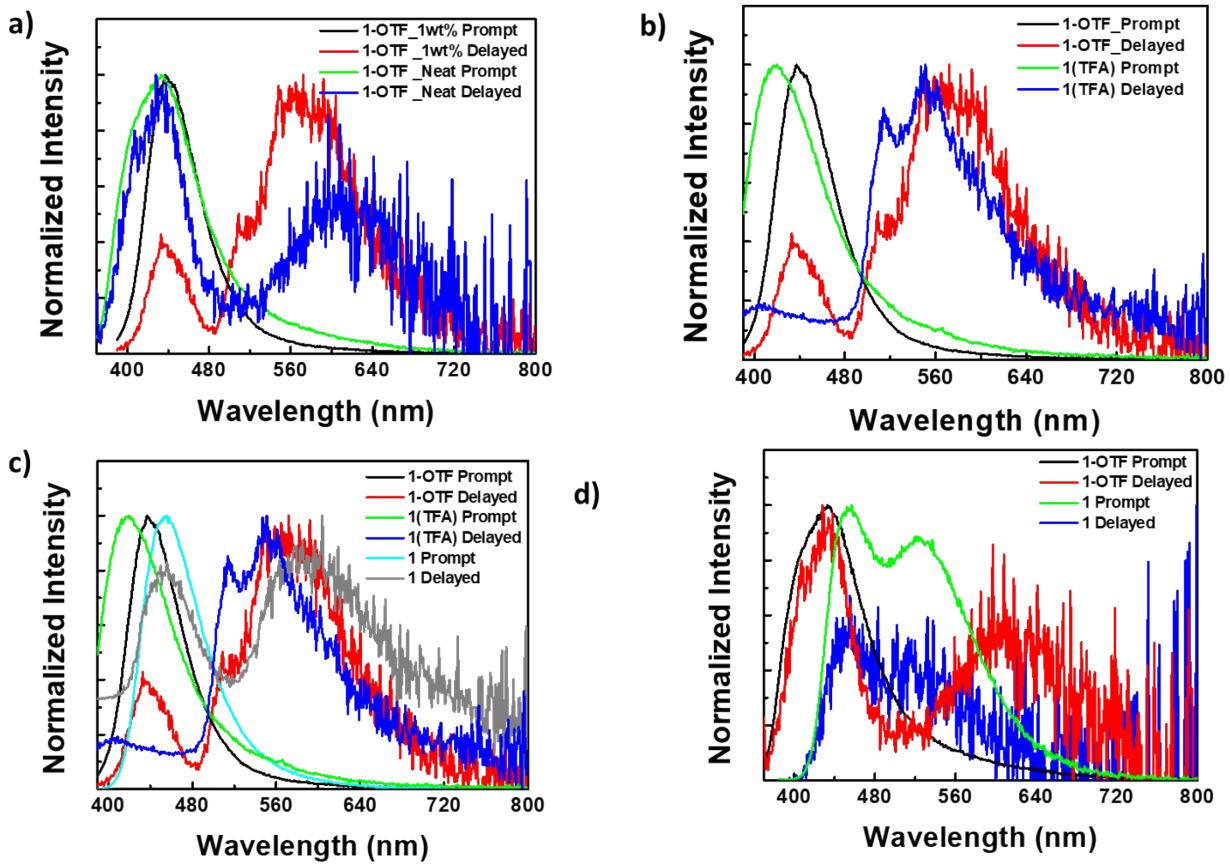

Figure S76. Prompt and delayed spectra for (a) **1-OTF** doped in PMMA matrix (1 wt%) neat film [λ_{ex} = 360 nm], (b) **1-OTF and 1 (exposed to TFA)** doped in PMMA matrix (1 wt%) [λ_{ex} = 380 nm], (c) **1-OTF,1 and 1 after exposed to TFA** in PMMA matrix (1 wt%) [λ_{ex} = 380 nm] (d) **1-OTF,1 and 1 after exposed to TFA** in neat film [λ_{ex} = 360 nm and 380 nm respectvly] under vacuum [absence of oxygen]

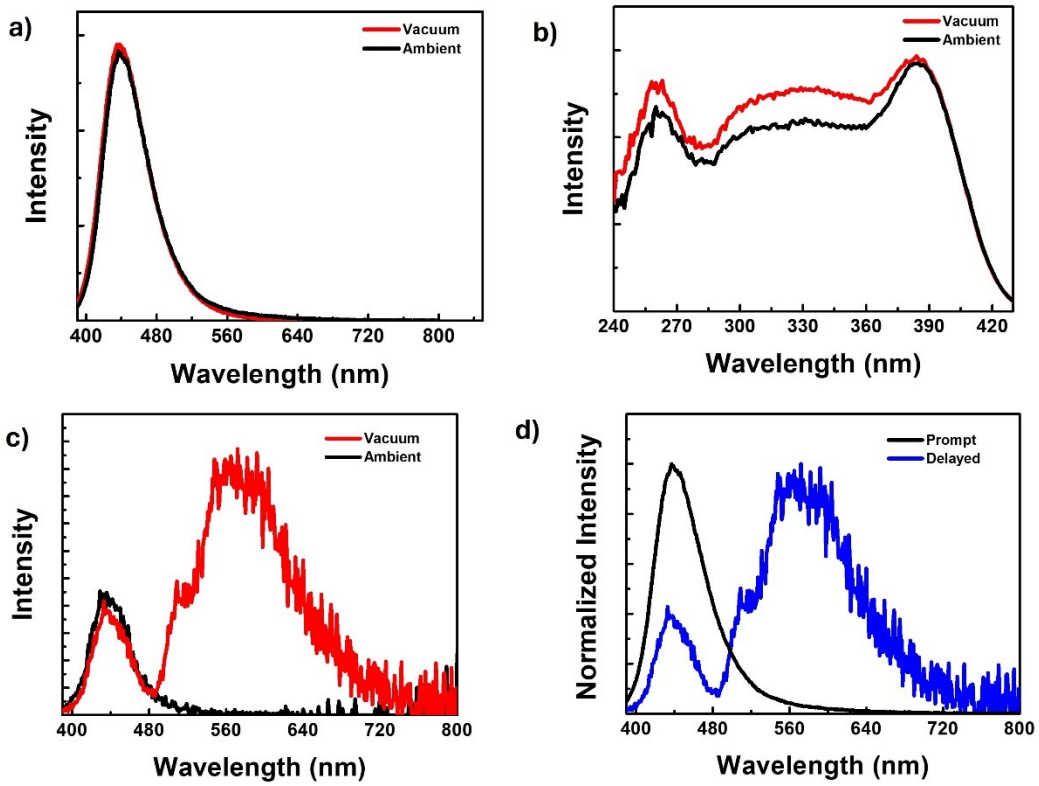

Figure S77. (a)Fluorescence spectra (b) excitation spectra corresponding to emission maxima (c) delayed fluorescence spectra [50 μs delay] under vacuum [absence of oxygen] and ambient atmosphere [presence of oxygen] at 298 K for **1-OTF** doped in PMMA matrix (1 wt%) [λ_{ex} = 380 nm]. (d) Prompt and delayed spectra for **1-OTF** doped in PMMA matrix (1 wt%) [λ_{ex} = 380 nm] under vacuum [absence of oxygen].

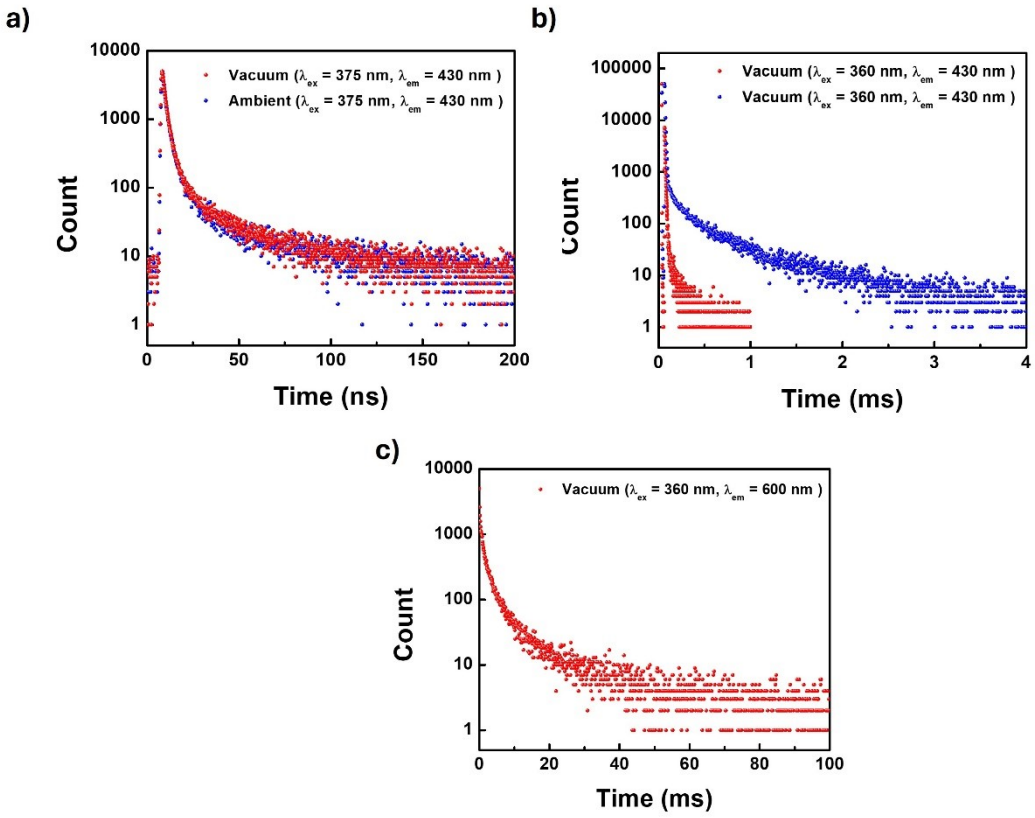

Figure S78. (a) fluorescence lifetime decay [λ_{ex} = 375 nm and λ_{ex} = 430 nm], (b) delayed fluorescence lifetime decay [λ_{ex} = 380 nm and λ_{ex} = 430 nm] and (c) phosphorescence lifetime decay [λ_{ex} = 380 nm and λ_{ex} = 600 nm] under vacuum [absence of oxygen] and ambient atmosphere [presence of oxygen] at 298 K for **1-OTF** doped in PMMA matrix (**1** wt%) [λ_{ex} = 380 nm].

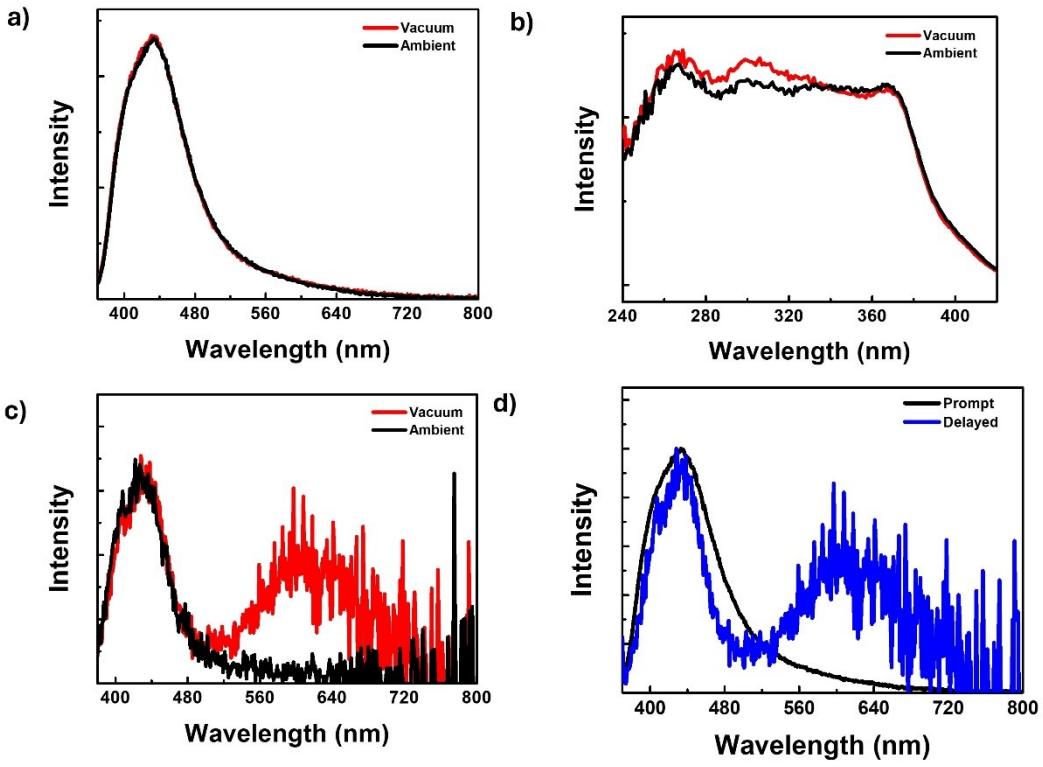

Figure S79. (a) Fluorescence spectra (b) excitation spectra corresponding to emission maxima (c) delayed fluorescence spectra [50 μs delay] under vacuum [absence of oxygen] and ambient atmosphere [presence of oxygen] at 298 K for **1-OTF** in neat film [λ_{ex} = 380 nm]. (d) Prompt and delayed spectra for **1-OTF** in neat film (1 wt%) [λ_{ex} = 380 nm] under vacuum [absence of oxygen]

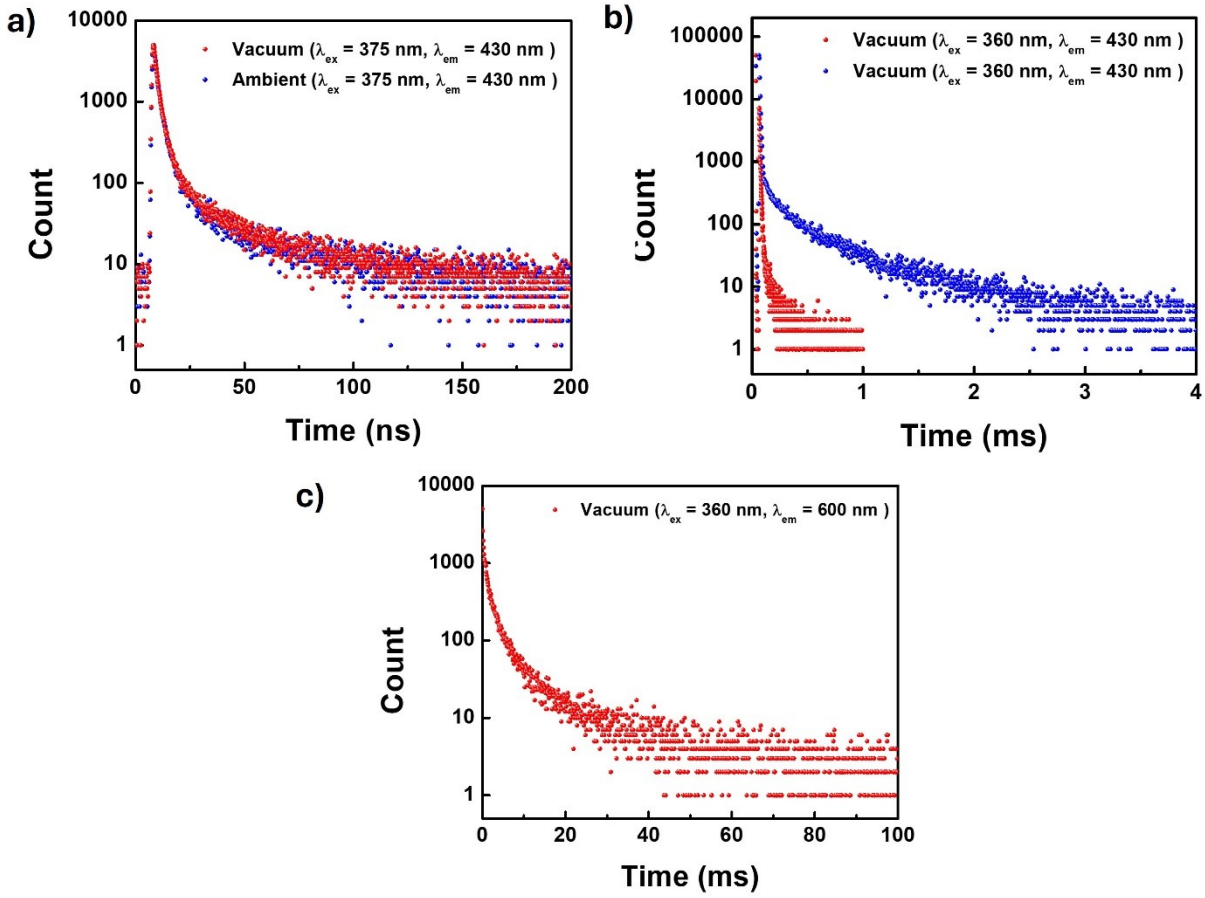

Figure S80. (a) fluorescence lifetime decay [λ_{ex} = 375 nm and λ_{ex} = 430 nm] (b) delayed fluorescence lifetime decay [λ_{ex} = 380 nm and λ_{ex} = 430 nm] (c) phosphorescence lifetime decay [λ_{ex} = 380 nm and λ_{ex} = 600 nm] under vacuum [absence of oxygen] and ambient atmosphere [presence of oxygen] at 298 K for **1-OTF** in neat film [λ_{ex} = 380 nm].

Table S23: Fluorescence, Delayed fluorescence and Phosphorescence lifetime for **1-OTF** in 1wt% doped film in PMMA and neat film at 298 K under vacuum.

	Fluorescence (ns)				**Delayed fluorescence (µs)**				**Phosphorescence (ms)**			
	λ_{ex} (nm)	λ_{em} (nm)	τ_1 (A_1[%])	τ_2 (A_2)[%])	λ_{ex} (nm)	λ_{em} (nm)	τ_1 (A_1 [%])	τ_2 (A_2 [%])	λ_{ex} (nm)	λ_{em} (nm)	τ_1 (A_1[%])	τ_2 (A_1)[%])
1wt% PMMA												
vacuum	375	430	3.74 (86.84)	11.86 (13.15)	380	430	6.13 (95.72)	59.86 (4.28)	380	570	91.41 (78.19)	379.99 (21.87)
Ambi	375	430	3.87 (88.45)	11.53 (11.55)	375	430	5.02 (82.90)	12.04 (17.10)				
Neat												
vacuum	375	430	2.51 (67.40)	26.25 (32.60)	380	430	85.18 (30.88)	564.86 (67.78)	380	600	1.05 (56.45)	7.92 (43.55)
Ambi	375	430	2.16 (70.56)	22.35 (29.44)	375	430	5.60 (90.95)	46.50 (9.05)				

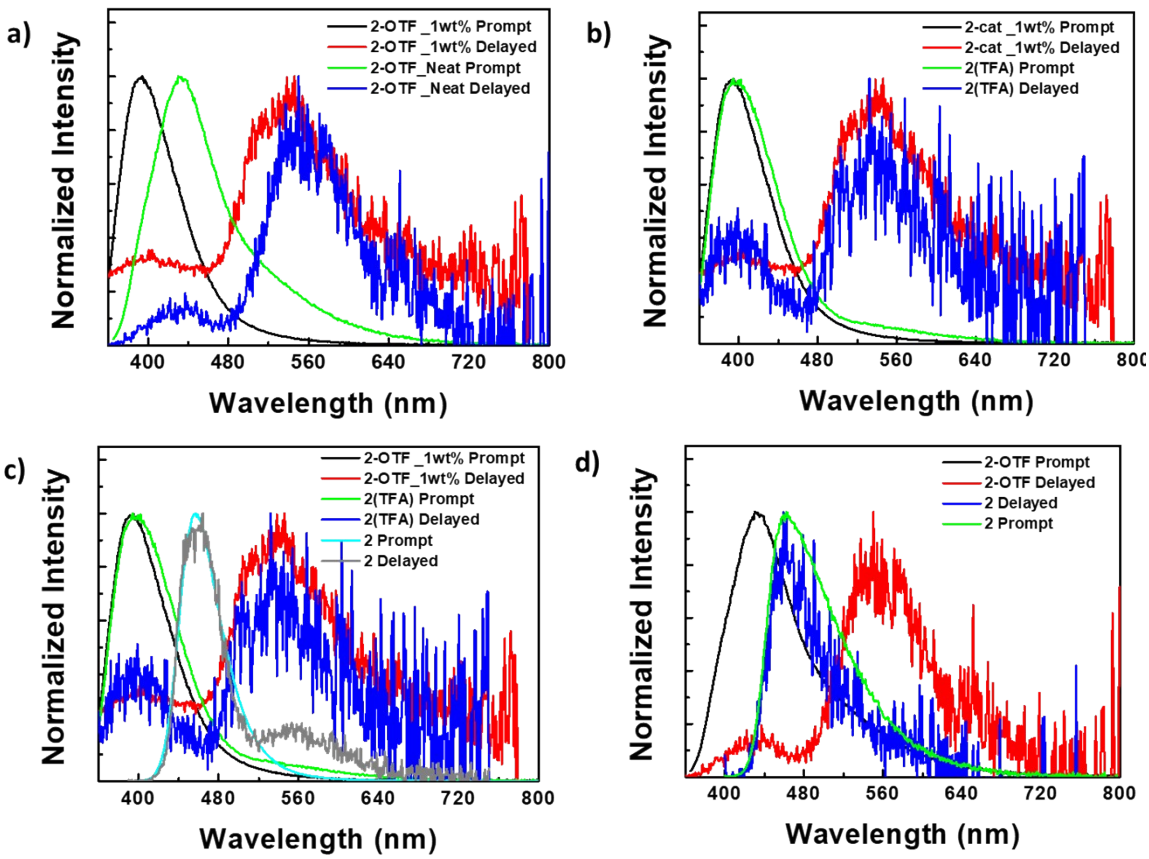

Figure S81. Prompt and delayed spectra for (a) **2-OTF** doped in PMMA matrix (1 wt%) neat film [λ_{ex} = 350 nm], (b) **2-OTF** and 2 (exposed to TFA) doped in PMMA matrix (1 wt%) [λ_{ex} = 350 nm], (c) **2-OTF**, **2** and **2** after exposed to TFA in PMMA matrix (1 wt%) [λ_{ex} = 350 nm], (d) **2-OTF**,**2** and **2** after exposed to TFA in neat film [λ_{ex} = 350 nm and 390 nm respctivly] under vacuum [absence of oxygen]

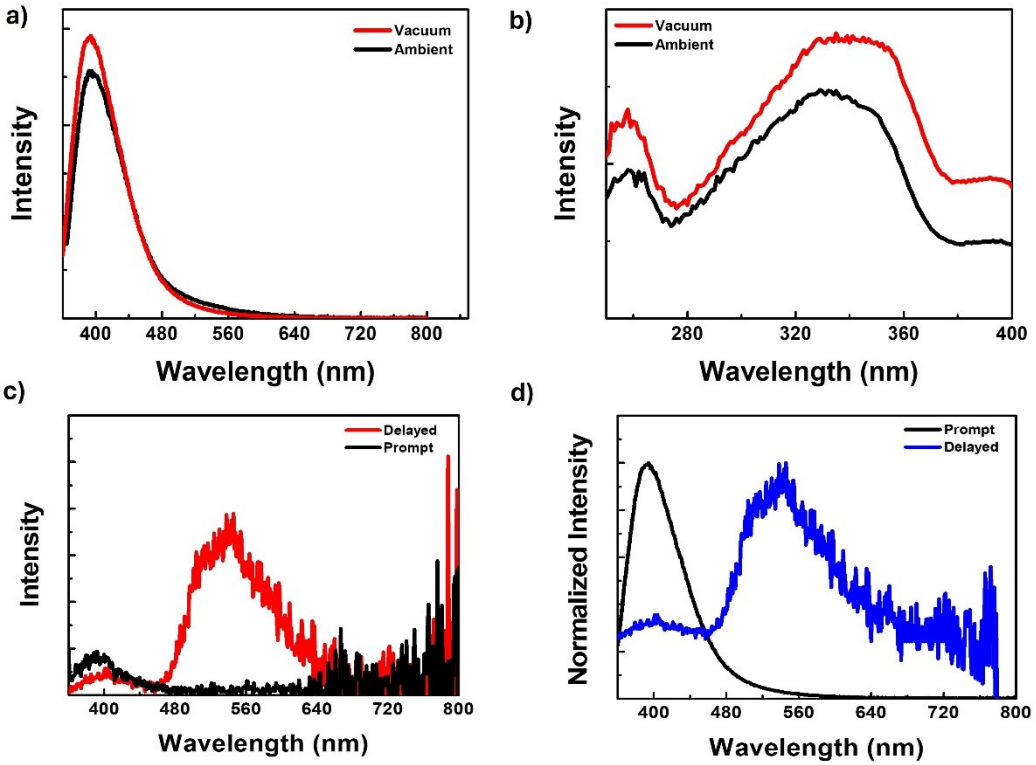

Figure S82. (a) Fluorescence spectra (b) excitation spectra corresponding to emission maxima (c) delayed fluorescence spectra [50 μs delay] under vacuum [absence of oxygen] and ambient atmosphere [presence of oxygen] at 298 K for **2-OTF** doped in PMMA matrix (1 wt%) [λ_{ex} = 350 nm] (d) Prompt and delayed spectra for **2-OTF** doped in PMMA matrix (1 wt%) [λ_{ex} = 350 nm] under vacuum [absence of oxygen]**.**

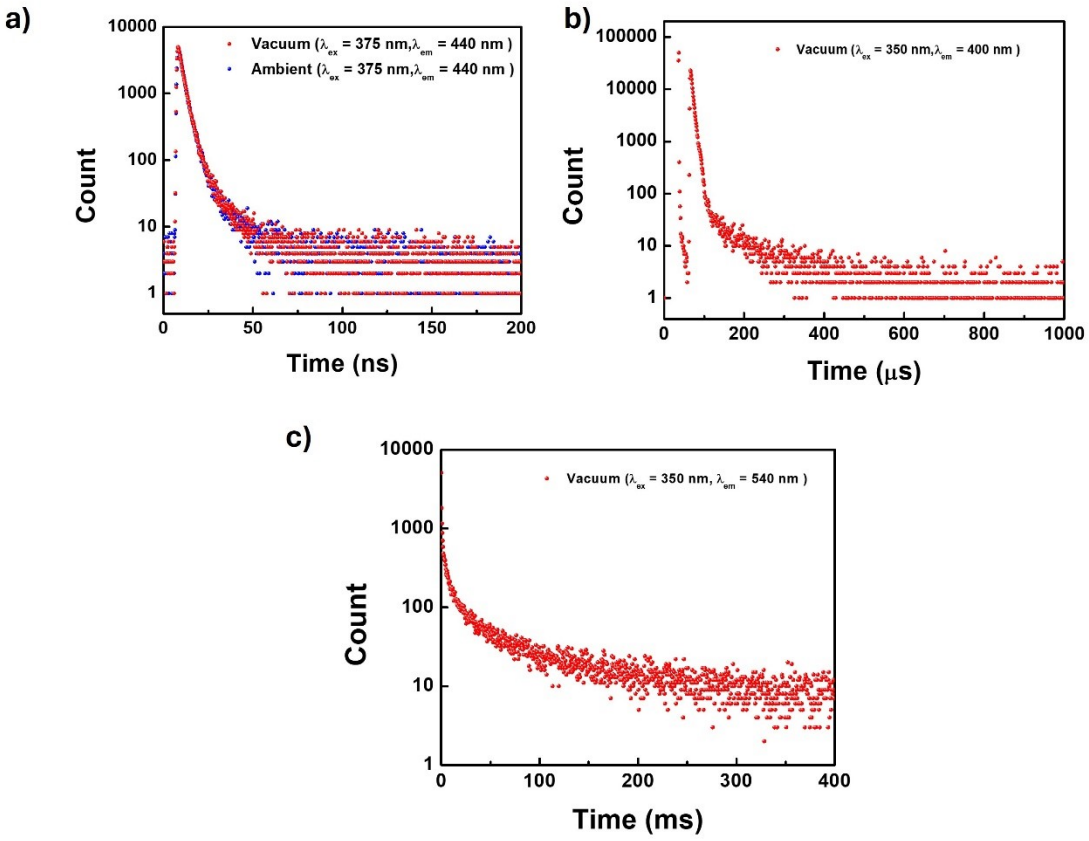

Figure S83. (a) fluorescence lifetime decay [λ_{ex} = 375 nm and λ_{ex} = 400 nm] (b) delayed fluorescence lifetime decay [λ_{ex} = 350 nm and λ_{ex} = 400 nm] (c) phosphorescence lifetime decay [λ_{ex} = 350 nm and λ_{ex} = 540 nm] under vacuum [absence of oxygen] and ambient atmosphere [presence of oxygen] at 298 K for **2-OTF** doped in PMMA matrix (1 wt%) [λ_{ex} = 350 nm].

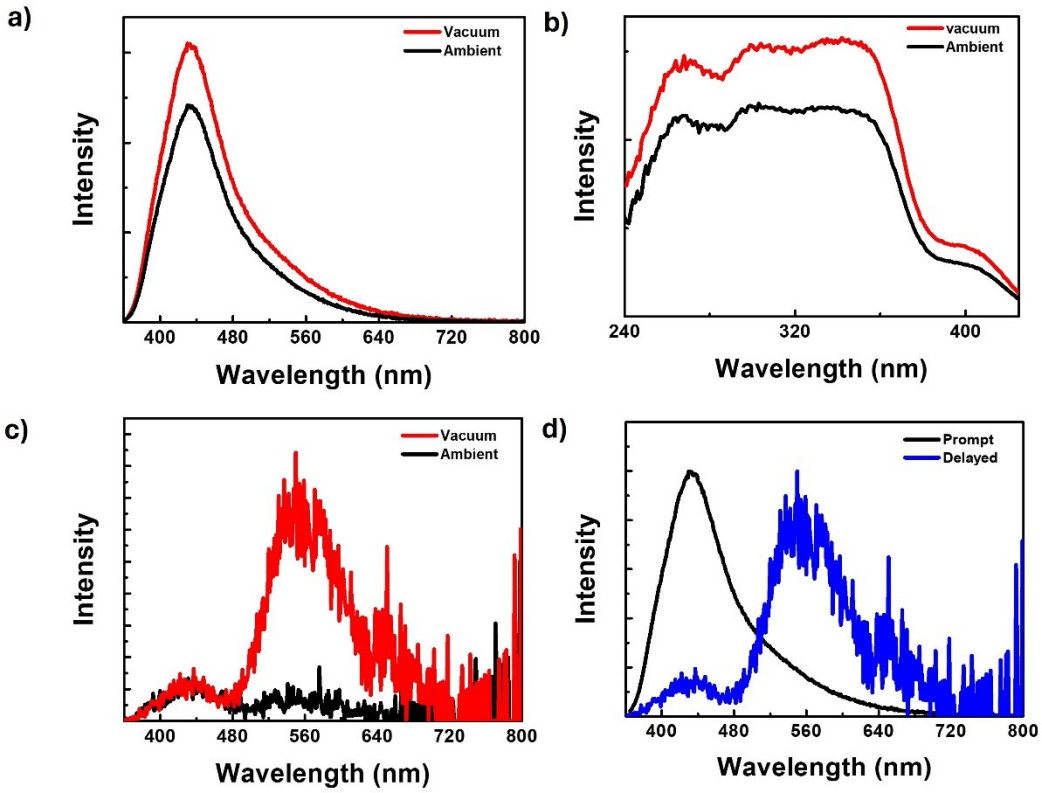

Figure S84. (a) Fluorescence spectra (b) excitation spectra corresponding to emission maxima (c) delayed fluorescence spectra [50 μs delay] under vacuum [absence of oxygen] and ambient atmosphere [presence of oxygen] at 298 K for **2-OTF** in neat film [λ_{ex} = 380 nm] (d) Prompt and delayed spectra for **2-OTF** in neat film (1 wt%) [λ_{ex} = 350 nm] under vacuum [absence of oxygen].

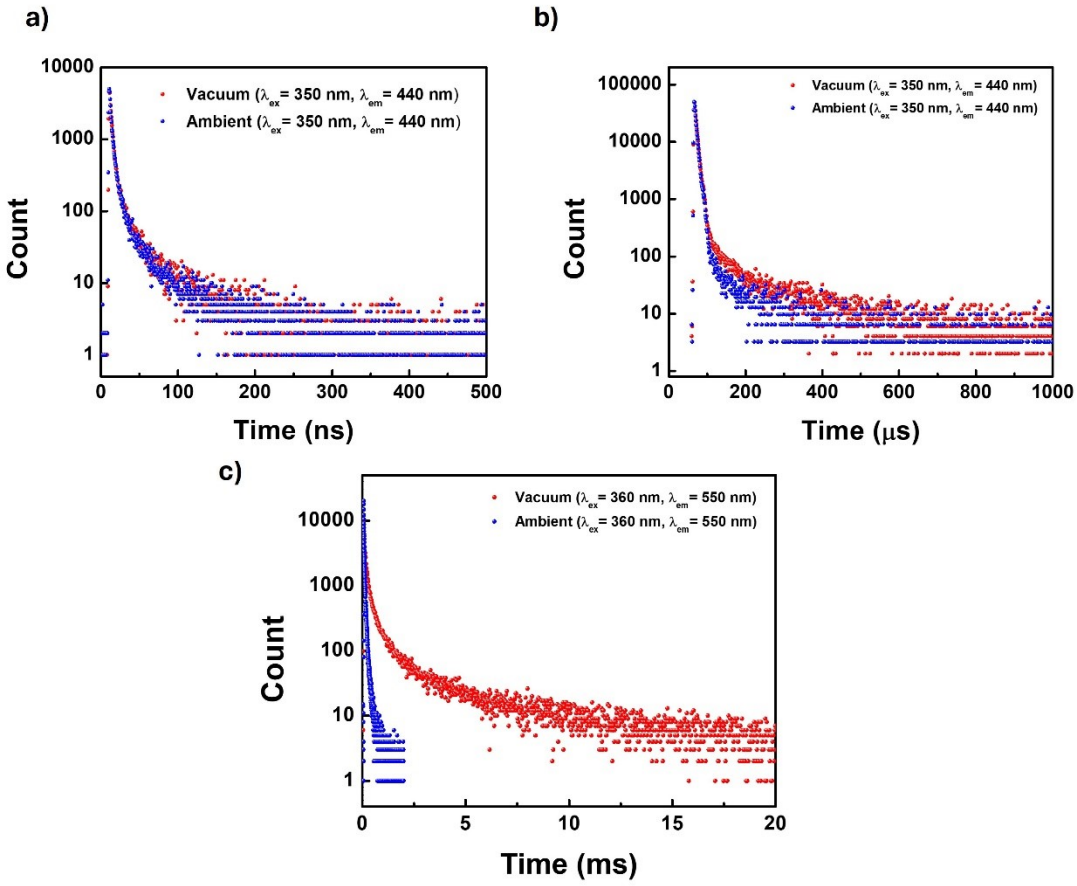

Figure S85. (a) fluorescence lifetime decay [λ_{ex} = 375 nm and λ_{ex} = 440 nm] (b) delayed fluorescence lifetime decay [λ_{ex} = 350 nm and λ_{ex} = 440 nm] (c) phosphorescence lifetime decay [λ_{ex} = 360 nm and λ_{ex} = 550 nm] under vacuum [absence of oxygen] and ambient atmosphere [presence of oxygen] at 298 K for **2-OTF** in neat film [λ_{ex} = 350 nm].

Table S24: Fluorescence, Delayed fluorescence and Phosphorescence lifetime for **2-OTF** in 1wt% doped film in PMMA and neat film at 298 K under vacuum.

	Fluorescence (ns)				**Delayed fluorescence(μs)**				**Phosphorescence (ms)**			
	λ_{ex} (nm)	λ_{em} (nm)	τ_1 (A_1 [%])	τ_2 (A_2 [%])	λ_{ex} (nm)	λ_{em} (nm)	τ_1 (A_1 [%])	τ_2(A_2 [%])	λ_{ex} (nm)	λ_{em} (nm)	τ_1 (A_1[%])	τ_2 (A_2 [%])
1wt% PMMA												
vacuum	375	400	2.86 (84.78)	11.80 (13.34)	380	400	6.11 (95.16)	76.10 (4.84)	380	540	5.01 (34.17)	60.60 (65.83)
Ambi	375	400	2.82 (86.66)	11.38 (13.34)								
Neat												
vacuum	375	430	3.51 (67.52)	30.80 (32.48)	375	430	6.83 (85.02)	96.86 (14.98)	360	550	0.33 (49.74)	2.85 (50.26)
Ambi	375	430	3.90 (68.49)	33.15 (31.51)	375	430	6.25 (94.27)	67.53 (5.73)	360	550	30.32 μs (70.40)	111.29 μs (29.60)

Table S25: List of spin-orbital coupling values for **1-OTF** and **2-OTF** between different singlet and triplet energy levels obtained theoretically using B3LYP/6-31G(d) level of theory.

Transition	**SOC (cm^{-1})**	
	1-OTF	**2-OTF**
$S_0 \rightarrow T_1$	0.1691	1.0000
$S_0 \rightarrow T_2$	0.4812	6.3970
$S_0 \rightarrow T_3$	0.8530	0.6300
$S_1 \rightarrow T_1$	0.1000	8.2239
$S_1 \rightarrow T_2$	0.3952	0.6211
$S_1 \rightarrow T_3$	0.2914	0.6765
$S_1 \rightarrow T_4$	0.4297	1.3815
$S_1 \rightarrow T_5$	0.3142	8.6291

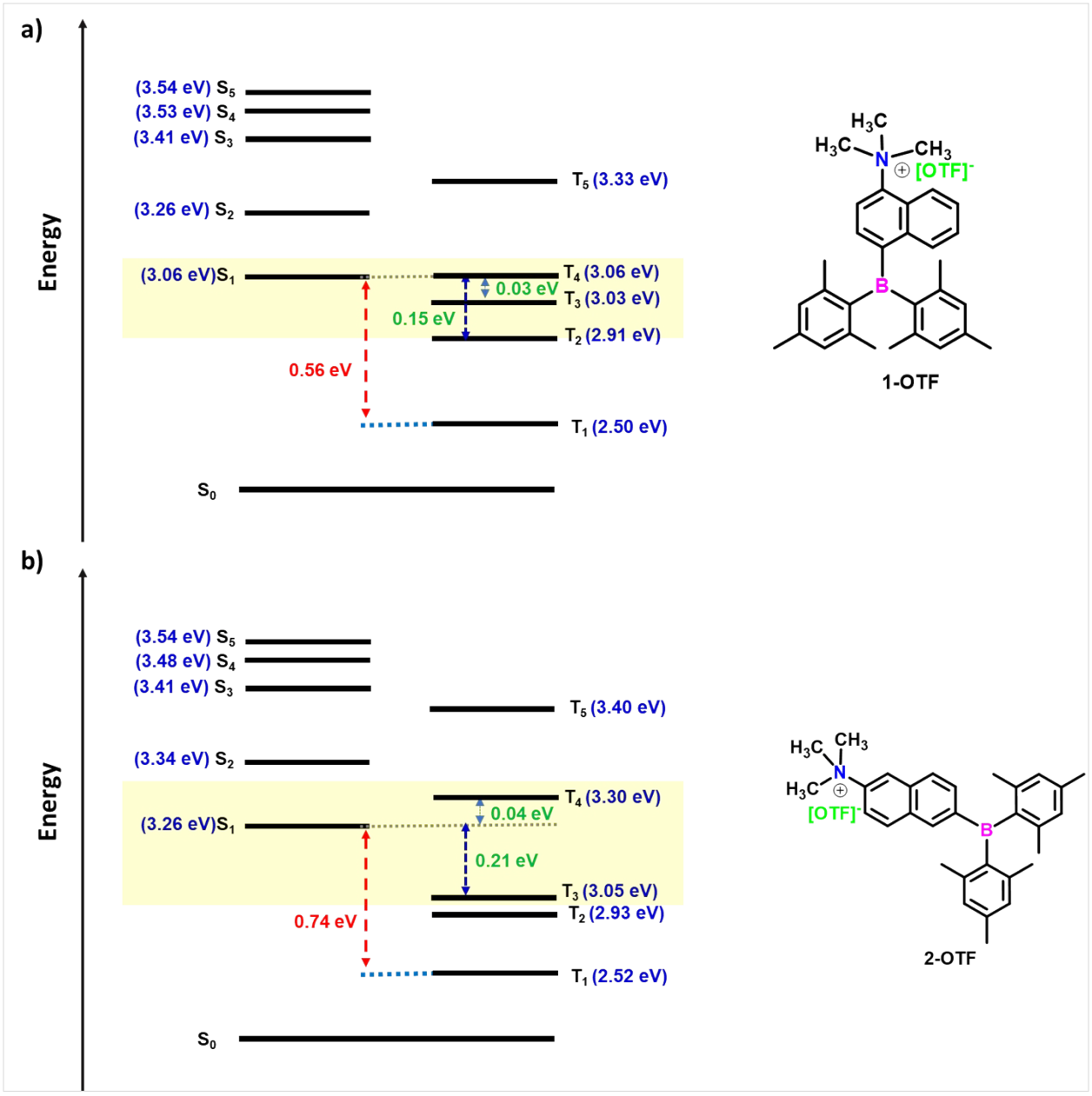

Figure S86. Energy level diagram showing singlet-triplet energy gap, and possible ISC channel for **1-OTF** and **2-OTF** [energy levels in the diagram are not up-to-scale, most possible T_n state involved in for spin-crossover according to the energy difference are highlighted in yellow box] (Energy levels are calculated from singlet and triplet vertical transitions through TD-DFT using 6-31G (d, p)/B3LYP level of theory).

Table S26. Three photon absorption properties of compounds **1** and **2**

800 nm excitation	$\beta \times 10^{-11}$ (cm.W^{-1})	$\gamma \times 10^{-23}$ (cm^3/W^2)	$\sigma_{3PA} \times 10^{-78}$ (cm^6.s^2)	Im [$\chi^{(3)}$]$\times 10^{-15}$ (e.s.u.)	$n_2 \times 10^{-16}$ (cm^2/W)	Re [$\chi^{(3)}$]$\times 10^{14}$ (e.s.u.)
1	-	3.0	6.2	-	4.9	3.8
2	-	3.9	8.1	-	5.6	4.4
Reference (DCM)	0.07	-	-	0.3	0.1	0.08

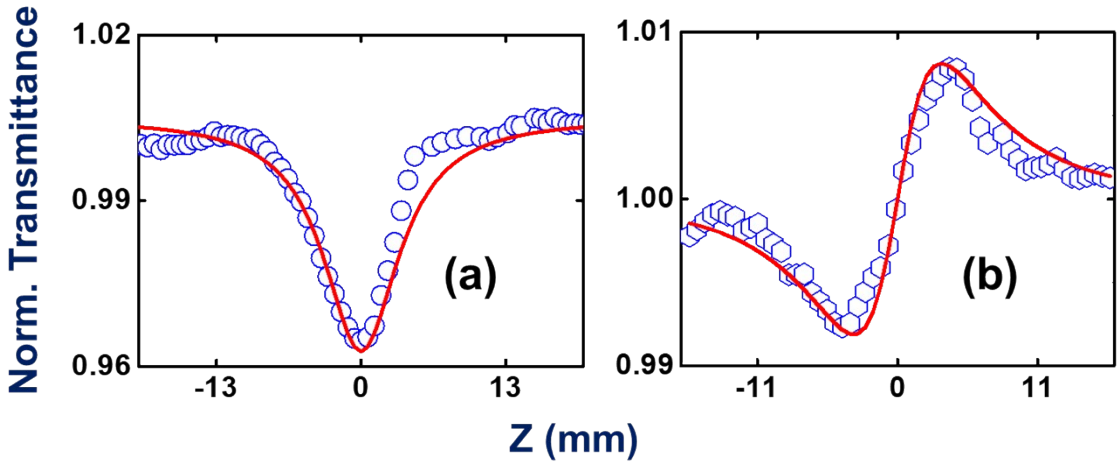

Figure S87. (a) Open aperture and (b) closed aperture data of the solvent DCM. Open symbols are the experimental data, while the solid lines represent the theoretical fits to the data.

Reference

1. R. J. Errington, Advanced practical inorganic and metal organic chemistry, Blackie academic & professional, London, 1997.
2. W. F. Armarego and C. L. L. Chai, Purification of laboratory chemicals, Elsevier, UK, 2013.
3. K. Kumar, R. J. Tepper, Y. Zeng, and M. B. Zimmt, *J. Org. Chem*. **1995**, 60, 4051-4066
4. X. Liu, M. Xiang, Z. Tong, F. Luo, W. Chen, F. Liu, F. Wang, R. Q. Yu, and J. H. Jiang, *Anal. Chem*. **2018**, 90, 5534−5539
5. (a) G. M. Sheldrick, Crystal structure refinement with SHELXL, Acta Crystallogr., Sect. C: Struct. Chem., **2015**, 71, 3-8; (b) G. M. Sheldrick, A short history of SHELX, Acta Crystallogr., Sect. A: Found. Crystallogr., **2008**, 64, 112; (c) A. L. Spek, Single-crystal structure validation with the program PLATON, J. Appl. Crystallogr., **2003**, 36, 7; (d) G. M. Sheldrick, Program for Crystal Structure Solution. SHELXS-97, University of Göttingen, Göttingen, Germany, 1997.

6. a) Frisch, M. J.; Trucks, G. W.; Schlegel, H. B.; Scuseria, G. E.; Robb, M. A.; Cheeseman, J. R.; Scalmani, G.; Barone, V.; Mennucci, B.; Petersson, G. A., et al. Gaussian 09, Revision D.01, Gaussian, Inc., Wallingford CT, **2013**. b) Lee, C.; Yang, W.; Parr, R. G. Development of the Colic-Salvetti Correlation-Energy Formula into a Functional of the Electron Density. Phys. Rev. B 1988, 37, 785-789.
7. (a) K. Goushi, K. Yoshida, K. Sato, C. Adachi, Nat Photonics 2012, **6**, 253–258 (b) K. Masui, H. Nakanotani, C. Adachi, Org Electron 2013, **14**, 2721–2726. (c)T. Nakagawa, S. Y. Ku, K. T. Wong, C. Adachi, Chem. Commun., 2012, **48**, 9580–9582. (d) G. Méhes, H. Nomura, Q. Zhang, T. Nakagawa, C.Adachi, Angew. Chem. Int. Ed.,2012, **51**, 11311–11315. (e) N. Notsuka, H. Nakanotani, H. Noda, K. Goushi, C. Adachi, J. Phys. Chem. Lett., 2020, **11**, 562–566.